

**A DESIGN OPTIMIZATION STUDY OF SERRATED STEEL  
GRIPPERS WITH SPECIAL REFERENCE TO SFOPM**

*A THESIS*

Submitted by

**OOMMEN THOMAS**

*for the award of the degree*

*of*

**DOCTOR OF PHILOSOPHY**



**MECHANICAL ENGINEERING DIVISION  
SCHOOL OF ENGINEERING  
COCHIN UNIVERSITY OF SCIENCE AND TECHNOLOGY, KOCHI.  
KOCHI-22**

**DECEMBER 2016**

## **THESIS CERTIFICATE**

This is to certify that the thesis entitled “**A DESIGN OPTIMIZATION STUDY OF SERRATED STEEL GRIPPERS WITH SPECIAL REFERENCE TO SFOPM.**” submitted by **Oommen Thomas, Reg. No. 3182** to the Cochin University of Science and Technology, Kochi for the award of the degree of Doctor of Philosophy, is a bona-fide record of the research work carried out by him under my supervision and guidance, at the Division of Mechanical Engineering, School of Engineering, Cochin University of Science and Technology. The contents of this thesis, in full or in parts, have not been submitted to any other University or Institute for the award of any degree or diploma.

Kochi- 682022

23-12-16

**Dr. V. N. Narayanan Namboothiri**

(Research Guide)

## **DECLARATION**

I hereby declare that the work presented in this thesis entitled **A DESIGN OPTIMIZATION STUDY OF SERRATED STEEL GRIPPERS WITH SPECIAL REFERENCE TO SFOPM** is based on the original research work carried out by me under the supervision and guidance of Dr. V N Narayanan Namboothiri, Associate Professor, Division of Mechanical Engineering, School of Engineering, for the award of degree of Doctor of Philosophy with Cochin University of Science and Technology. I further declare that the contents of this thesis, in full or in parts, have not been submitted to any other University or Institute for the award of any degree or diploma.

Kochi- 682022  
23-12-16

**Oommen Thomas**  
Reg. No. 3182

## ACKNOWLEDGEMENT

I bow my head before God Almighty for the blessings showered upon me throughout this research programme.

I would like to express with great pleasure, my deep sense of obligation and gratitude to my supervising guide Dr. V.N. Narayanan Namboothiri, Associate Professor, Division of Mechanical Engineering, School of Engineering, CUSAT for his invaluable guidance, constant support and encouragement during the entire course of my research work.

My heartfelt thanks are due to Dr. K.E. George, Principal, AISAT, Kalamassery and Dr. Rani Joseph, Professor, Department of Polymer Science and Rubber Technology for the invaluable help, support and guidance they had extended to me.

I wish to place my special thanks to the doctoral committee members Dr. P.S. Sreejith, Principal, CUCEK and Dr. N. H. Jayadas, Professor, Division of Mechanical Engineering, School of Engineering, CUSAT for their guidance, encouragement and support.

I am grateful to Dr. M.R.R. Panicker (Principal), Dr. Biju N.(HOD), Dr. P. S. Tide, Dr. G. Ajithkumar and Dr. James Varghese of SOE and Dr. Thomas Kurian, Dr. Sunil K. Narayanan Kutty and Dr. Bipinbal P.K. of the Department of Polymer Science and Rubber Technology for their support and encouragement.

I extend my sincere thanks to Dr. Thomas Tharian Scientist, VSSC, Valiyamala, and Mr. Gopalakrishnan, Manager, Brahmos Aerospace, Trivandrum and Mr. K.R. Rohith, Department of Polymer Science and Rubber Technology and Mr. Dilip, Scientist, VSSC, for their invaluable help and support in the execution of my work.

I would like to acknowledge my earnest thanks to M/s STIC (Sophisticated Testing and Instrumentation Centre, India) and M/s Rubber Park India for their laboratorial support.

My unbound gratitude goes to my beloved parents Late K.O. Thomas and Saramma Thomas who took a lot of pain to help me and blessed me with their prayers.

I am deeply indebted to my wife Susan and my son Abel for their understanding, tolerance, support and unlimited patience without which I would not have completed this study.

**Oommen Thomas**

## ABSTRACT

**KEYWORDS:** Serrated steel gripper; design optimization; contact stress; stress assisted diffusion; impactive gripper; sheet fed offset printing machine.

Gripper is a generic term for prehension devices used in printing, robotic and other applications. Serrations are usually provided on the gripping surfaces of the gripper jaws for achieving good grasp. The serrations experience high contact stress since the areas of contact are small. The operations of grippers are often repetitive and hence the serrations experience high cyclic contact stress which can adversely affect its durability and requires periodic replacement as in the case of grippers of sheet fed offset printing machine (SFOPM). The dearth of literature often renders the design of serrations ad-hoc and suboptimal.

In this thesis, an optimization framework to quickly arrive at design solutions to maximize the durability and performance of a serrated gripper is developed; the stress assisted diffusion of carbon near the contact surface of serrated steel grippers are explored and modelled; and the feasibility of Acrylonitrile-butadiene rubber (NBR) as a lining material for the gripper explored. Grippers of sheet fed offset printing machines are selected as a reference for the purpose of the study. However, the findings are applicable for any similar serrated steel gripper.

A framework for optimized design of serrations on a gripper jaw is developed as follows. The serrations are considered as an array of hemispherical projections on the jaw surface in contact with an elastic half space. The grasping force of the gripper is used to estimate the contact force on each serration. The von Mises stress developed on the serrations for various sizes of hemispherical projections are determined assuming Hertzian contact. The procedure is repeated for different grasping forces

and the results are analysed. Similarly, the values of deformation of serration are also determined for the corresponding values of serration sizes and forces. The optimum size of serrations is found to be a trade-off between the von Mises stress and deformation. From these results, the optimum design parameters are determined.

A cut section of used serrated steel gripper is examined using Field Emission Scanning Electron Microscope (FESEM) with Energy-dispersive X-ray Spectrometer (EDS) and clustering of carbon near the serrations is observed. The stress assisted diffusion of carbon atoms due to high stress cyclic loading of serrations of the gripper, leading to the redistribution of carbon near the surface is modelled. An elastic plastic finite element model coupled with simulation of stress assisted diffusion of carbon is employed for the purpose. Kinematic hardening rule is used to estimate the dissipated plastic strain energy due to the contact stress and these results are transferred to the nodes of a very fine square grid. Potential gradient due to dissipated plastic strain energy coupled with modified Fick's law are employed to simulate the stress assisted diffusion of carbon near the surface of a serration on the gripper jaw. Measures for quantifying the redistribution of carbon are introduced and the effect of the number of cycles, loading condition and temperature on the redistribution of carbon in steel are explored.

The feasibility of replacing serrated steel grippers with impactive grippers having a suitable lining material like silica reinforced nitrile butadiene rubber for applications like SFOPM are explored. The effect of silica loading on the static frictional coefficient of nitrile rubber when paired with different types of papers is investigated. The influence of silica loading on the mechanical properties of nitrile rubber and its changes due to natural ageing is also examined. The change in mechanical properties due to ageing was found to be marginal and the feasibility of silica loaded NBR as a lining material for gripper jaw surfaces is established.

# TABLE OF CONTENTS

ACKNOWLEDGEMENTS .....	i
ABSTRACT.....	ii
LIST OF TABLES .....	vi
LIST OF FIGURES.....	vii
ABBREVIATIONS.....	x
NOTATION.....	xi
<b>CHAPTER 1 INTRODUCTION</b>	
1.1 General.....	01
1.2 Motivation behind the research work .....	03
1.3 Objectives of the work.....	05
1.4 Research methodology.....	06
1.5 Outline of the thesis.....	07
<b>CHAPTER 2 OVERVIEW OF LITERATURE</b>	
2.1 Introduction .....	08
2.2 Grippers .....	08
2.3 Contact stress.....	10
2.3.1 Characteristics of contact stress.....	11
2.4 Contact elements.....	12
2.5 Cyclic plasticity .....	14
2.6 Diffusion and stress assisted diffusion.....	16
2.6.1 Diffusion.....	17
2.6.2 Stress assisted diffusion .....	20
2.7 Reinforcement of rubbers with particulate fillers .....	22
2.8 Acrylonitrile-butadiene rubber (NBR).....	24
2.9 Conclusion.....	25
<b>CHAPTER 3 A FRAMEWORK FOR OPTIMISED DESIGN OF SERRATIONS ON A GRIPPER</b>	
3.1 Introduction .....	26
3.2 Workholding grippers .....	27
3.3 Sprue picker grippers for de-molding .....	28
3.4 Sheet fed offset printing machine (SFOPM).....	28
3.4.1 Print quality, registration and importance of grippers .....	31
3.5 Framework for optimized design of serrations on a gripper .....	32
3.5.1 Grasping forces.....	33

3.5.2	Stresses on gripping surface .....	34
3.5.3	Summary of the methodology .....	34
3.5.4	Assumptions and calculations .....	36
3.5.5	Description of the procedure .....	39
3.5.6	Results and discussions .....	41
3.5.7	Conclusions .....	44

**CHAPTER 4 SHORT RANGE DIFFUSION OF CARBON IN  
STEEL GRIPPERS DUE TO CYCLIC CONTACT  
STRESS**

4.1	Introduction .....	46
4.2	Experimental setup.....	46
4.2.1	Major design considerations of the experimental setup.....	48
4.3	Experimental procedure .....	49
4.4	Methodology of simulation of carbon diffusion.....	52
4.5	Results of simulation.....	64
4.6	Discussion on the results of simulation.....	77
4.7	Conclusions .....	81

**CHAPTER 5 FEASIBILITY OF SILICA LOADED NBR AS  
LINING MATERIAL FOR IMPACTIVE GRIPPER**

5.1	Introduction .....	82
5.1.1	Objectives and background .....	83
5.2	Experimental.....	85
5.2.1	Materials .....	85
5.2.2	Preparation of samples .....	85
5.2.3	Tests .....	86
5.3	Results and discussion.....	87
5.4	Conclusions .....	93

**CHAPTER 6 SUMMARY AND CONCLUSIONS**

APPENDIX.....	97
REFERENCES.....	104
LIST OF PAPERS BASED ON THESIS.....	116
CURRICULAM VITAE.....	117



## LIST OF TABLES

<b>Table</b>	<b>Title</b>	<b>Page</b>
4.1	Properties of steel, AISI 4320.....	56
5.1	Formulation of mixes (in phr). ....	85
5.2	Co-efficient of static friction of NBR loaded with different amounts of silica, when paired with different types of paper.....	87

## LIST OF FIGURES

Figure	Title	Page
2.1	Two spheres in contact.....	11
2.2 (a)	Schematic illustration of the Bauschinger effect .....	15
2.2 (b)	The Bauschinger effect in a hysteresis loop for an austenitic material. ....	15
3.1	Gripper inserts with serrations.....	27
3.2	Sprue picker grippers for de-molding. ....	28
3.3	Four Color Sheet fed Offset Printing Machine with perfecting. ....	28
3.4	Four Color Sheet fed Offset Printing Machine with perfecting and Schematic of two adjacent printing units. ....	29
3.5	Gripper arrangement in a typical sheet fed offset printing machine and Serrations on a printing gripper.....	30
3.6	Serrations on the gripping surface. ....	32
3.7	Stresses along the axis of a hemisphere of 0.9 mm diameter at 50N load. ....	35
3.8	Maximum von Mises stress vs. diameter of hemisphere (projection), $d$ for different loads with constant gap, $\gamma$ . ....	41
3.9	Displacement of contact surface, $\alpha$ vs. diameter of hemisphere (projection), $d$ for constant $\gamma$ .....	42
3.10	Maximum von Mises stress vs. groove width $\gamma$ for constant $\rho$ . ....	43
3.11	Displacement vs. groove width $\gamma$ for constant $\rho$ . ....	44
4.1	Photograph of the fabricated experimental setup .....	47
4.2	CAD model of the main unit of the experimental set-up.....	47
4.3	The serrated portion of a printing gripper cut into three pieces and the balance portion .....	49
4.4	CARL ZIESS make SIGMA™ HD FESEM.....	50
4.5	Clustering of carbon near the surface of a serration in a printing gripper after subjecting to cyclic stress. ....	51

4.6	Meshed axisymmetric model for analysis and it's zoomed in view with enlarged view of mesh at the sphere of influence shown in inset .....	55
4.7	Schematic of bilinear hardening model and the residual area .....	57
4.8	The position of the region of interest (shown in red) on a gripper serration and the region of interest and the co-ordinate system. ....	59
4.9	Nodal definitions for finite difference method. ....	62
4.10	Equivalent stress assuming perfectly elastic material (Zoomed in view at the region of contact is shown in inset).....	65
4.11	Equivalent stress assuming bilinear elastic-plastic model (Zoomed in view at the region of contact is shown in inset) .....	65
4.12	Equivalent plastic strain assuming bilinear elastic-plastic model (Zoomed in view at the region of contact is shown in inset).....	66
4.13	Dissipated plastic strain energy density. ....	66
4.14	Dissipated plastic strain energy density along Y axis through the point of contact. ....	67
4.15	Vector plot showing Potential gradient.....	67
4.16	Laplacian of the potential gradient. ....	68
4.17	3D plot of carbon concentration for 50N load after $10^7$ cycles (at $30^\circ\text{C}$ ) .....	69
4.18	Gradient plot of carbon concentration for 50N load after $10^7$ cycles.....	69
4.19	3D plot of carbon concentration for 50 N load after $10^8$ cycles .....	70
4.20	Gradient plot of carbon concentration for 50 N load after $10^8$ cycles.....	70
4.21	3D plot of carbon concentration for 40 N load after $10^8$ cycles .....	71
4.22	Gradient plot of carbon concentration for 40 N load after $10^8$ cycles.....	71
4.23	3D plot of carbon concentration for 50 N load after $10^7$ cycles, at $20^\circ\text{C}$ .....	72
4.24	Gradient plot of carbon concentration for 50 N load after $10^7$ cycles at $20^\circ\text{C}$ .....	73
4.25	3D plot of carbon concentration for 50 N load after $10^7$ cycles, at $40^\circ\text{C}$ .....	73

4.26	Gradient plot of carbon concentration for 50 N load after $10^7$ cycles at $40^\circ\text{C}$ .....	74
4.27	3D plot of carbon concentration for 50 N load after $10^7$ cycles, at $50^\circ\text{C}$ .....	74
4.28	Gradient plot of carbon concentration for 50 N load after $10^7$ cycles at $50^\circ\text{C}$ .....	75
4.29	Maximum and minimum carbon concentrations after stress assisted diffusion due to cyclic contact stress at different temperatures.....	76
4.30	Range of carbon concentration (difference between maximum and minimum values) after stress assisted diffusion at different temperatures.....	76
4.31	Standard deviation of carbon concentration after stress assisted diffusion at different temperatures.....	76
5.1	SEM micrographs of (a) NBR with 55 phr silica. (b) NBR with 65 phr silica. ....	89
5.2	Variations of Hardness of NBR with silica loading and natural ageing and Tear strength of NBR with silica loading and natural ageing .....	89
5.3	Variations of Swelling Index of NBR in oil with silica loading and Tensile strength of NBR with silica loading and natural ageing .....	91
5.4	Variations of Abrasion loss of NBR with silica loading and Elongation at break of NBR with silica loading and natural ageing. ....	92

## ABBREVIATIONS

DLC	Diamond-like carbon
EDM	Electro Discharge Machining
EDS	Energy-dispersive X-ray spectroscopy
EXPST	Experimental set up
FDM	Finite difference method
FE	Finite element
FEA	Finite element analysis
FESEM	Field Emission Scanning Electron Microscope
LM guide	Linear Motion guide
NBR	Acrylonitrile-butadiene rubber
NR	Natural rubber
RCF	Rolling Contact Fatigue
SEM	Scanning Electron Microscope
SFOPM	Sheet fed offset printing machine
TiC	Titanium carbide
TiN	Titanium nitride

# NOTATION

## English Symbols

$a$	Radius of circular area of contact between two spheres
$A$	The pre-exponential factor
$b$	Half width of rectangular contact area
$c$	Concentration (of Carbon / solute)
$d$	Diameter of sphere (Diameter of projection)
$d_c$	Critical diameter of sphere (Critical diameter of projection)
$D$	Coefficient of diffusion, Phenomenological coefficient
$D_0$	Maximal diffusion coefficient (at infinite temperature).
$E$	Young's Modulus (Elastic constant)
$e$	Trace of strain
$F$	Applied load
$h$	Spatial span of grid
$H$	Phenomenological coefficient
$H_m$	Hardening Modulus
$I$	Identity matrix
$i, j$	Spatial coordinates
$J, J_x$	Flux, Flux in X direction
$k$	Boltzmann's constant
$K$	Rate constant of chemical reaction
$l$	Length of rectangular contact area
$M, N, P$	Phenomenological coefficients
$n$	Time step number
$p_{max}$	Maximum pressure
$Q$	Activation energy (for diffusion)
$r$	Radius of the sphere (radius of projection)

$R$	Gas constant
$S_y$	Yield Stress
$t$	Time
$T$	Absolute temperature
$V$	Potential driving the diffusion
$w$	Partial molar strain energy
$W$	The total work done on the stressed body per mole addition of component

### Greek Symbols

$\alpha$	Displacement
$\beta$	The distance of any point on the axis from the tip of projection / hemisphere
$\gamma$	The groove width or the gap between projections/hemisphere
$\Delta t$	Pseudo time step/ time step (temporal span)
$\varepsilon_p$	Equivalent plastic strain
$E$	Strain (Greek capital letter epsilon)
$\theta, \lambda$	Lamé constants
$\mu_0$	The chemical potential in the unstressed state
$\mu_s$	The chemical potential in the stressed state
$\nu$	Poisson's ratio
$\zeta$	Friction coefficient of particle
$\rho$	Pitch of the serration
$\rho_c$	Critical pitch
$\sigma$	Stress, Equivalent stress
$\sigma_t$	Trace of stress
$\sigma_x, \sigma_y, \sigma_z$	Principal stresses
$\tau_{xy}, \tau_{xz}, \tau_{yz}$	Shear stresses

# CHAPTER 1

## INTRODUCTION

### 1.1 GENERAL

Grippers are active links between the handling equipment and the workpiece or in a more general sense between the grasping organ (normally the gripper fingers) and the object to be acquired. They are a universal component in automation (Monkman *et al.*, 2007). They ensure the position and orientation when carrying and mating the object to the handling equipment. They operate with industrial robots for handling and manipulation of objects; used for hard automation in assembling, microassembling, machining, and packaging. They are also employed in NC machines (tool change) and special purpose machines; and in hand-guided manipulators for remote prehension, medical, aerospace, and nautical applications. The other applications include workpiece turret devices in manufacturing technology, rope and chain lifting tools in load-carrying equipment and in sheet fed offset printing machines (SFOPM). They are also used in service robots as prehension tools potentially similar to prosthetic hands, and miniaturized grippers for delicate components in micro and nano applications. In any application, the primary function of a gripper is to provide a stable grasp. Different physical effects like friction, permeation, suction and adhesion are employed to guarantee a stable grasp, depending on the type of object, the forces involved and the nature of application.

According to Shiller and Dubowsky (1989), the gripping force constraint is defined as the maximum force that can be applied by the gripper on the payload for a grasp which depends upon the friction between the payload and the gripper. Since the gripping forces are usually limited by the characteristics of the gripper and the



payload, the payload may slip out of the gripper at high accelerations, or even low speeds along tight turns. Including these types of constraints in the algorithm of movement is a method to ensure that the manipulator motion is time optimal and safe for the payload. A method suggested by Tremblay and Cutkosky (1993) to prevent slippage to provide optimal grasping force is detecting localized slips on the gripping surface which precede gross slip, so the controller can modify the grasp force to prevent the object from slipping. However in certain applications, even localized slips can be detrimental to the quality of output. In applications where the load is large and when the application permits, high gripping forces with permeation can be profitably employed and the path need not be constrained. Serrations on the gripping surface are usually employed for the purpose. Due to the small areas of contact, the serrations on the jaw surfaces often experience high contact stress.

Contact stress may be described as follows. The theoretical contact area of two spheres, or between a sphere and a plane, is a point and the theoretical contact area of two parallel cylinders is a line. As a result, the pressure between two curved surfaces should be infinite. The infinite pressure at the contact should cause immediate yielding of both surfaces. In reality, a small contact area is being created through elastic deformation, thereby limiting the stresses considerably. These contact stresses are called Hertz contact stresses. The hertzian contact stress often assumes high values in applications similar to the serrated grippers, where the theoretical area of contact is a point or line. The maximum contact stress also increases as the value of elastic moduli of the contacting materials increases. Repetitive high contact stress can adversely affect its durability and may necessitate periodic replacement as in the case of grippers of SFOPM (sheet fed offset printing machine).

## 1.2 MOTIVATION BEHIND THE RESEARCH WORK

Contact is a complex nonlinear phenomenon and the contact behaviour of various applications, like contact stress on teeth of gears, rail wheel contact stress, rolling contact stress on ball bearings etc. are well researched. Literature is available on contact stress on teeth of gears by Tsay (1988), Vijayarangan, and Ganesan (1994), Bibel *et al.* (1995), Litvin *et al.* (2000), Chen and Tsay (2002), Hassan (2009), Pedrero *et al.* (2011), Gupta *et al.* (2012), Hwang *et al.* (2013) and others. These studies include the tooth contact stress analysis of spur, helical, spiral, bevel and undercut gears. Mathematical and computer programs using finite element methods are discussed. The variations of contact stress along the contact surface in a direction normal to the mating surface are also explored.

Patil *et al.* (2014, 2015) included friction also for contact stress calculations of gears. A spur gear finite element (FE) model was validated with the theoretical analysis under frictionless condition, based on Hertz's contact theory and similar FE models were constructed for helical gear pairs with different helix angles and the contact stresses of these models were evaluated for different coefficients of friction. The variation of contact stresses with helix angle and also with friction coefficients was also explored.

Numerous studies are also available on rail wheel contact stress by Paul (1975), Bogdanski *et al.* (1996), Yan and Fischer (2000), Pau *et al.* (2002), Ayasse and Chollet (2005), Piotrowski and Kik (2008), Zhao and Li (2011), Ekberg *et al.* (2014), Xin Zhao *et al.* (2016) and others. The studies include, numerical stress analysis of rail rolling contact fatigue cracks, distribution of contact pressure in wheel–rail contact area, wheel/rail rolling contact fatigue, dynamic stress intensity

factors of rail cracks at high speeds, estimation of the convective part of the dissipation power due to friction etc. Still, Eric Magel *et al.* (2016) had raised a number of issues which need to be addressed through further developments in understanding and mitigating strategies in rail wheel contact to reduce the risk of failures from RCF and wear.

Various studies are also available on rolling contact stress and fatigue as in ball bearings by Zwirlein and Schlicht (1982), Jiang and Sehitoglu (1996, 1999), Jiang *et al.* (2002), Desimone *et al.* (2006), Popescu *et al.* (2006), Gabelli *et al.* (2008), Weinzapfel and Sadeghi (2013), Bomidi *et al.* (2013), Wardhpande *et al.* (2014), El-Thalji and Jantunen (2015) and others. The studies include investigation of rolling contact fatigue mechanisms, rolling contact failure models, elastic-plastic stress analysis of rolling contact etc. Numerical models of sub-surface initiated spalling in rolling contacts and dynamic models of wear evolution in rolling bearings are also developed. A comprehensive review of microstructural evolution and empirical life prediction models for RCF of bearing steels in the gigacycle regime by Arakere (2016) is available. Literature is also available in stress assisted diffusion of carbon in bearing steel due to rolling contact stress.

Studies are even available in various biomedical applications in joint contact like hip contact stress by Henak *et al.* (2014), Wang *et al.* (2016); dental biomechanics by Magne and Belser (2002), Dejak *et al.* (2012) and contact stress on knee implants by Seo *et al.* (2016) etc. on topics like modelling and simulation of hip joint surface contact stress, tooth-to-tooth contact, evaluation of contact pressure at articular surface of knee implant etc.

Serrated steel grippers are used in many applications like robots, workholding devices, printing machines etc. Serrations are provided on the gripper jaw(s) for a firm grip on the object to be handled. Small contact areas of the serrations result in high contact stress and these stresses are often repetitive. However no study has been reported in the case of contact stress on serrated steel grippers. The repetitive cyclic stress on the serrations and its effects need to be understood. This has been the motivation behind the research work.

### **1.3 OBJECTIVES OF THE WORK**

The serrated steel grippers of sheet fed offset printing machines (SFOPM) are observed to have limited life due to wear. The grippers are critical to the quality of printing and the periodic replacement of grippers requires sizable expense that adds to the maintenance cost of a printing press.

The main objectives of the study are

- To determine the contact stresses and corresponding deformations experienced by the serrations of a gripper and explore its relationship with the design parameters like size and pitch.
- To develop a framework for optimal design of the serrations on a serrated gripper based on the above relationships.
- To examine the microscopic alterations if any, at the contact surface and subsurface of serrated steel grippers, due to the cyclic contact stress as a result of the gripping action and to draw conclusions from the examination.
- To explore and evaluate an inexpensive and easily replaceable material suitable for lining the jaw surface of gripper for providing adequate grasp without serrations.

Grippers of SFOPM are selected as a reference for the purpose of the study. However, the findings are applicable for any similar serrated steel gripper used elsewhere.

## 1.4 RESEARCH METHODOLOGY

The major steps of the research and the methodology followed are briefly presented below.

- Gripping should ideally be done without causing any damage to the gripped object. If the tips of the serrations are sharp and pointed, it will hold the object firmly but may perforate and damage it. In the case of SFOPM, the gripped object is paper on which printing is to be done. If the tips are flat, its sharp corners can also damage the gripped object in case of any misalignment. So rounded tips are preferred and hence the serrations on the gripper jaw are approximated to hemispherical projections for the purpose of analysis.
- The major design parameters of the serrations are the radius of the hemispherical projections and the gap between these projections. Determine the maximum stress and deformation for different design parameters using established analytical methods. Some relationship between the contact stress and the corresponding deformation with the design parameters is expected. Develop a framework for optimal design of the serrations based on these relationships.
- Design and fabricate an experimental setup to simulate the cyclic contact stress on a serrated gripper.
- Simulate the cyclic contact stress developed during the functioning of a serrated steel gripper under controlled conditions using the specially fabricated experimental setup.
- Microscopic changes are expected at the contact surface and subsurface of serrated steel grippers. Examine the cross section of the serration subjected to cyclic contact stress and draw conclusions.
- It is expected that NBR is a suitable lining material for gripper jaw surface due to its frictional and oil resistant properties. Explore using experimental methods, the frictional and mechanical properties of NBR samples with suitable reinforcements to verify the suitability.
- Explore using experimental methods, the variation in its mechanical properties due to ageing.

## **1.5 OUTLINE OF THE THESIS**

**Chapter 1** presents the introduction, motivation, objectives and methodology of this research work.

**Chapter 2** reviews literature on grippers, contact stress, cyclic plasticity, diffusion, stress assisted diffusion, reinforcement of rubber with particulate fillers, and NBR.

**Chapter 3** develops and demonstrates a framework to arrive at the optimum design parameters of serrations of a gripper jaw.

**Chapter 4** explores the microscopic alterations near the contact surface of a used serrated steel gripper with the help of a newly designed experimental setup and FSEM with EDS, and models the observed clustering of carbon atoms near the surface of the serrations using an elastic plastic finite element model coupled with simulation of stress assisted diffusion of carbon.

**Chapter 5** examines the feasibility of replacing serrated steel grippers with impactive grippers having a suitable lining material like silica reinforced nitrile butadiene rubber (NBR), for applications like SFOPM.

**Chapter 6** summarizes the main findings of the research and conclusions.

## CHAPTER 2

### OVERVIEW OF LITERATURE

#### 2.1 INTRODUCTION

In this chapter, literature on grippers, contact stress, cyclic plasticity, diffusion and stress assisted diffusion, reinforcement of rubber with particulate fillers, and NBR are reviewed. The contact elements in the commercial FEA software used are also reviewed.

#### 2.2 GRIPPERS

Grippers are subsystems of handling mechanisms which provide temporary contact with the object to be grasped. Prehension is achieved by force producing and form matching elements (Monkman *et al.*, 2007). Grippers can be generally classified depending on the nature of prehension as Impactive (prehension is achieved by impactive forces), Astrictive (prehension is achieved by binding force produced by a field like vacuum or electric field), Ingressive (prehension is achieved by permeation of objects to be gripped) and Contigutive (prehension by methods like chemical and thermal adhesion).

Gripping and holding of objects are key tasks for robotic manipulators. Accurate knowledge of the coefficient of friction is particularly important in the case of impactive grippers for gentle manipulating of objects. Typically, when robots manipulate objects, they must do so with a predetermined grasp force. Some robotic manipulators employ dynamic tactile sensing to detect when it is about to lose hold of a grasped object and take preventive measures like increasing the gripping force, before gross sliding occurs. Controlling the grasp force based on

the measured load has been discussed by Bicchi *et al.* (2000). These are highly nonlinear systems, and complex mathematical models are required for controller. Design of an adaptive neuro fuzzy inference strategy (ANFIS) for controlling input displacement of an adaptive compliant gripper is reported by Petković *et al.* (2012). This design of the gripper has embedded sensors as part of its structure. The use of embedded sensors in a robot gripper gives the control system the ability to control input displacement of the gripper and to recognize particular shapes of the grasping objects.

A different approach to a universal gripper is to replace individual fingers by a single mass of granular material that, when pressed onto a target object, flows around it and conforms to its shape. Upon application of a vacuum the granular material contracts and hardens quickly to pinch and hold the object without requiring sensory feedback (Brown *et al.*, 2010). A simple passive universal gripper, consisting of a mass of granular material encased in an elastic membrane which passively conforms to the shape of a target object, then vacuum hardens to grip it rigidly, later using positive pressure to reverse this transition, releasing the object and returning to a deformable state was developed by Amend *et al.* (2012). Using a combination of positive and negative pressure, the gripper can rapidly grip and release objects with complex geometries.

Grippers with shape memory actuators are also used in some applications, usually in microgripping (Roch *et al.*, 2003). AbuZaiter *et al.* (2016) reports the development of a micromanipulator with gripping mechanism using structure of a shape memory alloy.



### 2.3 CONTACT STRESS

One of the first experiments on impacting bodies was by Marci in 1639. Huygens in 1669, found that for a fully elastic impact, the normal velocities before and after the impact have the same magnitude but opposite direction. Newton derived experimentally the coefficient of restitution and postulated the impact hypothesis for central impacts with kinetic energy loss in 1686. Euler described the contact of two fully elastic impacting bodies with a massless spring, herewith defining the impact as a continuous process in the year 1738. Poisson in 1835, divided the impact into a compression and restitution phase and postulated the impulse hypothesis, which says that the impulses in the two impact phases can be related by a coefficient of restitution.

In the classical analytical work of Hertz (1882) the theory of elasticity was applied in contact mechanics. He investigated the elastic contact of two spheres and derived the pressure distribution in the contact area and the approach of the spheres under compression. However, very few problems involving contact can be solved analytically.

Hertz interpreted the elastic normal impact as a quasi-static process and derived a static solution, neglecting elastic wave propagation within the bodies. He showed that within the contact region, there is an elliptical distribution of the contact pressure and determined the compressive reaction force by integrating the pressure over the area. He then obtained the normal displacement at the surface of the body from the Boussinesq solution for a force applied normal to the surface of an elastic half space (Goldsmith, 1960; Timoshenko and Goodier, 1970). Routh (1889) developed a graphical procedure considering the normal and tangential impulse changes due to friction but the approach was not easily extensible to the three-dimensional case.

Hertz analysis of the contact between two elastic bodies remains even today as one of the most important examples of a solution to a classical problem in the theory of elasticity.

### 2.3.1 Characteristics of contact stress

1. Represent compressive stresses developed from surface pressures between two curved bodies pressed together;
2. Possess an area of contact. The initial point contact (in the case of spheres) or line contact (in the case of cylinders) become area contacts, as a result of the force pressing the bodies against each other;
3. Constitute the principal stresses of a triaxial (three dimensional) state of stress;
4. Cause the development of a critical section below the surface of the body;
5. Failure typically results in flaking or pitting on the bodies' surfaces.

Consider two solid elastic spheres held in contact by a force  $F$ , such that their point of contact expands into a circular area of radius  $a$ , as shown in Fig. 2.1.

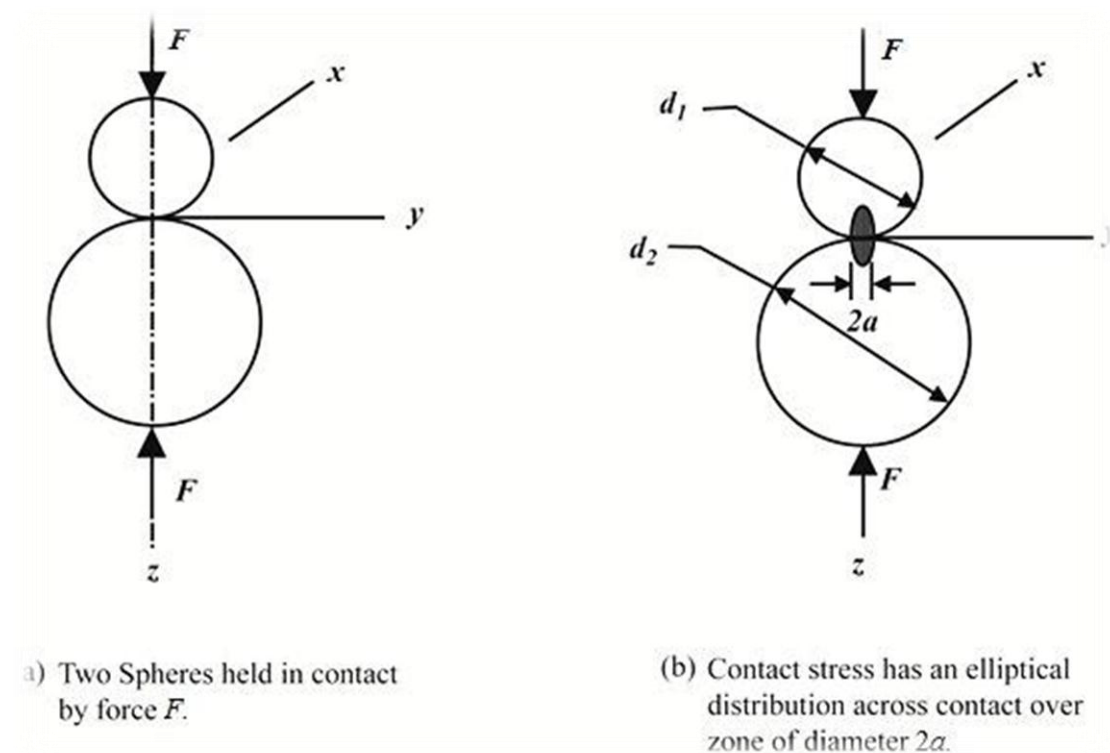


Fig. 2.1 Two spheres in contact. (Shigley, 1986)

Radius of circular area of contact between two spheres,

$$a = \left\{ \frac{3F}{8} \left[ \frac{(1 - \nu_1^2)/E_1 + (1 - \nu_2^2)/E_2}{(1/d_1 + 1/d_2)} \right] \right\}^{\frac{1}{3}} \quad (2.1)$$

where  $F$  is the applied load,  $E_1$  and  $E_2$  are the elastic constants and  $\nu_1$  and  $\nu_2$  are the Poisson's ratios of the materials of the spheres,  $d_1$  and  $d_2$  are the diameters of the spheres.

The maximum contact stress occurs at the centre of the point of contact and is,

$$p_{max} = \frac{3F}{2\pi a^2} \quad (2.2)$$

## 2.4 CONTACT ELEMENTS

A contact mechanics problem occurs when two bodies that are initially separated come into contact. For the modeling and analysis of this problem, either the finite element method or the multibody systems approach can be utilized. There is no doubt that the finite element analysis is the most powerful method to solve contact problems, but it relies on the knowledge and correct definition of a large number of properties including strain-displacement, stress-strain, boundary conditions, meshing, etc. (Flores *et al.*, 2016). Contact problems are highly nonlinear and require significant computer resources to solve. Popular commercial software for modelling of contact includes ANSYS, ABAQUS, NASTRAN, LS DYNA, ADAMS etc. ANSYS is used for the present study. Contact problems fall into two general classes: rigid-to-flexible and flexible-to-flexible. In rigid-to-flexible contact problems, one or more of the contacting surfaces are treated as rigid. (i.e., it has a much higher stiffness relative to the deformable body it contacts). In general, any time a soft material comes in contact with a hard material, the problem may be assumed to be rigid-to-flexible. The other class, flexible-to-flexible, is the more common type. In this case, both (or all) contacting bodies are deformable (i.e., have similar stiffness). An example of a flexible-to-flexible

contact is bolted flanges. The commercial FEA software employed here supports three contact models: node-to-node, node-to-surface, and surface-to-surface. Each type of model uses a different set of contact elements and is appropriate for specific types of problems.

The contact elements available in the commercial FEA software used here can be grouped into four general categories based on increasing levels of sophistication or complexity

- Point-to-point gap elements: CONTACT12, LINK10, COMBIN40, CONTAC52, CONTA178
- Point-to-line (or slide-line) contact elements: CONTAC26
- Point-to-surface contact elements: CONTAC48, CONTAC49
- Surface-to-surface contact elements: TARGE169, TARGE170, CONTA171, CONTA172, CONTA173, CONTA174

This software supports both rigid-to-flexible and flexible-to-flexible surface-to-surface contact elements. These contact elements use a "target surface" and a "contact surface" to form a contact pair. The target surface is modeled with either TARGE169 or TARGE170, for 2-D and 3-D, respectively and the contact surface is modeled with elements CONTA171, CONTA172, CONTA173, and CONTA174.

For surface-to-surface contact elements, either the augmented Lagrangian method (default) or the penalty method can be used. The augmented Lagrangian method is an iterative series of penalty updates to find the exact Lagrange multipliers (i.e., contact tractions). Compared to the penalty method, the augmented Lagrangian method usually leads to better conditioning and is less sensitive to the magnitude of the contact stiffness coefficient. However, in some analyses, the augmented Lagrangian method may require additional iterations, especially if the deformed mesh becomes

too distorted. As per ANSYS User's Group Conference discussions from the Mallett Technology Inc., some experienced analysts feel that "better" contact performance and results may be found when the penalty formulation alone is used.

The guidelines provided by the commercial FEA software for defining the contact faces in a model for the TARGE16x /CONTA17x elements include

- If a convex surface is expected to come into contact with a flat or concave surface, the flat/concave surface should be the target surface.
- If one surface has a fine surface mesh and, in comparison, the other has a coarse mesh, the fine mesh should be the contact surface and the coarse mesh should be the target surface.
- If one surface is stiffer than the other, the softer surface should be the contact surface and the stiffer surface should be the target surface.
- If higher-order elements underlie one of the external surfaces and lower-order elements underlie the other surface, the surface with the underlying higher-order elements should be the contact surface and the other surface should be the target.
- If one surface is markedly larger than the other surface, such as in the instance where one surface surrounds the other surface, the larger surface should be the target surface

## **2.5 CYCLIC PLASTICTY**

Due to the great complication involved in cyclic plastic deformation, most of the existing theories have limited capabilities to properly describe the experimentally observed cyclic plasticity phenomena (Jiang and Zhang, 2008). The stress-strain behaviour of metals under a cyclic loading is very miscellaneous and needs individual approaches for different metallic materials (Halama *et al.*, 2012). There are many different models that have been developed for the case of cyclic plasticity.

The Bauschinger effect is central in cyclic plasticity. Bauschinger effect is the phenomenon by which plastic deformation increases yield strength in the direction of

plastic flow and decreases it in other direction. This effect denotes the characteristics of the cyclic stress-strain relation, with a hysteresis loop with the dissipation of energy at each cycle. Upon loading, the yield strength is increased in the direction of the load, while simultaneously decreasing the yield strength in the opposite direction. After a number of load cycles, a relatively stable cyclic relation is approached, as shown in Fig. 2.2.

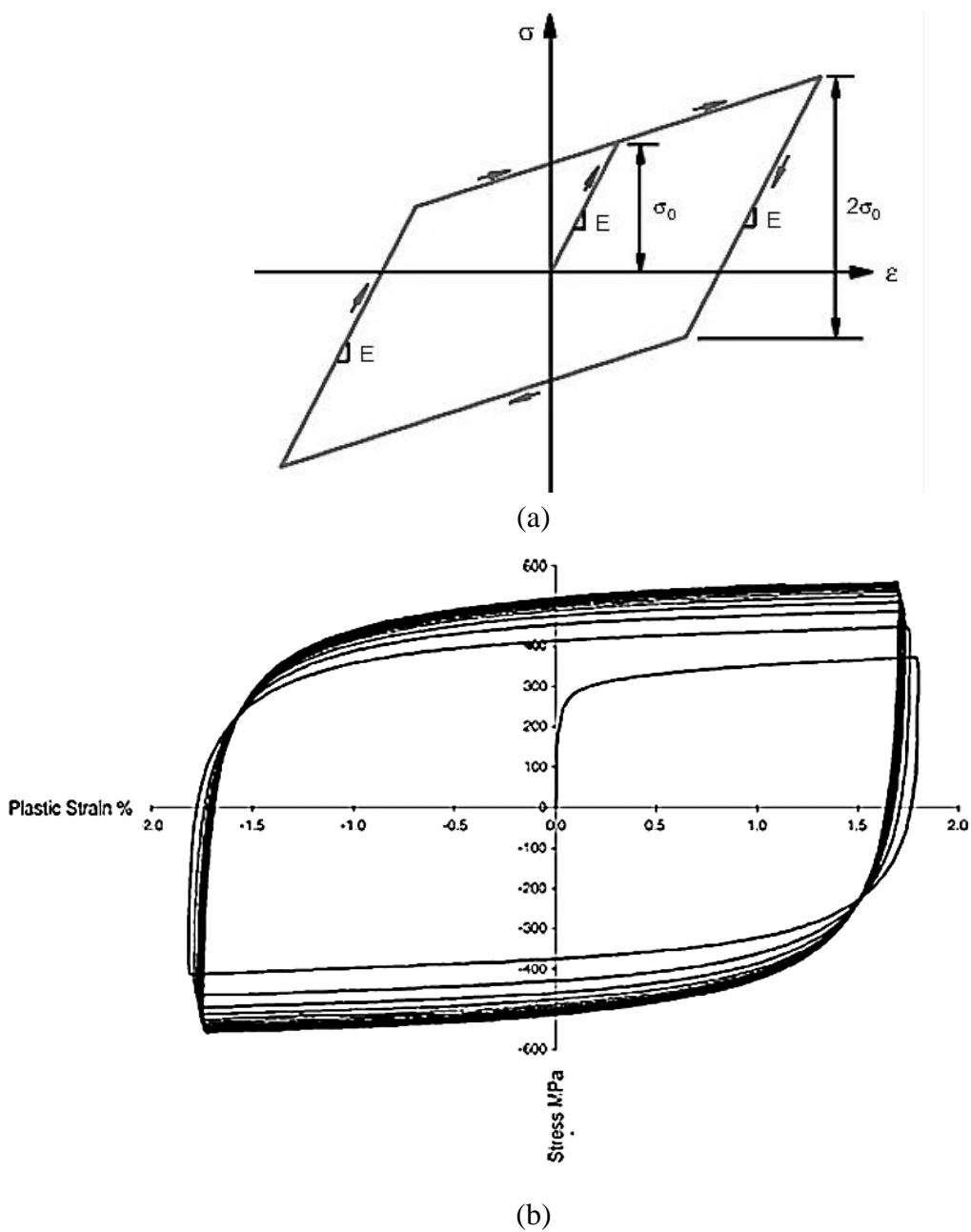


Fig. 2.2 (a) Schematic illustration of the Bauschinger effect (Jiang and Zhang, 2008); (b) The Bauschinger effect in a hysteresis loop for an austenitic material (Eeten, 2006).

Modelling the Bauschinger effect is essential for any model for cyclic plasticity, and it is noteworthy that this effect cannot be captured by isotropic hardening models. Fig. 2.2 (a) shows a schematic illustration of the Bauschinger effect with the immediate appearance of a stable loop. A real case is shown in Fig 2.2(b) which shows the difference between the initial cycle and the subsequent loops, which tend to stabilize after a number of cycles.

The behaviour of the material will depend much on the prior loads. Any overload as well as the introduction of non-symmetric loads will disturb the relation. The cyclic behaviour at a prescribed load is found to be significantly altered by previously higher strain ranges. This is sometimes termed the strain range effect. The hardening is not a unique material property. Neither can the hardening be modelled as a change of yield stress or modelled as isotropic hardening. If the hardening behaviour is isotropic, cyclic saturation of the stress response would mean that no more hardening would occur. However, tests with loading in several steps show that hardening will persist even after saturation on a prior load level (Jiang and Zhang, 2008). This finding is not in agreement with isotropic modelling, where cyclic saturation would prohibit any further hardening/softening.

## **2.6 DIFFUSION AND STRESS ASSISTED DIFFUSION**

Diffusion is a very significant and vast topic with development of scientific theories spanning over a century. Stress assisted diffusion is one of the offshoots of this branch of knowledge and is of particular interest in many engineering applications. In this section, a brief review of the major developments and applications in the field of stress assisted diffusion against a background of the development of diffusion theories is presented.

### **2.6.1 Diffusion**

Diffusion refers to the transport of matter by the motion of atoms or molecules down the gradient. Often, but not always, the gradient is that of concentration. Apart from concentration gradient, the other forces causing the drift of particles of matter include electric field, chemical gradient, temperature gradient, gravitational force, centrifugal force and stress gradient. The speed of diffusion is highest in gaseous state and lowest in the solid state of matter.

The significance of diffusion cannot be overemphasized. Diffusion occurs throughout the human body including metabolism and respiration and is essential for plant and human life. Some of the applications in engineering are doping of silicon for semiconductors, hydrogen embrittlement, various surface treatments like carburizing or nitriding, movement of neutrons in nuclear reactors etc.

Scientists have attempted to develop theories of diffusion using two approaches. One is the phenomenological approach and the other is the physical and atomistic approach. The earlier theories on diffusion like Fick's laws were all phenomenological in nature. After the discovery of Brownian motion of particles, diffusion theories like random walk based on the atomistic view also became popular.

As indicated above, the gradient causing the diffusion need not always be that of concentration. The diffusion caused by the stress gradient is referred as stress assisted diffusion. The theories on stress assisted diffusion are developed based on the general theories of diffusion. Hence a brief overview of the development of the general theories of diffusion, both phenomenological and atomistic is also given in this section.



The earlier studies of diffusion were on gases and liquids and the first systematic experimental studies were probably conducted by Graham (1829, 1833). Later, Graham (1868, 1869) also studied the diffusion of salts in liquids and to the uptake of hydrogen in metals. The next major advancement in diffusion was Fick's contributions. He developed a mathematical framework for Graham's observations and introduced the concept of Coefficient of Diffusion (Fick, 1855, 1995). Fick's first law in isotropic media can be expressed as

$$J_x = -D \cdot \frac{\partial c}{\partial x} \quad (2.3)$$

in one dimension.

In three dimensions it can be expressed as

$$J = -D \nabla c \quad (2.4)$$

Fick's second law can be written as

$$\frac{\partial c}{\partial t} = D \cdot \frac{\partial^2 c}{\partial x^2} \quad (2.5)$$

The contributions of Stephan (1879), Austen (1896) and Arrhenius (1889) are given in Appendix.

Arrhenius equation gives the dependence of the rate constant  $K$  of a chemical reaction on the absolute temperature  $T$ , and is given by

$$K = A e^{(-Q/RT)} \quad (2.6)$$

When applied to diffusion coefficient, it translates to

$$D = D_0 e^{(-Q/RT)} \quad (2.7)$$

The proposal that the diffusion in solids also obey Arrhenius law was apparently made by Dushman and Langmuir (1922).

The discovery of Brownian motion (Brown *et al.*, 1828) led to the atomistic approach by Albert Einstein (1905, 1906) and Smoluchowski (1906, 1916) which were later experimentally established by Perrin (1908, 1909).

The Einstein-Smoluchowski relation connects the diffusion coefficient and the mobility as follows.

$$D = \frac{kT}{\xi} \quad (2.8)$$

Frenkel disorder (Frenkel, 1926) was generalized by Wagner and Schottky (1930). Kirkendall's experiments (Kirkendall *et al.*, 1939; Kirkendall, 1942; Kirkendall and Smigelskas, 1947) had shown that the rate of diffusion of zinc is much greater than that of copper in alpha brass and that the interface shifts to compensate at least partially for the diffusion rate. In other words if the diffusion rates of two metals A and B into each other are different, the boundary between them shifts and moves towards the faster diffusing metal. Darken developed phenomenological equations based on the results of Kirkendall's experiments (Darken, 1948). In crystals, the jump probabilities of atoms often depend on the directions of preceding jumps as against pure random-walk diffusion where successive jumps are not correlated. Bardeen and Manning, brought out the significance of correlation in defect induced solid diffusion (Bardeen, 1949; Manning and Bruner, 1968). Grain boundary diffusion theories by Fisher and studies by Hoffman and Turnbull were published in Journal of Applied Physics (Fisher, 1951; Hoffman and Turnbull, 1951).

The developments of general theories on diffusion and some recent developments are tabulated in Appendix.

### 2.6.2 Stress assisted diffusion

The initial developments of stress assisted diffusion can be traced back to the theory of yielding and strain ageing of iron, based on the segregation of carbon atoms to form atmospheres around dislocations (Cottrell *et al.*, 1949). Strain ageing was interpreted as the migration of carbon atoms to free dislocations. The force needed to release a dislocation from its atmosphere was also roughly estimated.

The existence of a chemical potential to a mobile component anywhere within the solid under stress is demonstrated and a general equation for chemical potential is developed by Li *et al.* (1966). The chemical potential in the stressed state,

$$\mu_s = \mu_0 + w - W \quad (2.9)$$

Leeuwen (1974) described Stress assisted diffusion of hydrogen towards the tip of a notch or crack by adding a stress-dependent term to Fick's first and second law of diffusion. It was postulated that a critical combination of hydrogen concentration and stress will develop at the edge of the plastic enclave, and that this will produce an incremental crack growing from the edge of the plastic zone towards the notch or crack tip. Crack propagation is treated as a succession of incremental crack bursts.

Cottrell proposed a model for stress assisted diffusion,

$$\frac{\partial c}{\partial t} = D \nabla^2 c - M \nabla \sigma_t \cdot \nabla c \quad (2.10)$$

where  $c$  is the concentration of the solute, and the phenomenological coefficients  $D$  and  $M$  are regarded as constants (Cottrell, 1948).

Oriani (1969), Girffalco and Welch (1967) had also proposed similar models. Aifantis and Gerberich (1977) also found that the diffusivity varies linearly with the trace of stress and proposed the following model for stress assisted diffusion.

$$\frac{\partial c}{\partial t} = (D + N\sigma_t)\nabla^2 c + M \nabla\sigma_t \cdot \nabla c \quad (2.11)$$

Flynn (1973) proposed another mathematical model for stress assisted diffusion,

$$\frac{\partial c}{\partial t} = (D + N\sigma_t)\nabla^2 c + N \nabla\sigma_t \cdot \nabla c + P \text{tr}(\sigma \nabla^2 c) \quad (2.12)$$

where  $\sigma$  is the mechanical stress and the phenomenological coefficients  $D$ ,  $N$  and  $P$  are constants. It was also experimentally observed trend that the diffusivity varies linearly with the hydrostatic stress (Aifantis 1979; Varotsos *et al.*, 1980). Aifantis (1980) proposed a more generalized model for stress assisted diffusion as follows.

$$\frac{\partial c}{\partial t} = (D + N\sigma_t)\nabla^2 c - (M - N)\nabla\sigma_t \cdot \nabla c + K \text{tr}(\sigma \nabla^2 c) \quad (2.13)$$

It can be seen that equation (2.11) and equation (2.12) are special cases of equation (2.13), when certain phenomenological coefficients assume zero values.

Usually the stress,  $\sigma$  is taken as the mechanical stress in the body in the absence of diffusion as it is assumed that the state of stress is unaffected by diffusion. But the change in  $\sigma$  with diffusion may not be negligible for some materials. Wilson and Aifantis had suggested a coupled stress-assisted diffusion theory which can be represented by a system of partial differential equations as follows (Wilson and Aifantis, 1979; Aifantis, 1980).

$$\operatorname{div} \boldsymbol{\sigma}^0 = 0, \quad \boldsymbol{\sigma}^0 = \lambda e^0 I + 2 G \mathbf{E}^0, \quad \operatorname{curl}^2 \mathbf{E}^0 = 0 \quad (2.14)$$

$$\frac{\partial c}{\partial t} = (D + N\sigma_t^0)\nabla^2 c - (M - N)\nabla \sigma_t^0 \cdot \nabla c \quad (2.15)$$

$$\operatorname{div} \boldsymbol{\sigma}^+ = 0, \quad \boldsymbol{\sigma}^+ = \lambda e^+ I + 2 \theta \mathbf{E}^+ - \lambda c I, \quad \operatorname{curl}^2 \mathbf{E}^+ = 0 \quad (2.16)$$

where,  $\mathbf{E}$  (Greek capital letter, Epsilon) is the strain,  $e$  is the trace of strain and  $\lambda$  and  $\theta$  are Lamé constants of the material and the superscripts  $0$  and  $+$  indicate the corresponding values without and during diffusion respectively.

On solving, the diffusive flux,

$$\mathbf{J} = -(L + N\sigma_t^0)\nabla c + M c \nabla \sigma_t^0 \quad (2.17)$$

Subsequent to the development of above theories, much research were conducted in many areas related to diffusion like the simulation of diffusion on various applications (El-Mellouhi *et al.*, 2008; Tjaden *et al.*, 2016; Dubbeldam *et al.*, 2016), diffusion in polymers and composites (Robeson *et al.*, 2015; Klepach and Zohdi, 2014), thermo elastic diffusion (Sherief and Hussein, 2016; Abbas *et al.*, 2015), grain boundary diffusion (Tang *et al.*, 2015; Heuer and Azar, 2015), stress diffusion in special applications like lithium ion batteries (Song *et al.*, 2013) failure mechanism of a multilayered thin film (Raghavan *et al.*, 2013), Hydrogen embrittlement (Robertson *et al.*, 2015; Seita *et al.*, 2015) etc. to name a few.

## 2.7 REINFORCEMENT OF RUBBERS WITH PARTICULATE FILLERS

Rubbers in general are seldom used in their pristine form due to lack of hardness, strength properties and wear resistance required for practical applications. The performance related properties of rubbers are enhanced by the process of curing. The properties could be enhanced by the use of fillers, such as carbon black and silica

which has been found to offer improvement in the mechanical properties of rubber. There are many reports on the reinforcement of natural rubber, Nitrile rubber, Styrene Butadiene rubber etc. by furnace blacks. The results of the studies by Ramesan (2005) indicate that carbon black is good reinforcing filler for dichlorocarbene modified styrene butadiene rubber. Carbon black is a colloidal form of elemental carbon produced by partial combustion of oil or natural gases. The particle size of carbon black particles usually varies from 10-500 nm. The D 24 ASTM standard defines the nomenclature of different carbon blacks.

Generally precipitated silica is used as reinforcing filler in non-black rubber products to improve the mechanical properties, particularly tensile strength, tear resistance, abrasion resistance and hardness (Thongsang *et al.*, 2012). Silica is a crystalline compound occurring abundantly as quartz, sand and many other minerals. Though natural silica is more economical, precipitated silica is usually used as a filler material for rubber. They have particle sizes as small as the carbon black besides an extremely reactive surface (Nunes *et al.*, 2000). The types of synthetic silica are precipitated, pyrogenic, aerogels and hydrogels. Precipitated silica and pyrogenic (fumed) silica are being used for elastomer reinforcement. Silica has weaker filler polymer interactions and stronger filler-filler interactions in comparison to carbon black. Though it does not provide the same level of reinforcement as that of carbon of the same particle size, this can be compensated by using coupling agents. The combination of silica with a coupling agent has higher reinforcing effect and different dynamic mechanical properties compared to carbon black (Okel *et al.*, 1999). The reinforcing effect of silica is stronger compared to carbon black and the filler content can be reduced without any negative influence on the property profile. This will also result in better elasticity as the ratio of elastic component (rubber) to damping filler is higher. The

covalent silica-polymer network is more stable compared to the carbon black-polymer network. This results in a lower rate of breaking and reformation of the silica-polymer bonds during a deformation cycle, and a lower value for the loss modulus.

The particle size, surface area, specific surface activity/chemical composition and structure/ porosity are the primary filler characteristics influencing elastomer reinforcement. The reinforcement effect is mainly influenced by the size of the filler particles and then the surface area. Experience has shown that substantial improvement in the physical properties of vulcanizates generally cannot be expected from siliceous fillers greater than 50 millimicrons in average particle size, or less than 50 square meters per gram in specific surface area (Bachmann *et al.*, 1959). The principal requirement for rubber reinforcement is sufficiently small domain size, less than about 1  $\mu\text{m}$ . Sufficiently small filler can give good reinforcement, even when matrix/ domain bonding is poor (Rodriguez and Hamed, 1993; Ames *et al.*, 1996). The interaction between filler and rubber are attributed to physical interactions like Van der Waals forces, or chemical reactions as in the case of a silica-coupling agent system (Brinke, 2002).

## **2.8 ACRYLONITRILE-BUTADIENE RUBBER**

Acrylonitrile-butadiene rubber (NBR) often referred as nitrile rubber is an oil resistant synthetic rubber produced from a copolymer of acrylonitrile and butadiene. Nitrile rubbers are manufactured by emulsion co-polymerisation of butadiene with acrylonitrile. It is commonly considered as the workhorse of industrial and automotive rubber products industries and is widely used in applications where oil resistance is required. Nitrile rubber in the unfilled form has very low tensile strength. A variety of fillers are used in the rubber industry to modify the physical properties of elastomeric

materials (Ramesan, 2005; Donnet and Custodero, 2011) and NBR is no exception (Donnet and Custodero, 2011; Rodgers and Waddell, 2011). Carbon and silica are the most commonly used fillers used to modify the properties of nitrile rubber (Fultz and Evans, 1998; Schwaiger and Blume, 2000). Silica has been staged as notable filler for rubber to obtain high performance passenger tires (Bachmann *et al.*, 1959; Wolff, 1996; Donnet, 1998). Unlike hydrocarbon rubbers such as NR, SBR and the like, nitrile rubber exhibits comparatively better reinforcement with silica because of its improved dispersion (Donnet and Custodero, 2011; Rodgers and Waddell, 2011).

## **2.9 CONCLUSION**

In this chapter, an overview of literature on grippers, contact stress, cyclic plasticity, diffusion, stress assisted diffusion, reinforcement of rubbers with particulate fillers, and NBR have been undertaken. The contact elements available in the commercial FEA software used are also discussed. A framework for optimised design of serrations on a gripper is presented in the next chapter.



## CHAPTER 3

### A FRAMEWORK FOR OPTIMISED DESIGN OF SERRATIONS ON A GRIPPER

#### 3.1 INTRODUCTION

Grippers are commonly used in printing, robotic and other applications. Grippers are also used in many applications including modular manufacturing, but gripper design is an important and often overlooked aspect, of a complete assembly system (Causey and Quinn, 1998). As indicated by Zhang *et al.* (2001), the design of gripper jaws is often ad-hoc and suboptimal, even though grippers are widely used for automated manufacturing, assembly and packing. In any application, the gripper has to grasp the part securely and a long life for the gripper is always desirable.

In this chapter, a few applications of serrated grippers are discussed and a short description of SFOPM is provided and the significance of grippers in an SFOPM is explained. A framework for optimised design of serrations on a gripper jaw is developed. Though the framework is illustrated based on SFOPM, the same methodology is suitable for any similar application.

A gripper is a device which enables the holding of an object for manipulation. It can be attached to a robot or it can be part of a fixed automation system. Often grippers are provided with serrations to increase the grasping efficiency. Serrations provide an additional grasp for those applications in which gripping force and finger friction are not sufficient to effectively hold the part. Steel grippers with serrations are widely used in many industrial and positioning applications like printing machines, robots, work holding devices etc. The grippers are usually manufactured in various materials including steel alloys, polymers, rubber etc. The usual steel alloys for serrated

grippers are M-2 high speed tool steel, C-12 tungsten carbide, AISI 8620 steel, AISI 4320 steel etc., hardened to about Rc 60. The images of some serrated gripper inserts are given in Fig. 3.1.



Fig. 3.1 Gripper inserts with serrations (Fairlane Products, USA; Carr Lane manufacturing, USA)

Grippers form the link between all kinds of work pieces and the manipulating machine concerned. Grippers further enhance the performance capability of automated handling devices. These devices include not only industrial robots but also insertion devices, manipulators and special feed devices for automatic machines, testing machines and batch-assembly systems. A few applications where grippers with serrated jaws are employed are described below.

### 3.2 WORKHOLDING GRIPPERS

Work holding grippers can be manual like a bench vice or it can be a holding and positioning jaw attached to a robot. Serrations on the work-holding grippers help to hold the part securely. Replaceable work-holding grippers are used to extend the life of expensive jaws, fixtures and jigs. Images of replaceable gripper inserts are shown in Fig. 3.1. They are also ideal for holding and positioning irregularly shaped work-pieces. Image of swivel ball units that can be used as a contact bolts or as a rest pad are shown in Fig. 3.1. As contact bolts, these swivel-ball units are ideal for evenly distributing clamping pressure on sloped or uneven surfaces.

### 3.3 SPRUE PICKER GRIPPERS FOR DE-MOLDING

Sprue picker grippers are used for the safe and precise removal of injection molding parts. The fingers are serrated for effective holding of the grasped parts. An image of the same is shown in Fig. 3.2.



Fig. 3.2 Sprue picker grippers for de-molding (Fipa GmbH, Germany)

### 3.4 SHEET FED OFFSET PRINTING MACHINE (SFOPM)

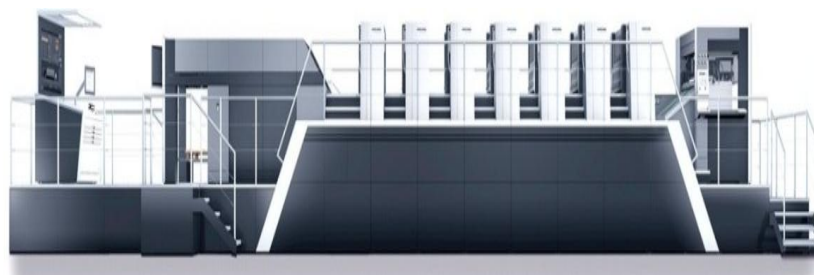
Sheet fed offset printing machines are presses for multi-color printing to achieve extremely high-quality results. Sheet fed refers to the feeding of individual pages of paper into the press in contrast to the web offset presses, where continuous roll of paper is fed into the machine. So the printing is carried out on single sheets of paper as they are fed to the press one at a time. They work according to the offset printing principle, which is a planographic printing system, based on the physical repulsion of water and printing ink. Sheet fed offset printing machines are used to produce magazines, calendars, high-quality advertising, packaging material and various other products in medium sized editions.

A four color SFOPM with perfecting is shown in Fig. 3.3. It has eight printing units

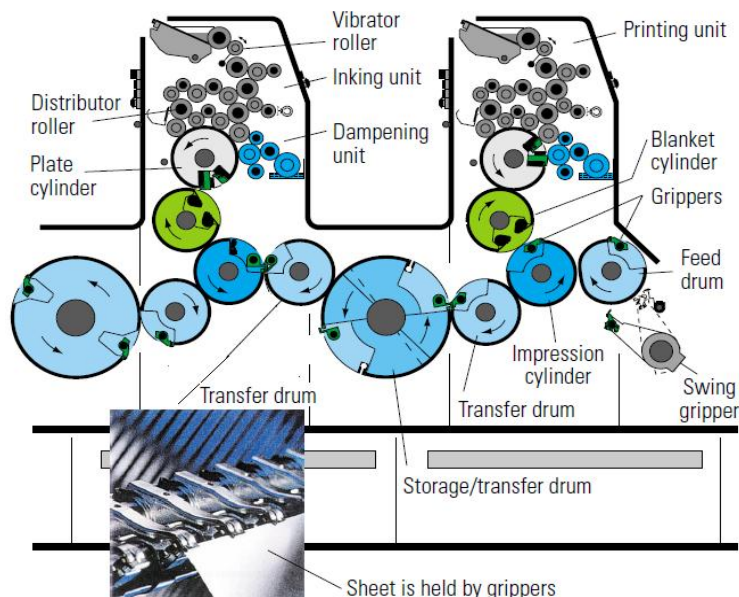


Fig. 3.3 Four Color Sheet fed Offset Printing Machine with perfecting (Heidelberg, Germany)

and can print four colors on one side of the sheet and four colors on the back of the sheet. Color offset printing is achieved by printing of individual color separations one by one, precisely one over the other. For achieving a good quality color print, a minimum of four color separations, viz. Cyan, Magenta, Yellow and Black are required. Separate masters, usually called printing plates or simply plates are made from the original image for each color separation using appropriate filters during plate making. The plate making is done with photochemical, photomechanical or laser engraving processes, such that the image areas corresponding to the particular color are rendered oleophilic or receptive to oils, such as ink and hydrophobic or repellent to water, while the non-image areas are rendered oleophobic or repellent to oils and hydrophilic or receptive to water.



(a)



(b)

Fig. 3.4 (a) Four Color Sheet fed Offset Printing Machine with perfecting (Heidelberg, Germany) and (b) Schematic of two adjacent printing units (Helmut Kipphan *et al.*, 2001).

The side view of an SFOPM and the schematic diagram of two adjacent printing units are reproduced in Fig. 3.4.

Each printing unit will be inked up with the respective color and the corresponding plate is loaded on the plate cylinder of each unit. During the printing process, the dampening rollers, inking rollers and all the three cylinders touch the adjacent element(s) with the required pressure and rotate at the same surface speed. Consequently, since oil and water do not mix with each other readily, the image areas are transferred to the substrate, usually paper, wound over the impression cylinder, through a blanket cylinder while the non-image areas do not.

A typical printing gripper has a serrated and a flat jaw. The gripper arrangement in a typical sheet fed offset printing machine, its sectional view and a photograph of the gripping surface of a serrated jaw are shown in Fig 3.5.

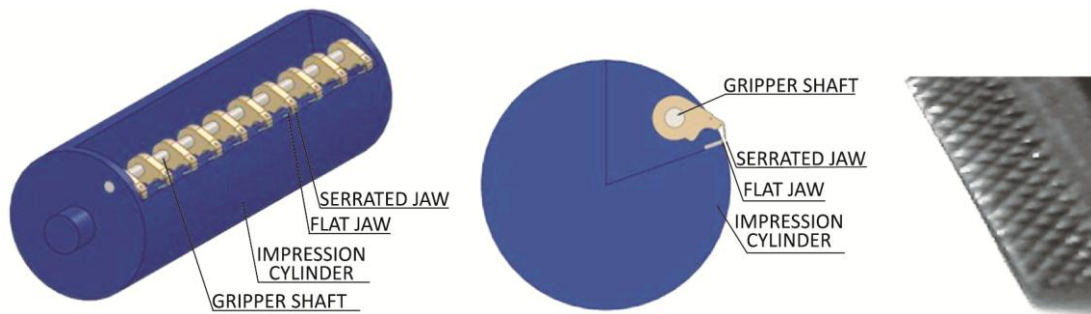


Fig. 3.5 Gripper arrangement in a typical sheet fed offset printing machine and Serrations on a printing gripper

The grippers are mounted on a shaft, called gripper shaft. The gripper shaft is mounted on a cylinder, called impression cylinder. The impression cylinder has only one degree of freedom, and can only rotate. The gripper shaft also has only freedom for rotation. The grippers are fixed on the gripper shaft and can be closed or opened by rotating the gripper shaft in clockwise or anticlockwise directions. During the

printing process, one edge of the paper (called leading edge), is held by the grippers and the paper is acted upon by forces including tensile force. So the paper has to be held between the two jaws of the gripper during the printing process. After printing, the gripper releases the paper and the next paper to be printed is grasped by the grippers. The gripping and releasing of paper is achieved by the closing and opening of the grippers at appropriate times. The feeding of paper and removal of paper to and from the grippers and timings for opening and closing of grippers are ensured in a printing machine through other mechanisms.

#### **3.4.1 Print quality, registration and importance of grippers**

Thus in a multicolor sheet fed offset press, the paper is held between the jaws, during transfer of the paper from one printing unit to another, as well as during the actual printing process. The sharpness and cleanness of a four-color print is greatly affected by the accuracy of the color register. In general, register refers to the accurate positioning of the sheets on the gripper for all repeated grips and the retention of this position during the processes the sheet undergoes, while it is being gripped. In the case of color offset printing, register refers to the accurate positioning of the printed image of each color separation on the substrate in relation to the sheet edges. Sheet fed presses use mechanical registration to relate each sheet to one another to ensure that they are reproduced with the same imagery in the same position on every sheet running through the press. The sheet transport from printing unit to printing unit has also to be extremely accurate and in register and the print images of the individual color separations must be accurately aligned. An accuracy of 10 microns to one another is required for high quality print jobs (Kipphan *et al.*, 2001). Hence the gripping should be such that the paper undergoes minimum unintended positional variation during the printing and the paper transfer.

Instead of serrated and flat steel jaws, some printing machines employ a serrated steel jaw along with a flat jaw with polymer inserts. In such an arrangement, the polymer inserts wear off very fast and needs frequent replacement.

### 3.5 FRAMEWORK FOR OPTIMIZED DESIGN OF SERRATIONS ON A GRIPPER

In many applications like that in an offset printing machine, one of the jaws of a two jaw sheet gripper is serrated. The serrations provide a kind of locking effect on the objects (like paper) being gripped in addition to the frictional gripping force and prevents slippage. Usually in sheet fed presses, one of the jaws will have a serrated surface and the other jaw a flat surface.

The gripper jaws are subjected to high contact stresses and the serrated surface particularly is more susceptible to deformation and wear. Hence the design of the serrations is of significance. In this chapter, we have developed a general framework for optimal design of serrations on a gripper considering printing gripper as an example. The contact stress on the serrations on the jaw during gripping is analyzed and the corresponding deformations are also determined. These results are used to develop the framework for optimum design of the serrations.

The sectional view of the serrations, with the actual and assumed shapes along with the coordinate system is shown in Fig. 3.6.

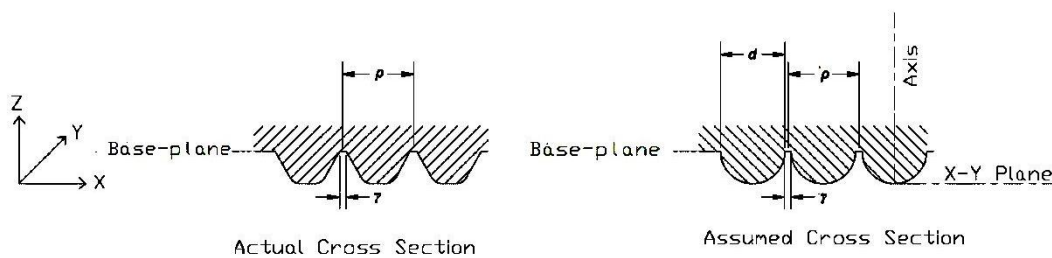


Fig. 3.6 Serrations on the gripping surface

The first sketch shows the actual cross section of the serrations. In the second sketch, the projections are approximated to hemispheres of diameter, ' $d$ ' for the purpose of analysis. The centre to center distance between each groove (or projection) on the serrated surface is referred to as pitch, ' $\rho$ '. The groove width or the gap between projections is referred to as ' $\gamma$ '. The plane containing the tip of all the projections is taken as the X-Y plane and the direction from this plane towards the center of the hemisphere is taken as the positive direction of Z-axis. (The X-Y plane coincides with the surface of the flat jaw when the gripper is closed). The line perpendicular to the X-Y plane passing through the center of a projection along the Z axis is referred to as the 'axis'. The distance of any point on the axis from the tip of projection is referred to as distance, ' $\beta$ '. The plane parallel to X-Y plane passing through the base of the grooves as shown in Fig. 3.6 is called 'base-plane'.

### **3.5.1 Grasping Forces**

A crucial problem in grasping is the choice of grasp forces so as to avoid, or minimize the risk of slippage (Bicchi *et al.*, 2000). The required grasp force can be arrived at from the force acting on the grasped object and the coefficient of friction between the object and jaws. In offset printing, the substrate, usually paper, is the grasped object and it passes between the blanket and impression cylinders of the press during printing. Several studies are available on the pressure distribution between the blanket and impression cylinders of an offset printing press. The printing pressure varies circumferentially and axially (Eschenbach and Wagenbauer, 1961; Vadivu *et al.*, 2006; Shuqin *et al.*, 2009). The tensile force acting on the paper during offset printing varies from start to finish during printing of each sheet depending on the angular position of impression cylinder at the moment. The gripping force of the grippers and the friction between paper and gripping surfaces ensure the positional



accuracy of the printed image on the paper. The coefficient of friction depends on the type of paper, humidity of atmosphere etc. (Inoue *et al.*, 1990; Back, 1991). The tensile force acting on the paper during offset printing is experimentally found to vary from 0 to about 70N (Kipphan *et al.*, 2001). The maximum gripping force acting on the paper varies between different designs and models of offset presses depending on the size of the machine and the number of grippers. These values were observed in different models of sheet fed offset presses and found to vary from 30N to 70N. Hence the study is made for forces in the range of 30N to 70N.

### **3.5.2 Stresses on Gripping Surface**

All points of the serrated surface experience stress. But the stresses will be more on the points within the projections (assumed as hemispheres). The maximum stress will be on points of the axes of projection shown in Fig. 3.6. In other words, in any plane perpendicular to the Z axis and passing through the hemisphere, the maximum stress will be at the center of the circle of intersection.

### **3.5.3 Summary of the Methodology**

The methodology adopted can be summarized as follows. The contact force per projection is estimated for different combinations of pitch ( $\rho$ ), groove widths ( $\gamma$ ) and gripping forces. Equal sharing of load by all projections of the gripper is assumed. The range of values of pitch  $\rho$  is varied judiciously from 0.2mm to 6mm, the range of gripping forces from 30N to 70N and the range of the groove width,  $\gamma$  from 0.1mm to 1 mm. For different combinations of these parameters, the normal stresses, shear stresses and von Mises stresses on the points of the axis of the projection are calculated. Plots are made for stresses at various distances,  $\beta$  along the axis of projection (in the Z-direction) starting from the contact point of the projection. A sample plot of the stress

distribution for pitch,  $\rho$  of 1mm, groove width,  $\gamma$  of 0.1mm (resulting in hemisphere diameter,  $d$  of 0.9 mm) and for gripping force of 50N is shown in Fig. 3.7.

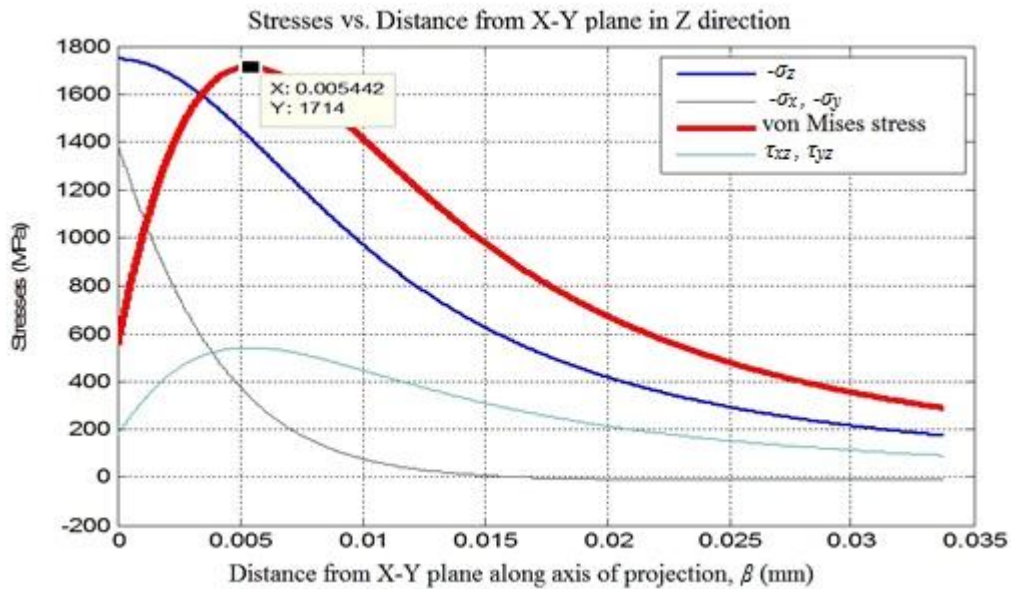


Fig. 3.7 Stresses along the axis of a hemisphere of 0.9 mm diameter at 50N load

The graph is plotted with distance of the point from contact surface,  $\beta$  along the abscissa and the corresponding stresses along the ordinate.

The maximum von Mises stress (1714 MPa) and the distance of the corresponding point from the tip of projection,  $\beta$  (0.005442 mm) is obtained from the graph (Fig. 3.7). It may be noted that this extreme value of stress is acting only at a point and the high stresses are experienced only over an extremely small area. Similar stress distribution plots are made for various combinations of pitches, groove widths and gripping forces. The maximum von Mises stresses taken from each of these stress distribution curves are tabulated and plotted. The displacements of the point of contact corresponding to above combinations are also calculated and graphs are plotted. These plots are used to develop meaningful relations to help optimization of serration.

### 3.5.4 Assumptions and Calculations

The gripping surface of the serrated jaw is considered as a two dimensional array of hemispherical projections on a plane, referred as 'base-plane', as shown in Fig. 3.6. The gripping surface of the flat jaw (jaw without serration) is considered as an elastic half space. Each projection on the serrated jaw is considered as an elastic hertzian (hemi) sphere contacting an elastic half space. It is assumed that all the contacts share the load equally. During the operation of a printing machine, the gripper jaws open and close with and without paper between them. The thickness of paper used is usually between 0.05 to 0.6 mm. Very thin paper will have negligible effect on the contact stress on jaw surfaces. As the thickness of paper increases, the tendency will be towards a reduction in the contact stresses on the projections. Hence, to arrive at a conservative estimate of contact stresses, the effect of paper between the jaws is neglected.

A serrated movable jaw (sometimes referred simply as gripper) and a flat fixed jaw (sometimes referred as gripper pad) are considered for the analysis. The analysis is valid for a serrated gripper pad and flat gripper as well. The width and breadth of a gripper pad in a typical sheet fed offset printing machine are 16 to 20 mm and 5 to 6 mm respectively. For the purpose of analysis, the dimensions of the contacting surface of gripper pad are taken as 18 mm and 6 mm. It is assumed that the thickness of gripper pad is fairly large compared to the size of the hemispheres of the serration. Due to high stresses involved, properly heat treated bearing steels like AISI 52100, M50 or M50NiL are some of the suitable materials for the jaws. Chrome alloy steel AISI 52100 with HRC 60-66, yield strength of 2030 MPa, Young's Modulus,  $E$  of  $2.03 \times 10^5$  MPa and Poisson's ratio,  $\nu$  of 0.3 is considered for both the jaws in the present analysis.

For finding the stresses and displacements, a Hertzian contact model is assumed. The solutions for Hertz contact remain valid until the applied load is sufficiently large, so as to initiate plastic deformation (Hill, 1998).

For the Hertzian contact stress theory, the fundamental assumptions are: (a) At the point of contact, the shape of each of the contacting surfaces can be described by a homogeneous quadratic polynomial in two variables; (b) Both surfaces are ideally smooth; (c) Contact stresses and deformations satisfy the differential equations for stress and strain of homogeneous, isotropic, and elastic bodies in equilibrium; (d) The stress disappears at a great distance from the contact zone; (e) Tangential stress components are zero at both surfaces, within and outside the contact zone; (f) Normal stress components are zero at both surfaces outside the contact zone; (g) The stress integrated over the contact zone equals the force pushing the two bodies together; (h) The distance between the two bodies is zero within, but finite outside the contact zone; (i) In the absence of an external force, the contact zone degenerates to a point (Hertz, 1882)

The formulae used are as follows (Timoshenko *et al.*, 1970; Shigley, 1986; Jackson and Green, 2005).

Radius of circular area of contact between two spheres,

$$a = \left\{ \frac{3F}{8} \left[ \frac{(1 - \nu_1^2)/E_1 + (1 - \nu_2^2)/E_2}{(1/d_1 + 1/d_2)} \right] \right\}^{\frac{1}{3}} \quad (3.1)$$

where  $F$  is the applied load,  $E_1$  and  $E_2$  are the elastic constants and  $\nu_1$  and  $\nu_2$  are the Poisson's ratios of the materials of the spheres,  $d_1$  and  $d_2$  are the diameters of the spheres. (In the present analysis, one surface is a plane and hence  $d_2$  is infinity). The maximum pressure occurs at the center of the contact area and is,

$$p_{max} = \frac{3F}{2\pi a^2} \quad (3.2)$$

The maximum stresses occur on the Z-axis. The principal stresses are given by

$$\sigma_x = -p_{max} \left\{ \left[ 1 - (z/a) \tan^{-1} \left( \frac{1}{z/a} \right) \right] (1 + \nu) - \left[ \frac{1}{2(1 + z^2/a^2)} \right] \right\} \quad (3.3)$$

$$\sigma_y = -p_{max} \left\{ \left[ 1 - (z/a) \tan^{-1} \left( \frac{1}{z/a} \right) \right] (1 + \nu) - \left[ \frac{1}{2(1 + z^2/a^2)} \right] \right\} \quad (3.4)$$

$$\sigma_z = -\frac{p_{max}}{1/(1 + z^2/a^2)} \quad (3.5)$$

And the corresponding shear stresses are

$$\tau_{xy} = 0 \quad (3.6)$$

$$\tau_{xz} = \tau_{yz} = \frac{\sigma_x - \sigma_z}{2} = \frac{\sigma_y - \sigma_z}{2} \quad (3.7)$$

Hence,

*von Mises stress*

$$= \left[ \frac{(\sigma_x - \sigma_y)^2 + (\sigma_y - \sigma_z)^2 + (\sigma_z - \sigma_x)^2 + 6(\tau_{xy}^2 + \tau_{yz}^2 + \tau_{zx}^2)}{2} \right]^{1/2} \quad (3.8)$$

Assuming same elastic constants for the spherical and plane surfaces, the displacement,

$$\alpha = 1.23 \left[ \frac{F^2}{E^2 r} \right]^{1/3} \quad (3.9)$$

where  $r$  is the radius of the sphere.

Also from geometry of Fig 3.6,

$$\rho = d + \gamma \quad (3.10)$$

### 3.5.5 Description of the Procedure

Consider for example a gripper serration of pitch 1mm, groove width 0.1mm and hemisphere diameter 0.9 mm for a gripping force of 50N. By geometry, the number of contact points (or projections) is 108. Assuming equal sharing of load by all projections, the load per contact point is 0.46296N. The radius of the area of contact,  $a$  and the maximum pressure at contact area,  $p_{max}$  are calculated. The normal, shear and von Mises stresses are calculated at various points along the Z axis passing through the centre (axis of projection) from the tip of projection towards the positive Z-direction at intervals numerically equal to one by thousandth of the contact area. The interval is chosen arbitrarily to obtain a good curve irrespective of load or hemisphere diameter of the serration. These stresses are then converted to appropriate units and plotted in Fig. 3.7. From the graph, the maximum von Mises stress is 1714 MPa occurring at a depth of 0.005442 mm from contact surface.

This procedure is repeated for various combinations of forces of 30N, 50N and 70N and hemisphere diameters of 0.1, 0.2, 0.3, 0.4, 0.65, 0.9, 1.1, 1.4, 1.9, 2.9 and 5.9 mm; keeping the groove width constant at 0.1mm. (These values are selected for the diameters to avoid distortion of results due to fractional hemispheres. The maximum diameter of 5.9 mm corresponds to three contact points on the 18mm  $\times$  6mm pad. The next biggest diameter of 2.9 mm corresponds to  $2 \times 6 = 12$  contact points. The minimum diameter of 0.1 mm corresponds to  $30 \times 90 = 2700$  contact points.) The value of maximum von Mises stress from each graph is taken. These values of maximum von Mises stresses (from all such graphs) are plotted against the corresponding hemisphere diameters, for different loads. The displacement of the point of contact,  $\alpha$  is calculated using equation 3.9. The variation of displacement,  $\alpha$  with the hemisphere diameter,  $d$  is also plotted.

This is repeated for different groove widths with the same forces (30N, 50N and 70N), keeping the pitch constant. The maximum values of von Mises stresses for different groove widths is consolidated and plotted. The corresponding displacements of the point of contact are also calculated and plotted.

The step by step procedure is summarised below.

1. Assume a value for width of groove between serrations, ' $\gamma$ ' ( $0.1\text{mm} \leq \gamma \leq 1\text{ mm}$ ).
2. Assume grasping force, ' $F$ ' ( $30\text{ N} \leq F \leq 70\text{N}$ ).
3. Assume diameter of hemisphere, ' $d$ ' ( $0.1\text{mm} \leq d \leq 6\text{ mm}$ ).
4. Calculate the number of contacts.
5. Calculate the load per contact.
6. Calculate the radius, ' $a$ ' of the area of contact of each hemisphere assuming Hertzian contact.
7. Calculate the maximum pressure ' $p_{max}$ ' using Hertz equation.
8. Calculate the displacement ' $\alpha$ ' at the contact.
9. Consider a point on the axis of hemisphere through the point of contact, at a distance ' $\beta$ ' from the surface ( $0 \leq \beta \leq 3a$ ).
10. Calculate the principal and shear stresses at a distance  $\beta$  from the point of contact (Start from the point of contact itself, i.e.,  $\beta = 0$ ).
11. Calculate the von Mises stress at the point (at distance,  $\beta$ ).
12. Increment  $\beta$  by  $(a/1000)$ ; i.e.,  $\beta = \beta + (a/1000)$ .
13. Repeat steps 10 to 12 till  $\beta = 3a$ .
14. Obtain the relationship between  $\beta$  and von Mises stress.
15. Get the maximum value of von Mises stress from the above relation. (This is the maximum von Mises stress experienced by the serration of the given size,  $d$  and groove width,  $\gamma$  at a load,  $F$ ).
16. Repeat the steps from 3 to 15 and get the maximum von Mises stress for different hemisphere diameters  $d$ , keeping the groove width,  $\gamma$  and the gripper load,  $F$  constant to obtain the relation between  $d$  and maximum von Mises stress.
17. Repeat the steps from 2 to 16 for different loads ( $30\text{ N} \leq F \leq 70\text{N}$ ) keeping the groove width,  $\gamma$  constant and obtain the relationship between  $d$  and maximum von Mises stress at different loads.

18. Calculate the displacement,  $\alpha$  of the contact point for each combination of  $d$  and  $F$ , keeping  $\gamma$  constant to get the relation between  $\alpha$ ,  $d$  and  $F$ .
19. Get the maximum von Mises stress for each combination of  $\gamma$  and  $F$ , keeping  $\rho$  constant.
20. Get  $\alpha$  for each combination of  $\gamma$  and  $F$ , keeping  $\rho$  constant.
21. The conclusions drawn from the relations obtained in steps 17, 18, 19, 20 provide the framework for optimum design of serrations.

Although the analysis is done in the context of printing grippers, it provides a methodology for development of design optimization framework for similar grippers.

### 3.5.6 Results and Discussions

Fig. 3.8 shows the variation of maximum von Mises stress with the hemisphere diameter,  $d$ , for a constant value of  $\gamma$  (0.1mm).

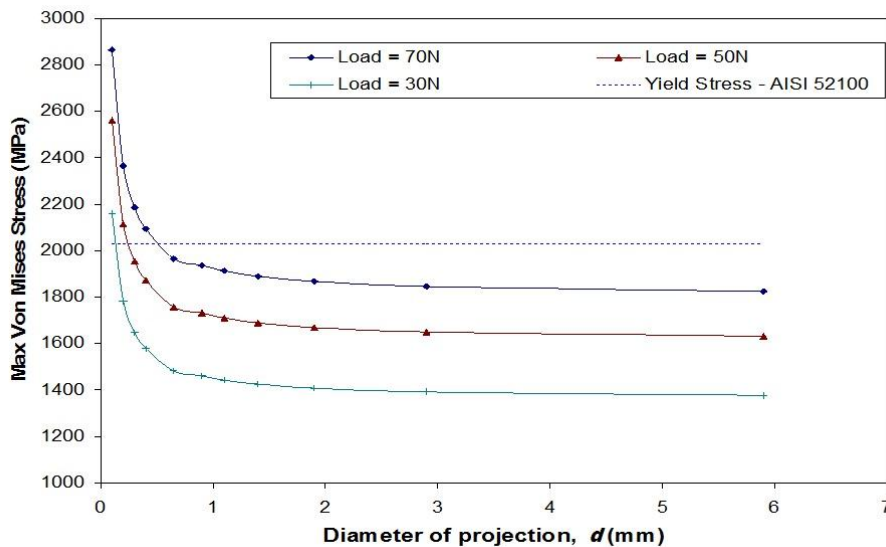


Fig. 3.8 Maximum von Mises stress vs. diameter of hemisphere (projection),  $d$  for different loads with constant gap,  $\gamma$ .

From the Fig. 3.8, it is evident that within the given load range, the maximum von Mises stress decreases as the  $d$  increases till a certain value, and then it remains more or less constant. Since  $\gamma$  is kept constant, a curve with pitch along the abscissa (instead



of  $d$ ) also will be of similar nature. This value of  $d$  is referred as critical hemisphere diameter,  $d_c$  and the corresponding value of  $\rho$  is referred as critical pitch,  $\rho_c$ .

The gripper is subjected to repeated loading and hence a lower value of maximum von Mises stress will result in higher fatigue life for the gripper. Hence it can be inferred from Fig. 3.8, that a value of  $d$  is equal to or more than the critical value,  $d_c$  is preferred for the durability of the serrations. In the given load range, the critical hemisphere diameter is about 0.9 mm and the corresponding critical pitch is 1 mm. The values of hemisphere diameter,  $d$  and the corresponding displacement,  $\alpha$  are plotted in Fig. 3.9.

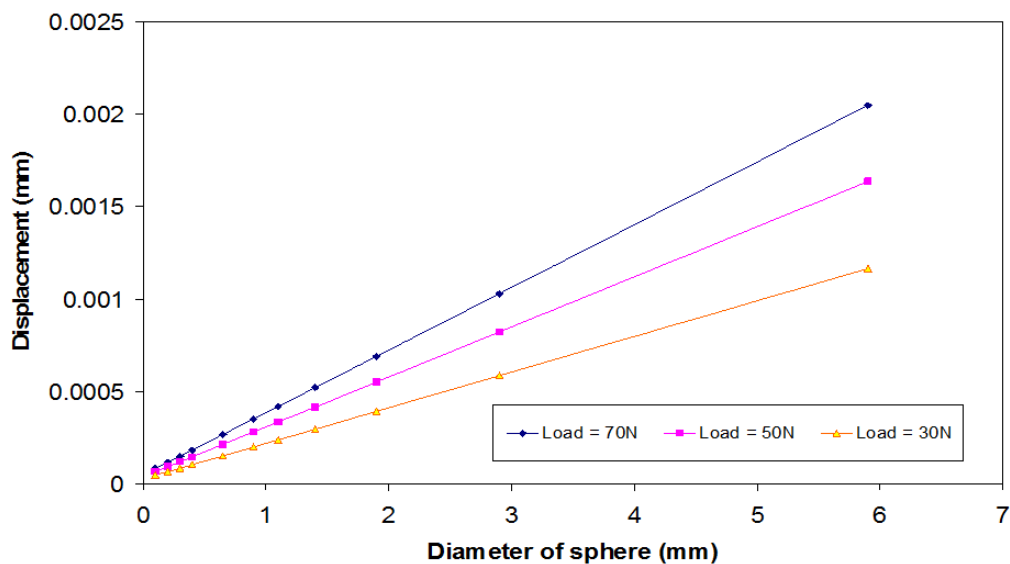


Fig. 3.9 Displacement of contact surface,  $\alpha$  vs. diameter of hemisphere (projection),  $d$  for constant  $\gamma$

The plot is made for a constant value of  $\gamma$  of 0.1mm. It shows that the displacement increases with  $d$  within the given range of loads.

Clearly, less deformation gives longer life and hence from Fig. 3.9, a lower hemisphere diameter is to be preferred. Also less displacement/deformation gives better accuracy of positioning of the paper during printing/paper transfer (register

accuracy) in the case of serrated gripper pad. In short, from Fig. 3.9, it can be inferred that the lower the hemisphere diameter, the better the life and better the register accuracy.

Considering Fig. 3.8 together with Fig. 3.9, it can be inferred that a hemisphere diameter of 0.9 is ideal for the durability and performance of a printing gripper. It may be noted that the above value of 0.9 is almost independent of load within the relevant range of loads.

To assess the effect of groove width, a plot with groove width  $\gamma$  on the abscissa and maximum von Mises stress on the ordinate is plotted for a constant pitch of 1mm in Fig. 3.10.

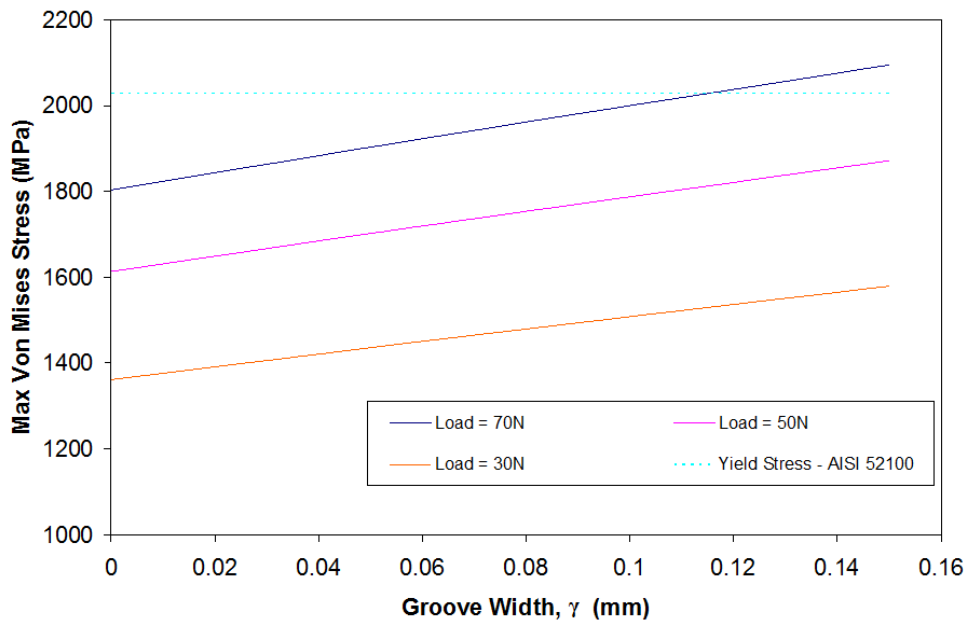


Fig. 3.10 Maximum von Mises stress vs. groove width  $\gamma$  for constant  $\rho$ .

It can be seen from Fig. 3.10, that the maximum von Mises stress increases as the groove width increases. Hence it is always better to have a lower value for  $\gamma$ , for the durability of the pad.

Another plot showing the relation between groove width,  $\gamma$  and displacement,  $d$  is given in Fig. 3.11.

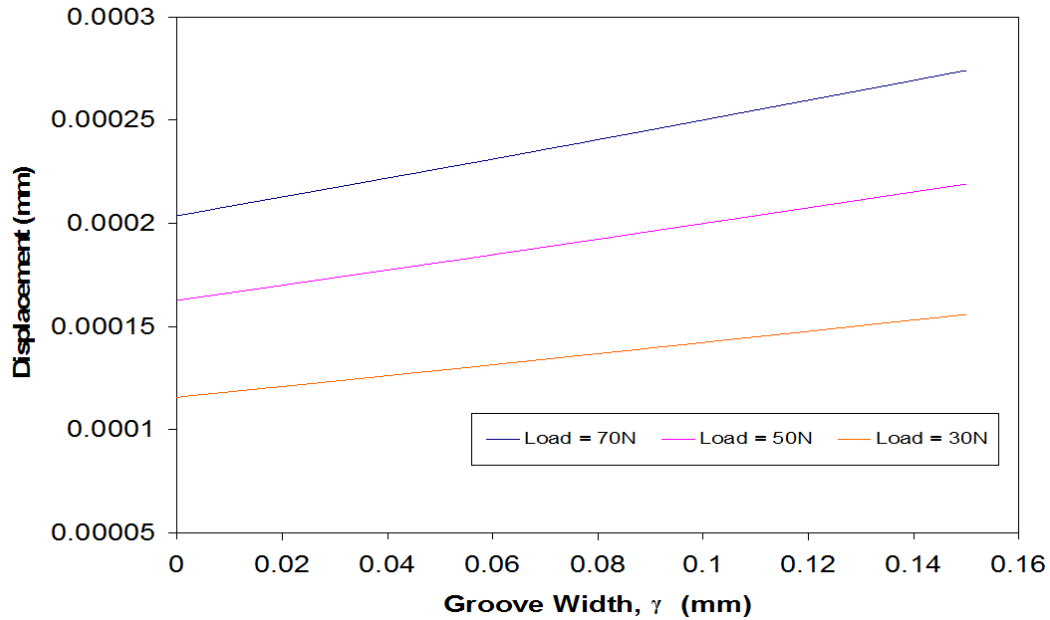


Fig. 3.11 Displacement vs. groove width  $\gamma$  for constant  $\rho$ .

Fig. 3.11 shows that smaller  $\gamma$  will result in smaller displacements and better life and register accuracy.

As discussed previously, the displacement assumes significance in the context of gripping operations which requires positional accuracy. In case of a printing gripper in an offset press, particularly for colour prints, the register accuracy is one of the major parameters affecting print quality. Hence the displacement has to be kept as low as possible in such applications if serrated gripper pad is used. However if the pad is flat and the gripper is serrated the effect of displacement is not significant.

### 3.5.7 Conclusions

A method to arrive at the optimum design parameters of serrations of a gripper jaw was discussed and the method was demonstrated in the context of a printing gripper. An optimum design should ensure long life for serrated gripper surface and good register

accuracy. For the design of serrations, the relevant geometrical parameters are pitch,  $\rho$ , hemisphere diameter,  $d$  and groove width,  $\gamma$ . From equation 3.10, it can be seen that the effect of only two of the three variables  $\rho$ ,  $d$  and  $\gamma$  need to be explored. In the present study, the effect of these variables on the durability of the gripper surface and on the register accuracy of the gripper is explored and the following conclusions were drawn.

- For a constant groove width, the maximum von Mises stress decreases as the pitch or hemisphere diameter increases till a critical value. Thereafter, it remains more or less constant.
- It is ideal to keep the hemisphere diameter at the critical value if the deflection corresponding to that pitch is acceptable for the application (Fig. 3.8 & Fig. 3.9).
- It has been found that a hemisphere diameter of 0.9 mm is ideal for the durability of gripper for the application considered in the present study. The above value is almost independent of load within the range of loads applicable in the context of a typical printing gripper.
- For finding the critical values of  $d$  for a different application or load range, the same method can be adopted.
- The lower the hemisphere diameter, the lower the displacement and hence better the register accuracy.
- The maximum von Mises stress and displacement increases with the groove width. Hence the groove width is to be kept as low as possible within the constraints of economical machining processes available.

A gripper in a sheet fed offset printing machine is selected for the analysis, as an example. The same methodology can be adopted for analysis on any two jaw gripper with serrated and flat pair of gripping surfaces. In the next chapter, the effect of high stress cyclic contact due to repetitive gripping operation near the surface of the gripper serration is simulated and analysis is carried out.

## **CHAPTER 4**

### **SHORT RANGE DIFFUSION OF CARBON IN STEEL GRIPPERS DUE TO CYCLIC CONTACT STRESS**

#### **4.1 INTRODUCTION**

Offset printing is achieved by printing different color separations exactly one over the other. Hence prevention of the slippage of paper is very crucial for the grippers of an offset printing machine. When the gripper is closed, the serrated jaw presses against the hard flat jaw with sufficient force to prevent any slippage of paper held between them during printing. The contact surface of each serration is very small and hence the stress will be high.

Assuming 25 working days per month and an average printing speed of 10,000 copies per hour, with eight hours per day operation for the press, a gripper will have to grip the paper ten million times in six months. Thus the serrated tip will be subjected to high stress cyclic loading. The contact stress creates an elastic gradient near the contacting surface of the serrations. The elastic gradient can result in stress assisted diffusion of carbon atoms at the surface of the serrations.

#### **4.2 EXPERIMENTAL SETUP**

To simulate the conditions of gripper, a newly designed experimental set-up (EXPST) is fabricated. The photograph of the fabricated model with the drive and controls is shown in Fig. 4.1. A CAD model of the main unit of EXPST is shown in Fig. 4.2.

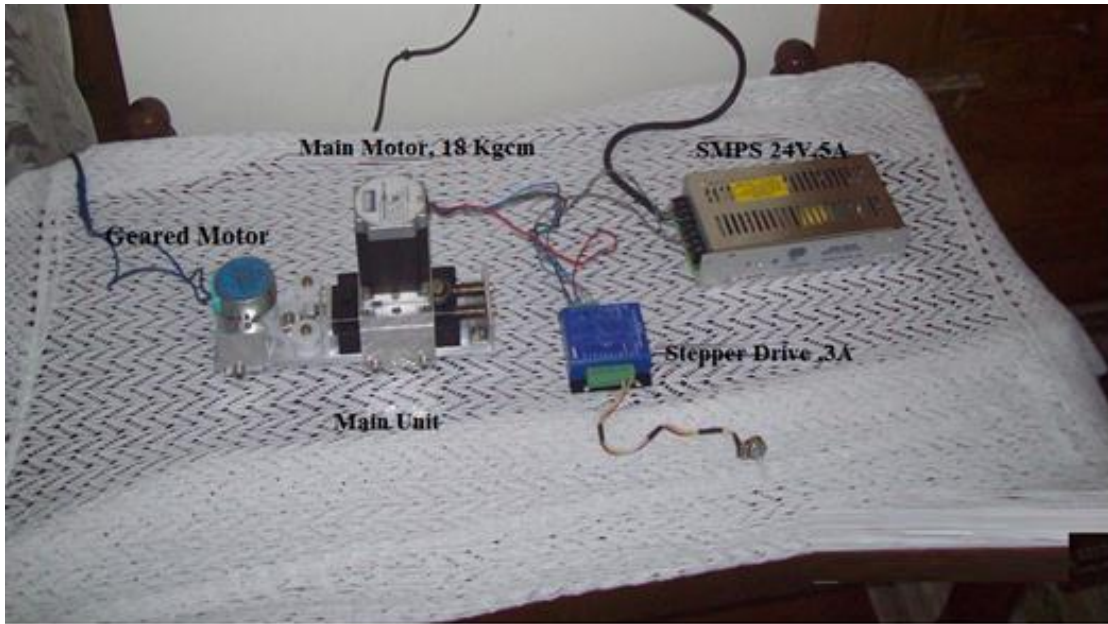


Fig. 4.1 Photograph of the fabricated experimental setup

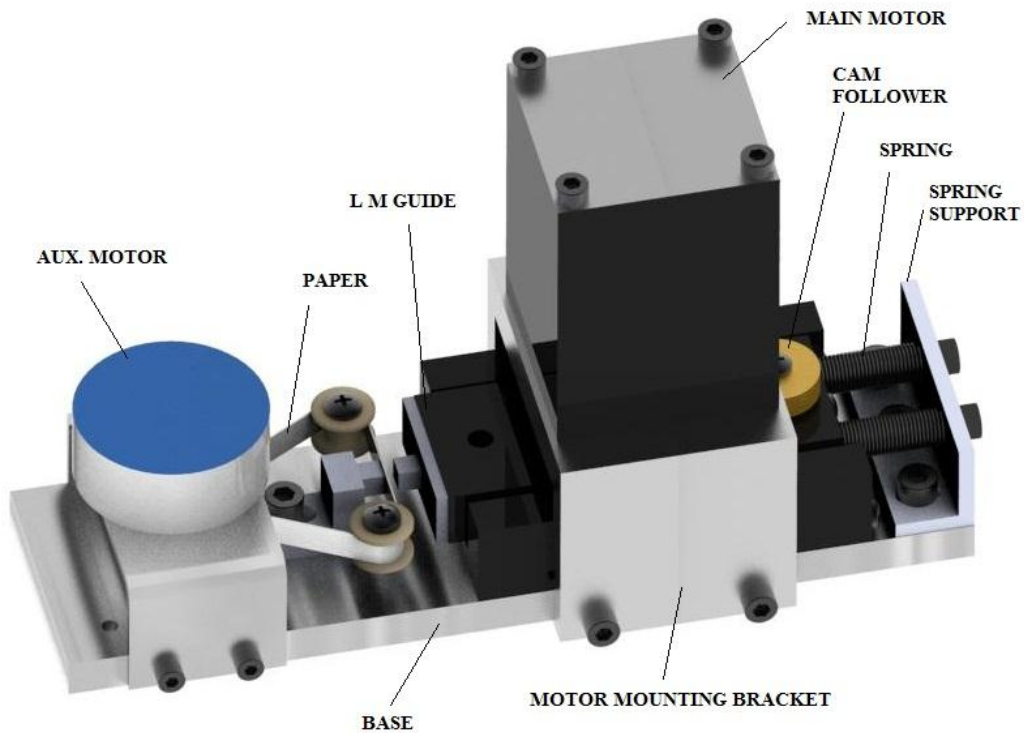


Fig. 4.2 CAD model of the main unit of the experimental set-up

The prime mover is a stepper motor with drive and a potentiometer is also provided for speed control. The main motor is mounted on a bracket fastened to a base. An LM guide is also fixed to the base. The motor drives a cam and the cam follower imparts

movement to the LM guide. The reverse motion of LM guide is ensured by two compression springs shown at right end. The force exerted by compression springs is transferred by the LM guide to the specimen to be experimented, the cut piece of gripper jaw in this case. A cut piece of the mating flat gripper is fixed on a bracket which is fixed to the base plate. The arrangement is such that if the motor and cam are removed, the jaws will be pressed against each other with the spring force. The motor and cam acts only to separate the contact. The force exerted by the gripper is adjusted by adjusting the spring force using the adjustable spring support at the extreme right end of the unit. The springs are designed such that the actual pressure exerted by the grippers of SFOPM can be simulated. An arrangement to pass a paper ribbon continuously between the jaws using an auxiliary motor is also provided to simulate the gripping process in an SFOPM.

#### **4.2.1 Major design considerations of the experimental setup.**

In SFOPMs, the gripping force of the grippers is provided by springs and the gripper is opened and closed with the help of cams. Hence the same method is adopted in the experimental setup also. The thickness of paper usually printed on an SFOPM varies from 0.05 mm to 0.7 mm and the gripper opens to a maximum gap of approximately 3 mm to facilitate entry and gripping of paper. The timing of the opening and closing of grippers is studied and typically the gripper is kept fully opened for  $26^{\circ}$  and fully closed for  $214^{\circ}$  for each rotation of the Impression cylinder. The experimental set up is also designed to maintain the same opening and closing angles. Hence a cam with radii 23 mm and 20 mm over a dwell of  $26^{\circ}$  and  $214^{\circ}$  respectively is planned for the experimental setup.

As indicated in sec 3.5.1 and 3.5.4, the maximum load on gripper is 70 N, on a gripper pad of size 18 x 6 mm. The experimental setup is designed for a gripper pad of size 6mm x 6 mm, for convenience. Hence max load required is  $70 \text{ N}/3 = 23.3 \text{ N}$ . Hence the springs of the experimental setup are designed such that the position of the spring holder can be set to produce a force of 23.3 N (or less) when the gripper is closed. An additional load of 3.6 N due to opening of grippers is make the maximum force on the cam to be 26.9 N. The maximum pressure angle of the cam is  $8.8^\circ$  at  $29.496^\circ$  from the start of lifting. A motor of torque 1.8 Nm is employed for the set up.

#### 4.3 EXPERIMENTAL PROCEDURE

The serrated portion of the printing gripper is cut into three pieces of size  $6\text{mm} \times 6\text{ mm}$  each. The cut pieces and the balance portion are shown in Fig 4.3. Wire cut EDM process is used for cutting to keep the temperature change during cutting to a minimum, to prevent any unintended microstructural change.

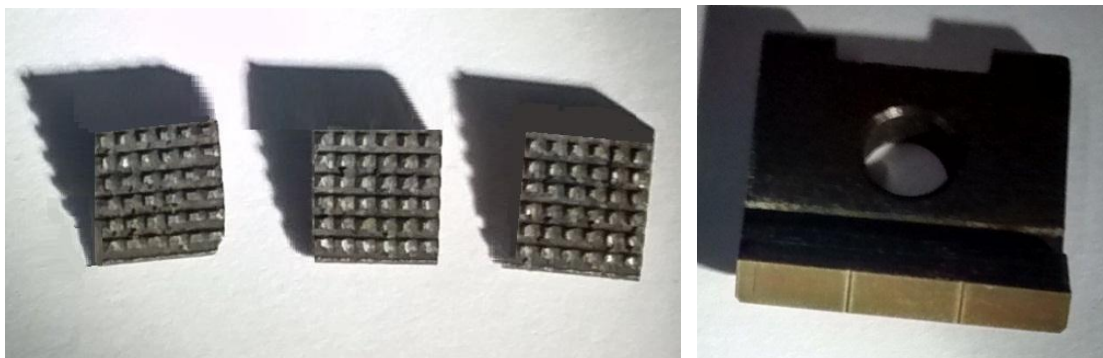


Fig 4.3 The serrated portion of a printing gripper cut into three pieces and the balance portion

The cut piece is mounted at the end of the LM guide. The bracket behind the spring is adjusted to approximately 16.75 N so that the force on each serration during closing is approximately 0.465 N. The motor is switched on so that each serration of the sample is subjected to intermittent loads of 0.465 N as in the case of actual gripping process.



After an hour, the sample is removed and the cross section of the serration is examined for the dispersion of carbon atoms using an SEM with EDS. The CARL ZIESS make SIGMA™ HD FESEM used for the purpose is shown in Fig 4.4.



- |                            |                           |
|----------------------------|---------------------------|
| 1. Electron optical column | 6. Personal Computer (PC) |
| 2. Specimen chamber        | 7. ON/OFF button          |
| 3. EDS detector            | 8. Plinth                 |
| 4. Monitors                | 9. WDX                    |
| 5. EBSD                    |                           |

Fig. 4.4 CARL ZIESS make SIGMA™ HD FESEM

The FESEM uses a focused beam of electrons to generate an image or to analyze the specimen. Electrons are liberated from a field emission source and accelerated in a high electrical field gradient. Within the high vacuum column these so-called primary electrons are focused and deflected by electronic lenses to produce a narrow scan beam that bombards the object. The focused electron beam scans the

surface of the specimen. As a result secondary electrons are emitted from each spot on the object. The angle and velocity of these secondary electrons relates to the surface structure of the object. A detector catches the secondary electrons and produces an electronic signal. This signal is amplified and transformed to a video scan-image that can be seen on a monitor or to a digital image that can be saved and processed further.

The carbon distribution near the surface of the serration, obtained through examination of a sectional plane along the axis of the serration using CARL ZIESS make SIGMA™ HD FESEM and OXFORD EDS with AZTEC software, shows regions of carbon clustering over a small area at the surface of the serration after subjecting to cyclic loading (Fig. 4.5).

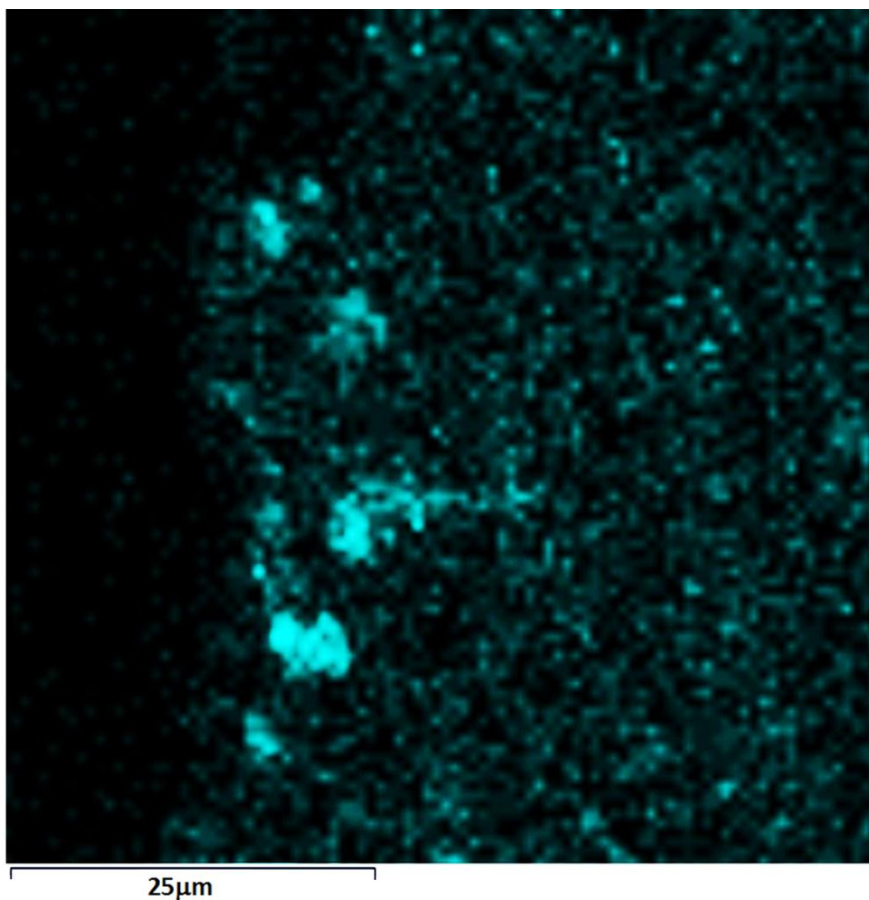


Fig 4.5 Clustering of carbon near the surface of a serration after subjecting to cyclic stress (Micrograph using ZIESS SIGMA™ FSEM with Oxford EDS with AZTEC software). The unaffected portion in the interior with original carbon distribution can be seen at the right part of the figure.

#### 4.4 METHODOLOGY OF SIMULATION OF CARBON DIFFUSION

Among the studies on the applications of stress assisted diffusion, those on the dark and white etching regions developed in bearing raceways due to stress assisted diffusion of carbon leading to microstructural changes (Swahn *et al.*, 1976; Mitamura *et al.*, 2007; Warhadpande *et al.*, 2014) are of particular interest. In the context of formation of dark and white etching bands due to rolling contact stress, it is reported in various studies that carbon diffuses over some microns within the bands, due to the stresses produced, and precipitates as carbide at the edge of the band (Buchwald and Heckel, 1968; Borgese, 1970). The redistribution of carbon and the resulting martensitic decay due to the rolling contact fatigue is also reported by Swahn *et al.* (1976). Warhadpande *et al.* (2014) developed a diffusion based model for rolling contact fatigue.

The theoretical work of Fick is regarded as the phenomenological basis of diffusion. Fick's first law postulates that the flux goes from regions of high concentration to regions of low concentration, with a magnitude that is proportional to the concentration gradient. If an elastic gradient is present, the Fick's first law is no longer the flux equation. The elastic gradient will induce a flux of atoms from a higher potential to a lower potential. The flux of atoms due to the potential gradient is to be added to that produced by the concentration gradient to arrive at the equation for total flux (Shewmon, 1991).

The carbon clustering near the surface formed by cyclic contact stress on a used steel gripper is shown in Fig. 4.5. It is very similar to the phenomenon of dark and white bands in bearing steel on the raceway of used ball bearings due to the interstitial diffusion of carbon atoms caused by rolling contact stress (Mitamura *et al.*, 2007; Warhadpande *et al.*, 2014).

It is well established that repeated loading of steel resulting in plastic deformation will induce stress assisted diffusion of carbon and the dark and white bands on used bearings is the result of redistribution of carbon due to stress assisted diffusion (Swahn *et al.*,1976; Warhadpande *et al.*, 2014). But no study is available for stress assisted diffusion in steel grippers.

In this chapter, the stress experienced by the serrations of a gripper is modeled and the redistribution of carbon due to stress assisted diffusion and the resulting clustering of carbon at the affected region near the surface of the gripper serration are simulated for the first time. Quantification parameters for the clustering of carbon are developed and the effects of the variation of load, the number of cycles and the variation of temperature on the clustering of carbon atoms due to diffusion are compared.

The procedure adopted is summarized in the following steps.

1. The force acting on the gripper is estimated from the force exerted on the gripper mechanism by the spring and the boundary conditions are that the flat jaw is fixed and the axis of the serration, perpendicular to the fixed flat jaw, is free to move only in one direction (along the axis of the serration).
2. The contact of one serration of the gripper is modeled using finite element analysis to get the nodal values of equivalent stress and equivalent plastic strain.
3. The area of stress strain curve at each of the above points is computed. These areas represent the dissipated plastic energy at the nodal points of the FE model.
4. A region of interest is defined to reduce the size of the problem and the values of dissipated plastic strain energy at the FE nodal points falling within the region of interest are filtered into a file which forms the input file for subsequent steps. Care is taken to ensure that the region of interest defined is larger than the diffusion affected region.
5. A very fine uniform square grid in the same coordinate system of step 2, with one of the nodes at the origin and with the gridlines parallel to X and Y axes is defined.
6. The values of the dissipated plastic strain energies at the nodes of finite element model, obtained in step 4, are interpolated to the nodes of the uniform square grid defined in step 5. The gradient of these values represent the potential for driving diffusion.

7. Computer simulation of stress assisted diffusion of carbon atoms at the gripper tip surface is conducted using MATLAB 2009.

A commercial FEM software (ANSYS 15.0) is used for steps 1 and 2, spread-sheet for steps 3 and 4 and a MATLAB program for steps 5, 6 and 7.

There are variations in the number of grippers, size of the gripper jaws and serrations per gripper jaw employed in different makes, models and sizes of offset printing machines. The maximum gripping force acting on the paper during offset printing also varies between different designs and models of offset presses and the maximum force is usually set between 30N to 70N. In this study, a model with a setting force of 50N and a gripping area  $18\text{mm} \times 6\text{mm}$  is considered. Thus the serrated area on the gripper, refer Fig. 3.5 and Fig. 4.3, shall be  $18 \times 6$  mm. The serration is approximated as a hemisphere of diameter 0.9 mm for the purpose of the study (Fig 3.6). Assuming a gap ( $\gamma$ ) of 0.1 mm between each serration, there will be 108 serrations per gripper tip.

The printing gripper pivoted on the gripper shaft, is configured such that, the contacting surfaces of serrated and flat jaws are parallel during contact. Since the contacting surfaces are parallel and area of contact is small, it is assumed that the contact load is shared equally by all the serrations and hence the contact of only one serration is modeled. The force acting per serration of 0.9 mm diameter is  $50\text{N} / 108 = 0.463\text{N}$ . As per the classical Hertzian theory of non-adhesive elastic contact, the maximum stress will be experienced on the axis of the hemisphere near the contact point.

The contact of the gripper tip is modeled using an elastic plastic model in commercial FEA software. An axisymmetric model with a coordinate system with the origin at the point of contact and directions of the axes as shown in Fig. 4.6 is employed. The

serration is modeled as a hemisphere with a radius of 0.45mm. The degree of freedom of the axis of the hemisphere in X direction is arrested. The zoomed in view of the mesh is also shown in Fig. 4.6. PLANE183 element type of size of 0.01mm with axisymmetric option is used for meshing the body.

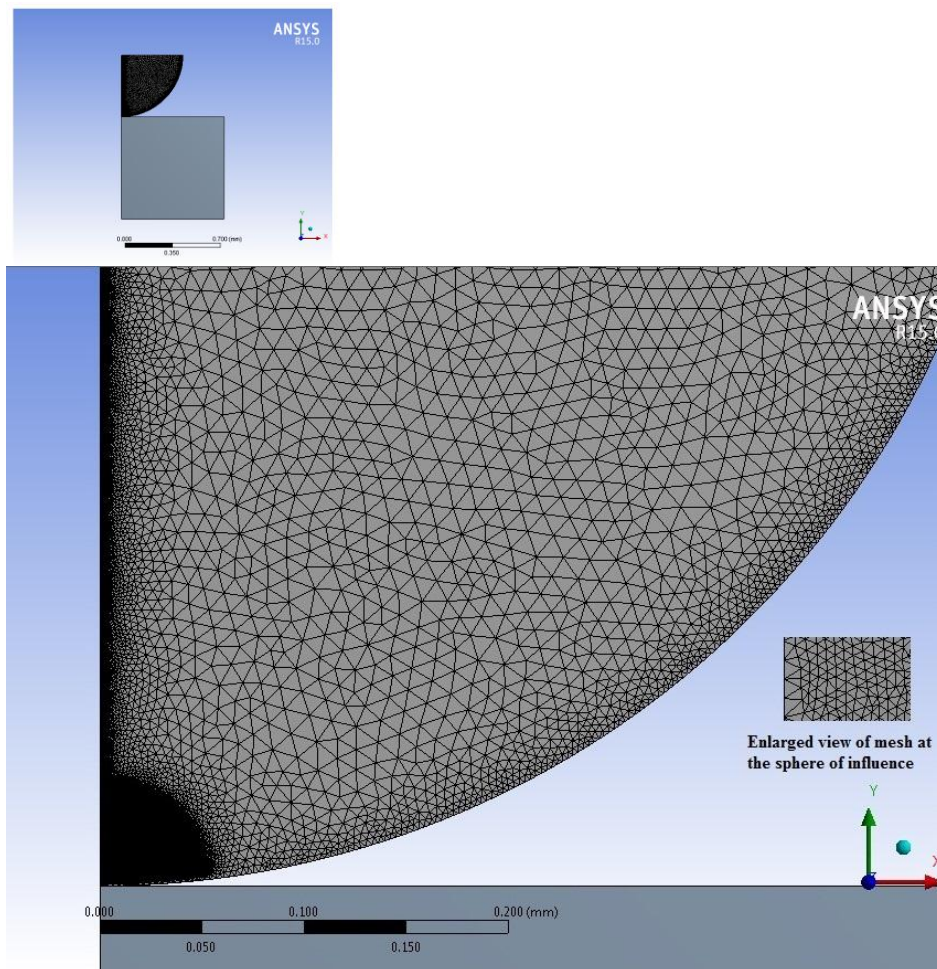


Fig. 4.6 Meshed axisymmetric model for analysis and its zoomed in view with enlarged view of mesh at the sphere of influence shown in inset

Since the contact analysis is a non-linear problem, the contact region must be finely meshed and accurately modeled to capture the geometric nonlinearity to get accurate results. Hence the elements along the contacting edge are refined to 3 microns size. Since the maximum stress occur near the contact point on the axis of the hemisphere passing through the point of contact, or more precisely through the center point of the

area of contact, the elements along and near this axis are also refined to 0.1 microns size. The elements very close to the point of contact are further refined using a sphere of influence of radius 50 microns with very fine mesh size of 0.05 microns. Enlarged view of mesh at the sphere of influence is shown in inset in Fig. 4.6. Thus the region of interest mentioned in step 4 will be having a mesh size of 0.05 microns. Special elements CONTA172 and TARGE169 are used for the contact.

Since the focus of study is on the serrations of the gripper tip, the contacting flat surface is modeled as a single element to reduce computational load. This has resulted in 1550001 elements including 301 contact elements resulting in 3104206 nodes for the axisymmetric model.

Before proceeding with the analysis, a pilot analysis is done in commercial FEA software with the same geometry, mesh, boundary conditions and assuming that the material is perfectly elastic with the same elastic modulus. This result is compared with the values obtained theoretically using Hertz contact equations to validate accuracy of the finite element analysis procedure adopted.

During actual gripping, the stress at the tip of the serration exceeds the yield strength, resulting in plastic deformation and work hardening. Bilinear kinematic hardening model is adopted and the von Mises stress and equivalent plastic strain at the nodes are determined. The material properties are given in Table 4.1.

Table 4.1 Properties of steel, AISI 4320

Property	Value
Elastic Modulus ( $E$ )	205 GPa
Poisson's ratio ( $\nu$ )	0.3
Yield strength( $S_y$ )	869MPa
Hardening Modulus ( $H_m$ )	8 GPa

The variation of contact stress and the corresponding plastic strain result in the variation of dissipated plastic strain energy at different points on the serrations of the gripper. This potential gradient can create a flux of carbon atoms.

The potential function,  $V$  at each node is the dissipated plastic strain energy at that node. The strain energy density at each node is obtained by determining the corresponding residual area under stress strain curve after the application and release of the load. The schematic of bilinear hardening model and the residual area representing dissipated plastic strain energy are shown in Fig. 4.7.

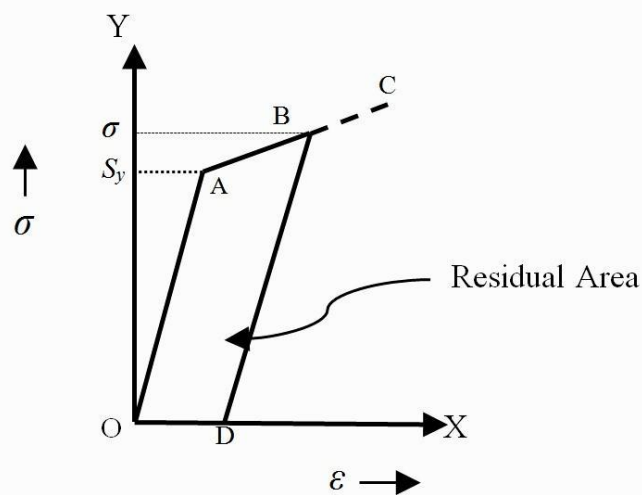


Fig. 4.7 Schematic of bilinear hardening model and the residual area

Fig. 4.7 shows the strain along the X-axis and stress along the Y-axis. OABC is the stress strain curve. OA and AC are the elastic and plastic regions respectively. The slope of OA is the elastic modulus,  $E$  and the slope of AC is the tangent modulus,  $H_m$ . The point A and B represent the yield stress and the maximum equivalent stress respectively. OD represents the equivalent plastic strain,  $\epsilon_p$ .



$$\begin{aligned}
\text{The residual area, OABD} &= \frac{1}{2}(\sigma - S_y)\varepsilon_p + S_y\varepsilon_p \\
&= \left(\frac{1}{2}\sigma - \frac{1}{2}S_y + S_y\right)\varepsilon_p \\
&= \left(\frac{1}{2}\sigma + \frac{1}{2}S_y\right)\varepsilon_p \\
&= \frac{1}{2}(\sigma + S_y)\varepsilon_p \tag{4.1}
\end{aligned}$$

The dissipated plastic strain energy density at the nodes are calculated by substituting the corresponding values of maximum equivalent stress,  $\sigma$  and the equivalent plastic strain,  $\varepsilon_p$  in equation (4.1).

The next step is to conduct the simulation of the diffusion of carbon atoms due to the potential gradient generated. The distribution of dissipated plastic strain energy density is same in any plane passing through the axis. Since the study is carried out to compare the variation of the diffusion of carbon with various parameters like load, cycles, and temperature, the simulation is done only in one plane to simplify the problem. The maximum stress will be experienced on the axis of the hemisphere near the point of contact. It was found that the plastic strain energy will be experienced only over a width of about 20 microns and a depth of 15 microns when a load of 0.463N (corresponding to 50N gripper load as mentioned above) is applied. However since the values at the adjacent nodes are also included in the equations and the calculations are repeated over millions of cycles, the MATLAB simulation is done for a larger area with a width of 53 microns symmetrical to the axis of the hemispherical serration and a depth 26.5 microns. This area is referred as the region of interest. The position of the region of interest and the region of interest with the coordinate system is shown in Fig 4.8. The center point of the contact area conveniently referred as the point of contact is the origin O.

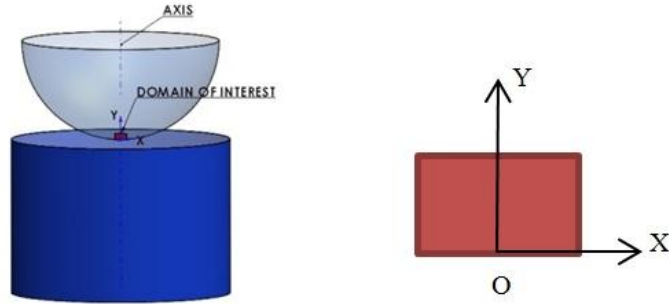


Fig 4.8 The position of the region of interest (shown in red) on a gripper serration and the region of interest and the co-ordinate system.

Thus the region of interest is perpendicular to the surface of contact and the axis divides the region of interest into two equal squares of 26.5 microns sides. The point of contact also lies on the axis. An Excel file with the Cartesian coordinates of the nodes and the respective values of dissipated plastic strain energy, falling within the region of interest forms the input for the simulation.

The nodes of any model discretized for finite element analysis need not be (and most commonly are not) spaced evenly. So the nodal values of equivalent stress and equivalent plastic strain and hence the dissipated plastic strain energy, obtained from the finite element analysis are distributed in a scattered manner. For the purpose of finding out the potential gradient for the simulation of diffusion of carbon atoms, these scattered data are interpolated to a fine uniform square grid. A MATLAB program is employed for this purpose.

Various built in functions like `griddata`, `interp2`, `TriScatteredInterp`, `scattered Interpolant` etc. with various options like `linear`, `natural`, `nearest`, `v4`, `cubic` etc. are available for interpolation of data in MATLAB. However `interp2` can be used for interpolation only when the input is uniform 2D data and hence not suitable for the purpose. `Griddata` fails when there are replicates or when the data has many collinear points. `Griddata` is

also unable to extrapolate beyond the convex hull of the data and outputs NaN (Not a Number) results unless the 'v4' option is used, which is slow and requires a lot of computer memory. Thus TriScatteredInterp and scatteredInterpolant class are the remaining methods available in MATLAB to perform triangulation-based scattered data interpolation. Both methods have linear, natural and nearest neighbor options. As the name implies, both the commands does interpolation only and not extrapolation. Both will return NaN for any value outside the convex hull of the data. However, NaN can be avoided and numeric results can be expected if the points are queried using the nearest neighbor method. The reason is that the nearest neighbor to a query point exists both inside and outside the convex hull.

The size of the grid is a trade-off between the accuracy of simulation and the time and cost of computation. For the present study, the grid size is finalized as  $1/3 \mu\text{m}$  after careful trials. That is, the nodal values of dissipated plastic strain energy are transferred to a uniform square grid with lines at a spacing of  $1/3 \mu\text{m}$ . Thus the region of interest is having width of 160 grids, corresponding to 53 microns symmetrical to the point of contact through a depth of 80 grids, corresponding to 26.5 microns. As explained above, the value of the plastic strain energy at each node of the square grid is derived from the value at the nearest node of the finite element mesh (nearest neighbor method). To ensure that the accuracy is not compromised by the use of the nearest neighbor method, more nodal vales are generated in the FE analysis. Hence to ensure accuracy of the method, the mesh size is refined to 0.05 microns as previously mentioned, at the region of interest shown in Fig.4.8 and 2050213 nodal values of the FE model are used to get 12,800 nodal values of the square grid in the region of interest.

The dissipated plastic strain energy at all the nodes of the square grid in the region of interest, estimated as above, represent the potential,  $V$  at each node of the grid. This potential,  $V$  at the nodal points of the grid in the region of interest is represented by an 80x160 array.

To model the diffusion of carbon atoms, the flux generated by this potential gradient must be added to that produced by the concentration gradient of carbon. Hence the Fick's law has to be modified with an additional term to incorporate stress assisted diffusion (Shewmon, 1991).

That is,

$$\frac{\partial c}{\partial t} = D \nabla \left[ \nabla c + \frac{c \nabla V}{kT} \right] \quad (4.2)$$

where

$$\text{Boltzmann constant, } k = 1.38064852 \times 10^{-23} \text{ m}^2 \text{ kg s}^{-2} \text{ K}^{-1}$$

This on expansion gives,

$$\frac{\partial c}{\partial t} = D \nabla^2 c + \frac{D}{kT} \nabla c \cdot \nabla V + \frac{Dc}{kT} \nabla^2 V \quad (4.3)$$

The diffusion coefficient,  $D$  and the activation energy,  $Q$  are related by the equation,

$$D = D_0 e^{\left(\frac{-Q}{RT}\right)} \quad (4.4)$$

where,  $D_0 = 2 \times 10^{-6} \text{ m}^2 \text{ s}^{-1}$  for carbon diffusion in  $\alpha$ -iron (Polonsky and Keer, 1995).

The activation energy for carbon in ferrite,  $Q = 84 \text{ KJ/mol}$  (Mitamura, 2007).

The gas constant,  $R = 8.314 \text{ J / mol. K}$ .

The temperature  $T = 303 \text{ K}$ , is assumed.

Applying finite difference method on equation (4.3),

$$\begin{aligned} \frac{c_{i,j}^{n+1} - c_{i,j}^n}{\Delta t} = & D \left[ \frac{c_{i+1,j}^{n+1} - 2c_{i,j}^{n+1} + c_{i-1,j}^{n+1}}{\Delta h^2} + \frac{c_{i,j+1}^{n+1} - 2c_{i,j}^{n+1} + c_{i,j-1}^{n+1}}{\Delta h^2} \right] + \frac{D}{kT} \left\{ \left[ \frac{c_{i+1,j}^{n+1} - c_{i,j}^{n+1}}{\Delta h} \right] \left[ \frac{V_{i+1,j}^{n+1} - V_{i,j}^{n+1}}{\Delta h} \right] \right\} + \\ & \frac{D}{kT} \left\{ \left[ \frac{c_{i,j+1}^{n+1} - c_{i,j}^{n+1}}{\Delta h} \right] \left[ \frac{V_{i,j+1}^{n+1} - V_{i,j}^{n+1}}{\Delta h} \right] \right\} + \frac{Dc_{i,j}^{n+1}}{kT} \left[ \frac{V_{i+1,j}^{n+1} - 2V_{i,j}^{n+1} + V_{i-1,j}^{n+1} + V_{i,j+1}^{n+1} - 2V_{i,j}^{n+1} + V_{i,j-1}^{n+1}}{\Delta h^2} \right] \end{aligned} \quad (4.5)$$

where, the nodes are as in Fig. 4.9.

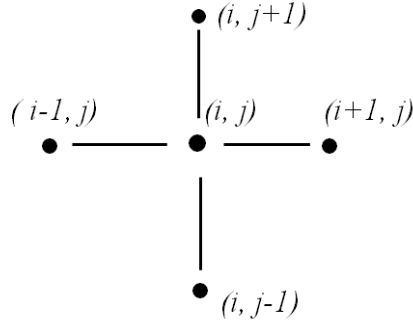


Fig. 4.9 Nodal definitions for finite difference method

Since there is no flow of carbon from or into the system, the total carbon concentration before and after diffusion remains unchanged. Hence,

$$c_{i,j}^{n+1} + c_{i-1,j}^{n+1} + c_{i+1,j}^{n+1} + c_{i,j-1}^{n+1} + c_{i,j+1}^{n+1} = c_{i,j}^n + c_{i-1,j}^n + c_{i+1,j}^n + c_{i,j-1}^n + c_{i,j+1}^n \quad (4.6)$$

Applying boundary condition (4.6) to equation (4.5), and solving,

$$\begin{aligned} c_{i,j}^{n+1} = & \frac{c_{i,j}^n + \frac{D\Delta t}{\Delta h^2} [c_{i,j}^n + c_{i-1,j}^n + c_{i+1,j}^n + c_{i,j-1}^n + c_{i,j+1}^n]}{1 + \frac{5D\Delta t}{\Delta h^2} - \frac{2D\Delta t}{kT\Delta h^2} V_{i,j}^{n+1} + \frac{D\Delta t}{kT\Delta h^2} V_{i+1,j}^{n+1} + \frac{D\Delta t}{kT\Delta h^2} V_{i,j+1}^{n+1} - \frac{D\Delta t}{kT} \nabla^2 V} \\ & + \frac{\frac{D\Delta t}{kT\Delta h^2} [c_{i+1,j}^{n+1} V_{i+1,j}^{n+1} - c_{i+1,j}^{n+1} V_{i,j}^{n+1} + c_{i,j+1}^{n+1} V_{i,j+1}^{n+1} - c_{i,j+1}^{n+1} V_{i,j}^{n+1}]}{1 + \frac{5D\Delta t}{\Delta h^2} - \frac{2D\Delta t}{kT\Delta h^2} V_{i,j}^{n+1} + \frac{D\Delta t}{kT\Delta h^2} V_{i+1,j}^{n+1} + \frac{D\Delta t}{kT\Delta h^2} V_{i,j+1}^{n+1} - \frac{D\Delta t}{kT} \nabla^2 V} \end{aligned} \quad (4.7)$$

The potential gradients which are the gradients of dissipated plastic strain energy are assumed not to change with time. i.e.,

$$V^{n+1} = V^n \quad (4.8)$$

For simplifying the analysis, it is assumed that

$$c_{i+1,j}^{n+1} = c_{i+1,j}^n \quad \& \quad c_{i,j+1}^{n+1} = c_{i,j+1}^n \quad (4.9)$$

as it will not have any significant effect on the results, for small time steps.

Hence (4.7) simplifies to

$$c_{i,j}^{n+1} = \frac{c_{i,j}^n + \frac{D\Delta t}{\Delta h^2} [c_{i,j}^n + c_{i-1,j}^n + c_{i+1,j}^n + c_{i,j-1}^n + c_{i,j+1}^n]}{1 + \frac{5D\Delta t}{\Delta h^2} - \frac{2D\Delta t}{kT\Delta h^2} V_{i,j}^n + \frac{D\Delta t}{kT\Delta h^2} V_{i+1,j}^n + \frac{D\Delta t}{kT\Delta h^2} V_{i,j+1}^n - \frac{D\Delta t}{kT} \nabla^2 V} + \frac{\frac{D\Delta t}{kT\Delta h^2} [c_{i+1,j}^n V_{i+1,j}^n - c_{i+1,j}^n V_{i,j}^n + c_{i,j+1}^n V_{i,j+1}^n - c_{i,j+1}^n V_{i,j}^n]}{1 + \frac{5D\Delta t}{\Delta h^2} - \frac{2D\Delta t}{kT\Delta h^2} V_{i,j}^n + \frac{D\Delta t}{kT\Delta h^2} V_{i+1,j}^n + \frac{D\Delta t}{kT\Delta h^2} V_{i,j+1}^n - \frac{D\Delta t}{kT} \nabla^2 V} \quad (4.10)$$

The variation in carbon concentration at each time step is calculated using equation (4.10) and used for modeling the flux of carbon atoms. In this model it is assumed that the change in carbon concentration will not affect the constitutive material behavior and hence the dissipated energy due to plastic deformation is not recalculated for subsequent cycles.

Case hardened steel AISI 4320, is the material of the gripper used. The original carbon content of the material is 0.17%. When the material is carburized, the carbon content of the surface increases to about 0.9%. The carbon content decreases as depth increases and reaches the original value of 0.17% at a depth of about 1mm from surface. The variation of concentration is almost linear and is assumed linear. Thus the initial carbon concentration is defined. An array of same size,  $80 \times 160$  is used to represent the initial carbon concentration of the region of interest at time step,  $n=1$ .

As indicated earlier, a typical gripper operates at about 10,000 copies per hour on average. The time for one cycle is  $3,600/10,000 = 0.36$  s. During operation the actual time of gripping is about 70% only and hence approximately 0.25 s. Hence each operation or cycle can be taken as one time step and  $\Delta t$  shall be 0.25s. However the

time step has to be kept at small values to prevent divergence of the finite difference solution. Hence a pseudo time step of  $\Delta t = 2 \times 10^{-5}$  s is adopted. The temperature is assumed as 303° K.

The distribution of potential,  $V$  at each node of the grid is the driving force for stress assisted diffusion. The Laplacian of the potential is the divergence of the gradient. It also is one of the variables of equation (4.10) for simulating stress assisted diffusion of carbon atoms. The potential gradient and its Laplacian in the region of interest are plotted for better understanding of the process.

To start with, equation (4.10) is applied for  $10^7$  times to arrive at the carbon distribution in the region of interest at the end of  $10^7$  time steps (cycles). The simulation is repeated for more cycles and for different loads. 3D Matlab plot showing the dissipated plastic strain energy density, 2D plot of dissipated plastic strain energy density along the Y axis through the point of contact and 3D Matlab plot with contour of the Laplacian of potential gradient are made for easy visualization. The vector plots indicating the direction and magnitude of the gradients of dissipated plastic strain energy (potential gradient) are also plotted. The 3D, contour and vector plots of carbon concentration for different load conditions and for different number of cycles and at different temperatures from 20° C to 50° C are calculated and plotted. The maximum and minimum values of the carbon concentration, its range and standard deviation in the region of interest are also calculated.

#### **4.5 RESULTS OF SIMULATION**

The equivalent stress values obtained from finite element analysis using FEA analysis for a gripper load of 50 N assuming perfectly elastic material with the same elastic modulus for validating the results is shown in Fig. 4.10.

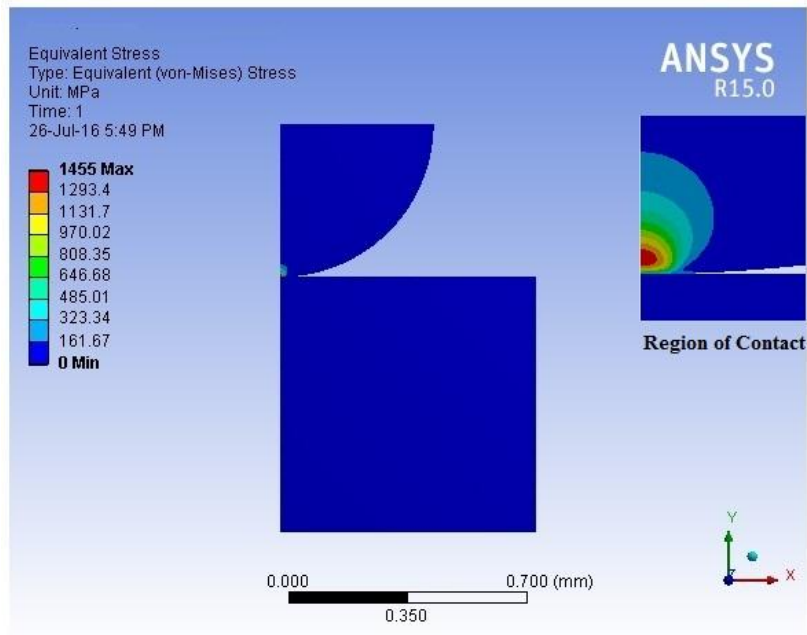


Fig. 4.10 Equivalent stress assuming perfectly elastic material  
 (Zoomed in view at the region of contact is shown in inset)

The results obtained from finite element analysis using FEA with the actual material properties are shown in Fig. 4.11 & Fig. 4.12.

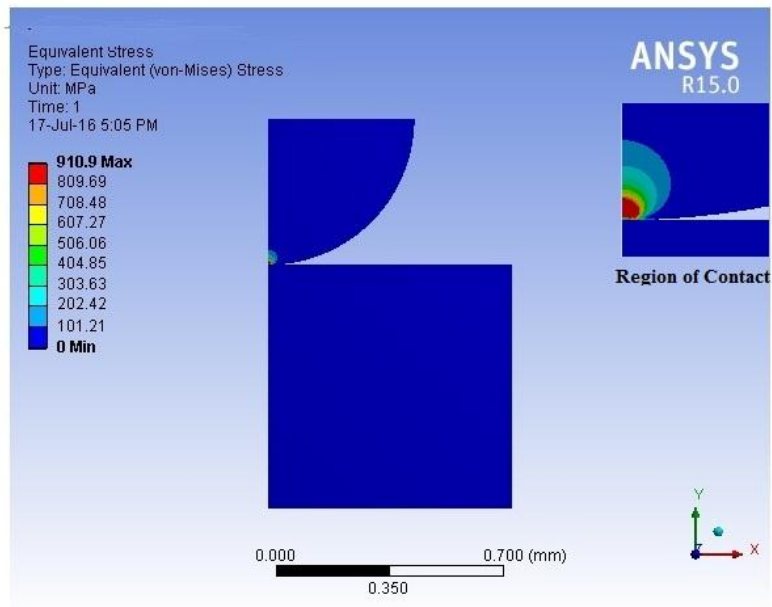


Fig 4.11 Equivalent stress assuming bilinear elastic-plastic model  
 (Zoomed in view at the region of contact is shown in inset)



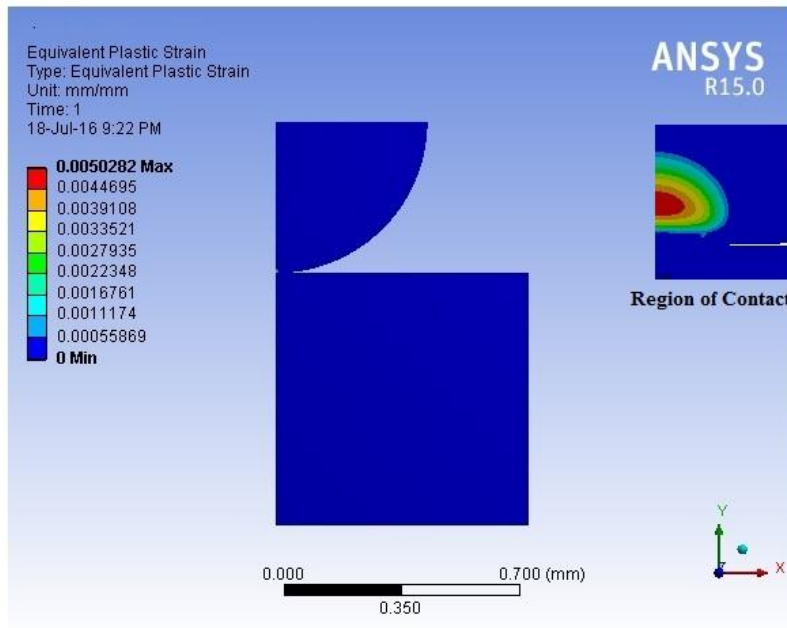


Fig. 4.12 Equivalent plastic strain assuming bilinear elastic-plastic model (Zoomed in view at the region of contact is shown in inset)

As indicated before, the variation in dissipated plastic strain energy results in the potential for stress assisted diffusion. The 3D mesh plot representing the dissipated plastic strain energy over the region of interest is shown in Fig. 4.13.

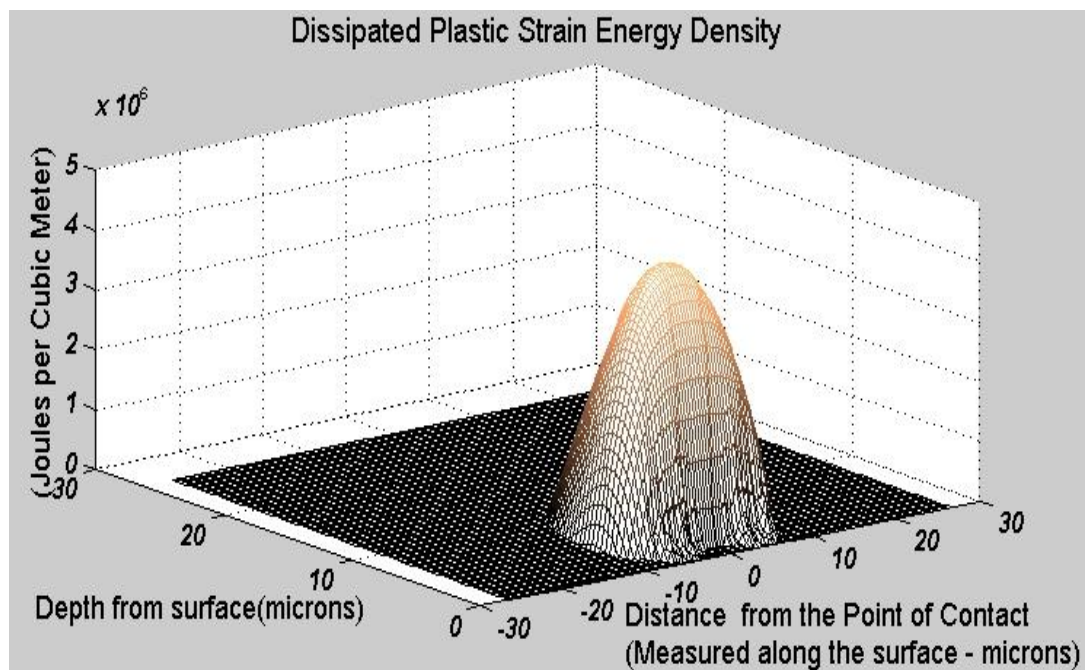


Fig. 4.13 Dissipated plastic strain energy density.

The points on the surface at distances from -26.5 to + 26.5 microns from the point of contact, as shown in Fig. 4.8, are given on the X axis and the depth of 26.5 microns is represented on the Y axis. The third axis represents the relative values of potential,  $V$ . The plot of the variation of dissipated plastic strain energy with the depth from surface of contact, along the axis, is shown in Fig. 4.14 and the vector plot showing the potential gradient is shown in Fig. 4.15.

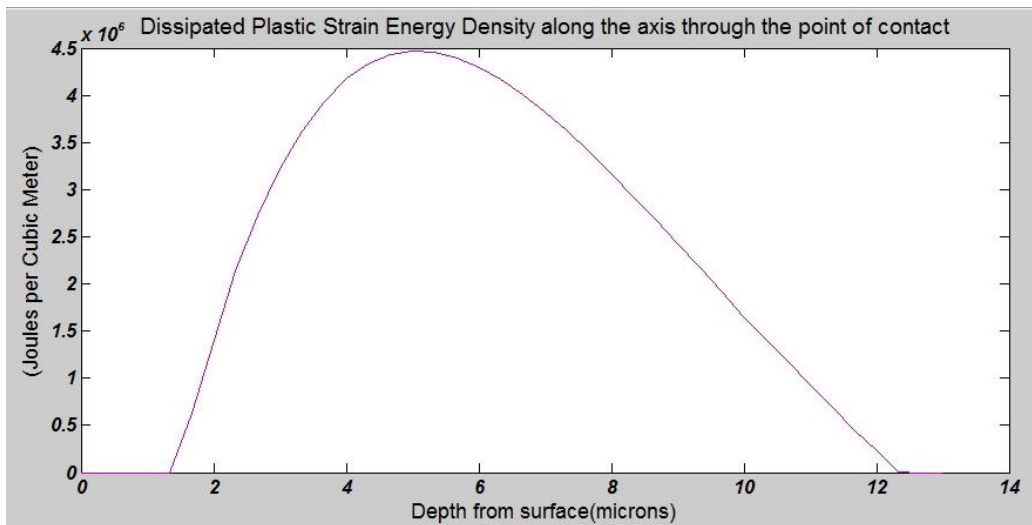


Fig. 4.14 Dissipated plastic strain energy density along Y axis through the point of contact. (Skewness is 0.0128 and kurtosis is 1.8044)

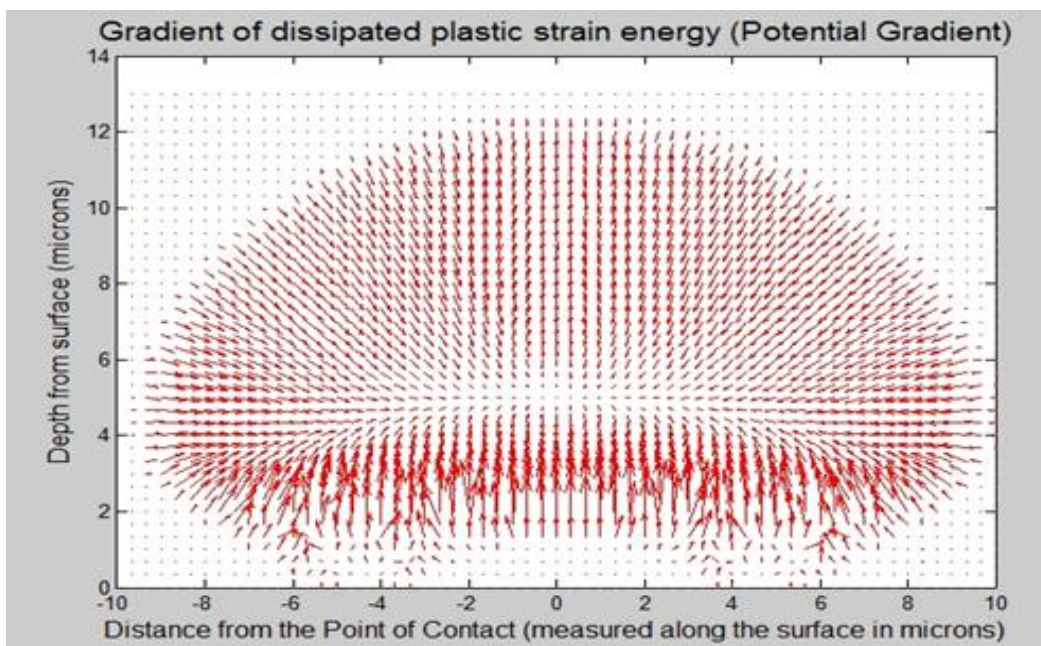


Fig. 4.15 Vector plot showing Potential gradient at 50N

The mesh plot of the Laplacian of the potential gradient in the region of interest is shown in Fig. 4.16.

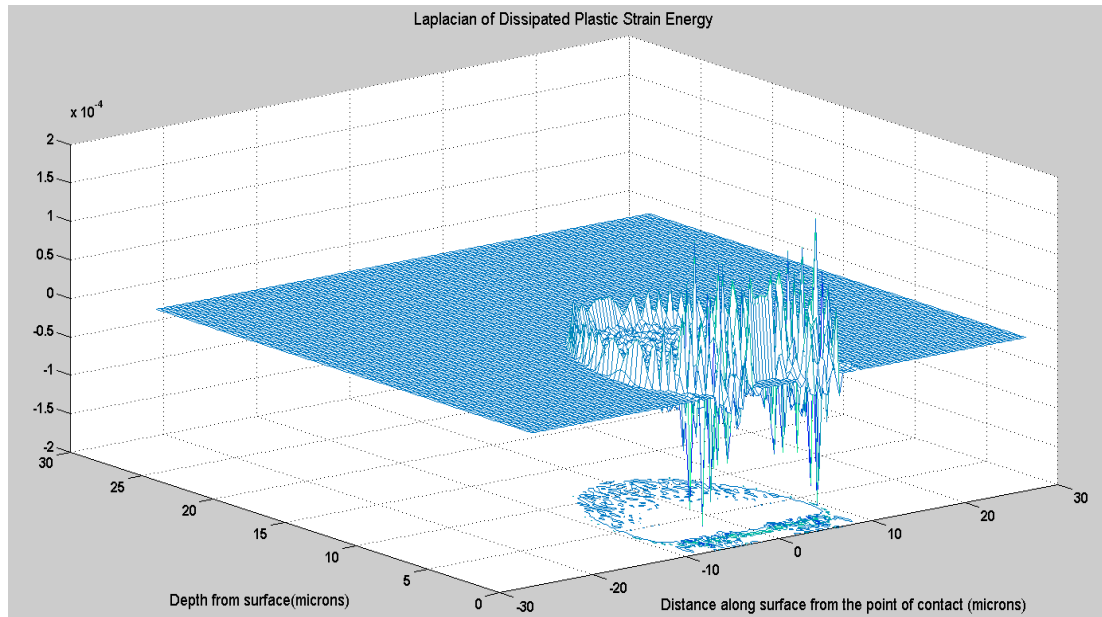


Fig. 4.16 Laplacian of the potential gradient.

Similar to Fig. 4.13, the points at a distance of -26.5 to +26.5 microns from the point of contact is represented on the X axis and the depth of 26.5 microns on the Y axis. The third axis represents the values of the Laplacian of dissipated strain energy density. The 2D contour plot showing the Laplacian of the potential gradient is also shown in the same figure.

Similarly the 3D Mesh plot along with the contour plot of the carbon concentration at the diffusion affected region after  $10^7$  cycles is shown in Fig. 4.17 and the corresponding vector plot, showing the gradient of carbon concentration in Fig. 4.18. The simulations are done assuming a temperature of  $30^{\circ}$  C. The 3D plots are generated in appropriate scales considering the maximum and minimum values of concentration and hence the scales may not be identical for all figures. The diffusion corresponding to all the conditions considered here occur within a region

of 26.66 microns  $\times$  13.33 microns (corresponding to 80  $\times$  40 gridlines). Hence the figures that follow are confined to this region for better clarity, rather than the entire region of interest. The statistical estimates discussed below are also based on this region.

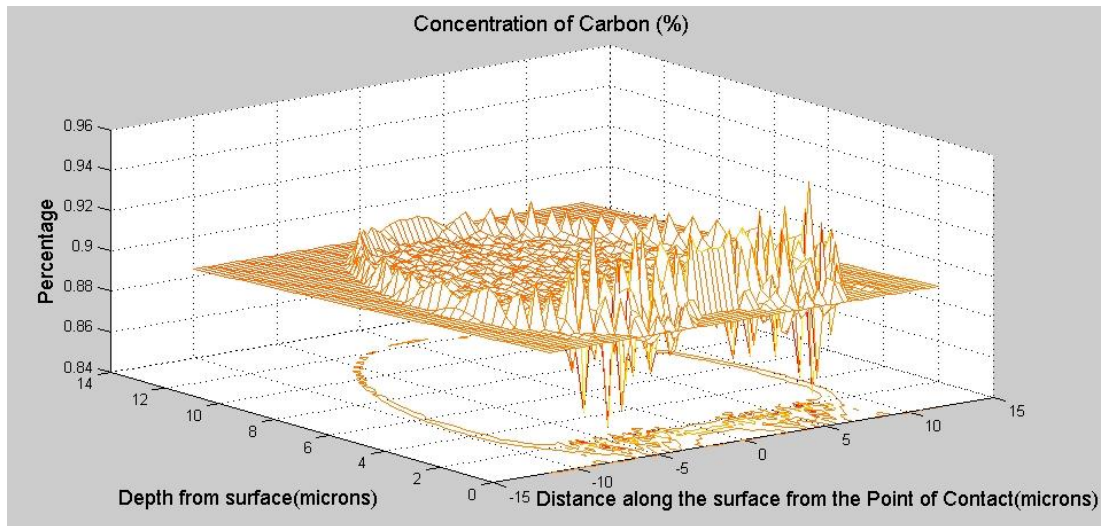


Fig. 4.17 3D plot of carbon concentration for 50N load after  $10^7$  cycles (at 30° C)

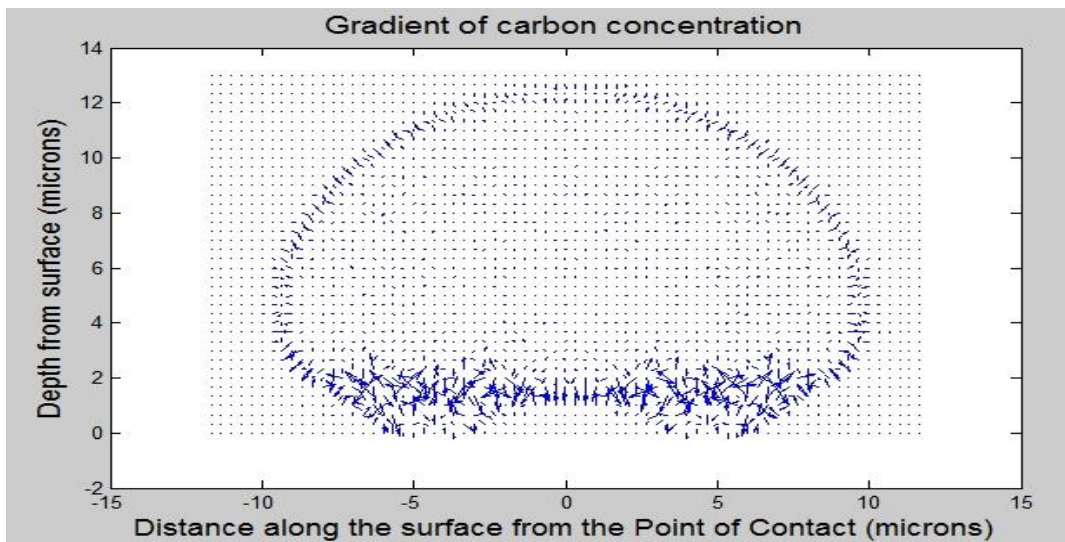


Fig. 4.18 Gradient plot of carbon concentration for 50N load after  $10^7$  cycles

The maximum and minimum nodal carbon concentrations corresponding to the above parameters (50N gripper load and  $10^7$  cycles) are 0.9525% and 0.8496% respectively resulting in a range of 0.1029 percentage points and a standard deviation of 0.0069.

3D mesh and contour plots of the carbon concentration at the diffusion affected region after a longer duration of  $10^8$  cycles under the same load and temperature is shown in Fig. 4.19 and the corresponding vector plot, showing the gradient of carbon concentration in Fig. 4.20.

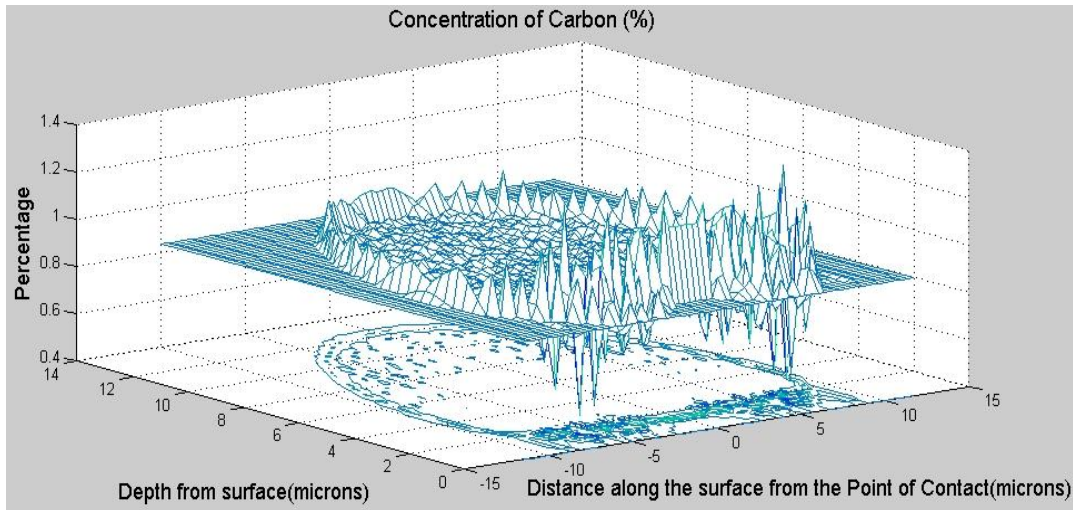


Fig. 4.19 3D plot of carbon concentration for 50 N load after  $10^8$  cycles

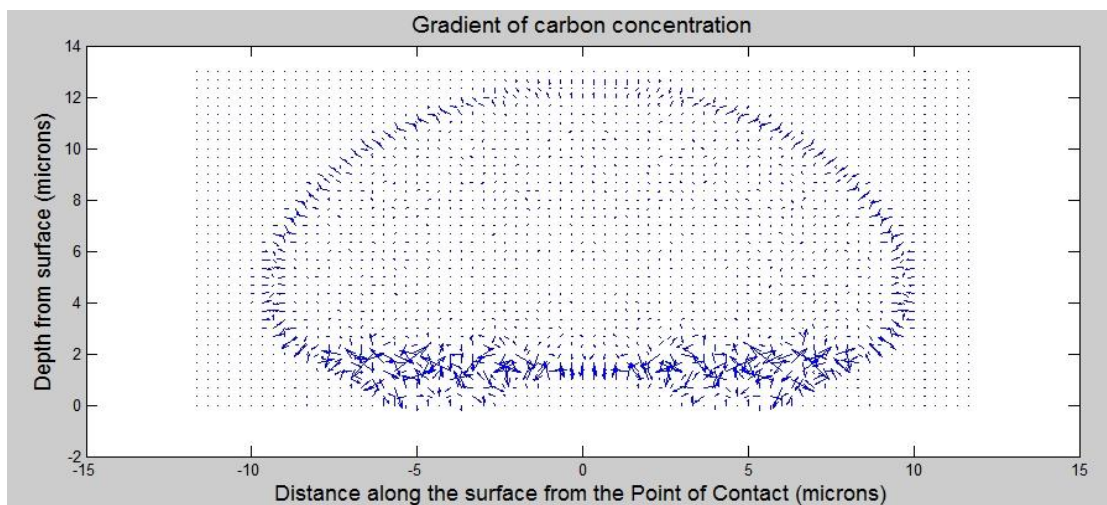


Fig. 4.20 Gradient plot of carbon concentration for 50 N load after  $10^8$  cycles

The corresponding maximum and minimum nodal carbon concentrations are 1.3837% and 0.4788% respectively resulting in a range of 0.9049 percentage points and a standard deviation of 0.0594.

3D mesh and contour plots of the carbon concentration at the diffusion affected region after  $10^8$  cycles with 40N gripper load is shown in Fig. 4.21 and the corresponding vector plot, showing the gradient of carbon concentration in Fig. 4.22.

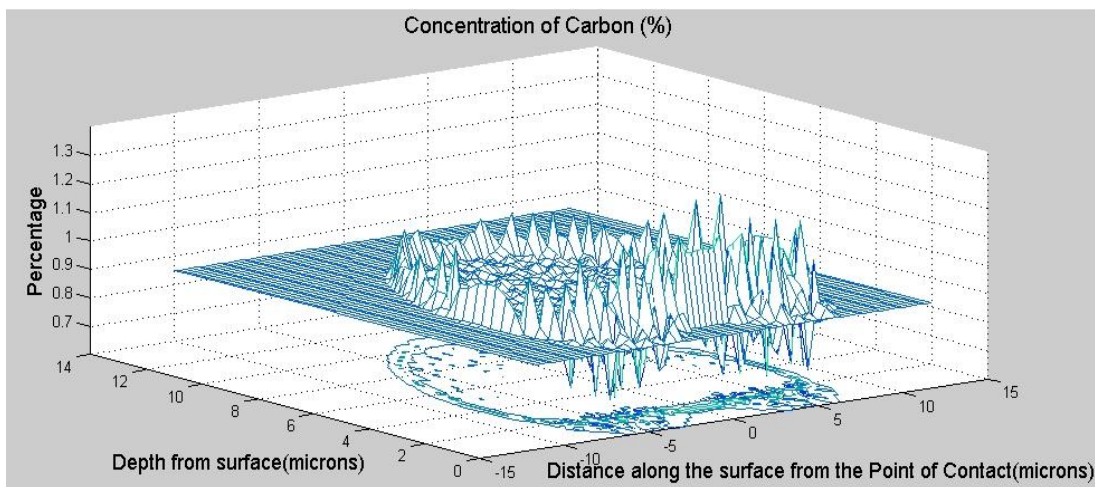


Fig. 4.21 3D plot of carbon concentration for 40 N load after  $10^8$  cycles

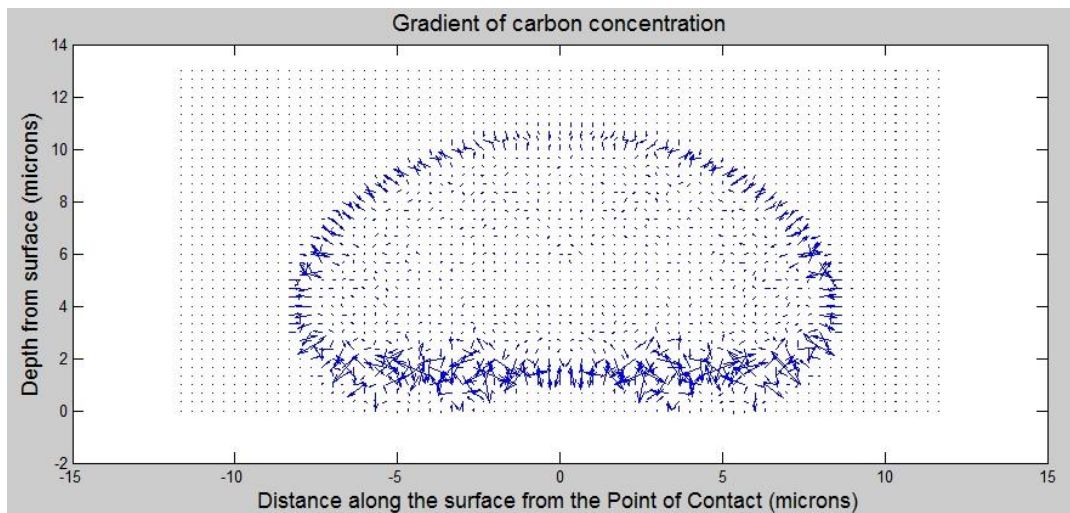


Fig. 4.22 Gradient plot of carbon concentration for 40 N load after  $10^8$  cycles

All the conditions of Fig. 4.21 and Fig. 4.22 are similar to Fig. 4.19 and Fig. 4.20 except that the load corresponding to Fig. 4.21 and Fig. 4.22 are of a lower value.

The corresponding maximum and minimum nodal carbon concentrations are 1.2306% and 0.6663% respectively resulting in a range of 0.5643 percentage points and a standard deviation of 0.0464.

3D mesh and contour plots of the carbon concentration at the diffusion affected region at a gripper load of 50N and for of  $10^7$  cycles at 20° C, 40° C and 50° C are shown in Fig. 4.23, Fig. 4.25, Fig. 4.27 and the corresponding vector plot, showing the gradient of carbon concentration in Fig. 4.24, Fig. 4.26 and Fig. 4.28 respectively. All the conditions of Fig. 4.23, Fig. 4.24, Fig. 4.25, Fig. 4.26, Fig. 4.27 and Fig 4.28 are same as those in Fig. 4.17 and Fig 4.18 except the temperature.

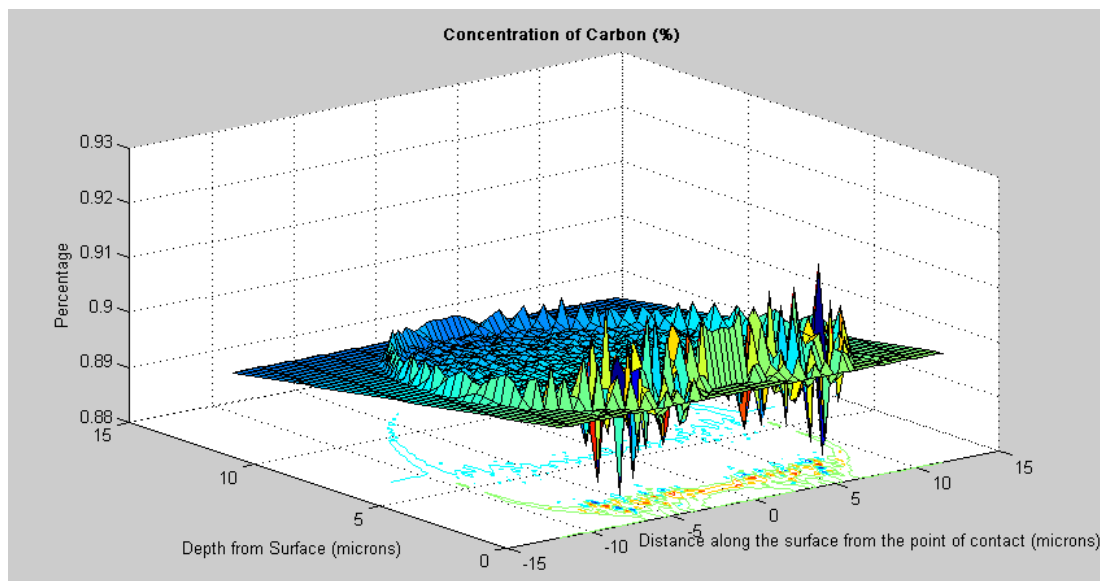


Fig. 4.23 3D plot of carbon concentration for 50 N load after  $10^7$  cycles, at 20° C

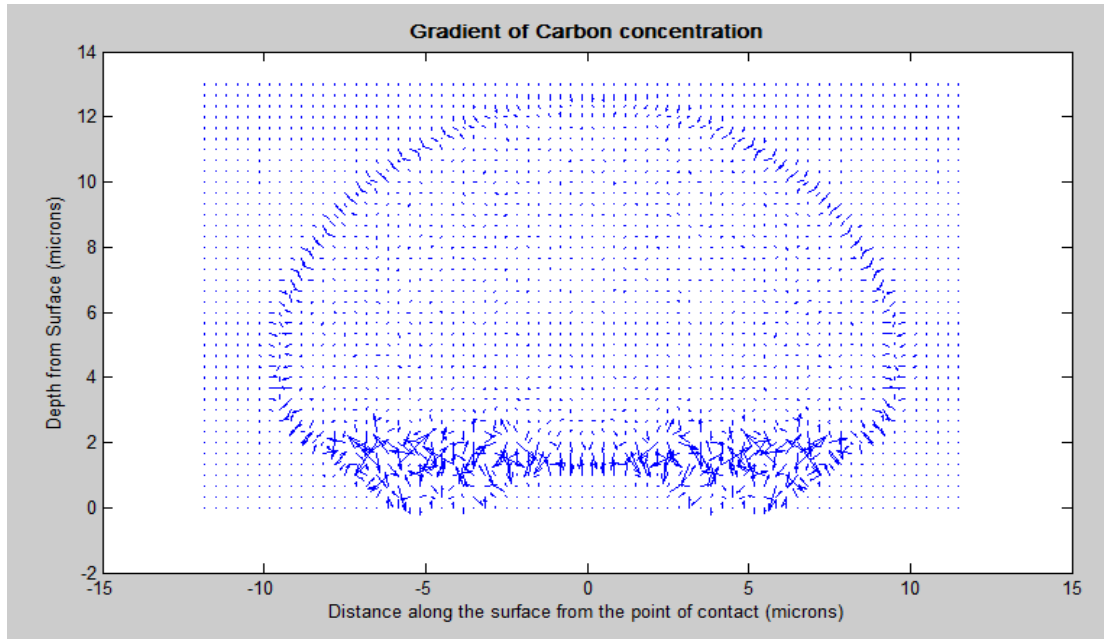


Fig. 4.24 Gradient plot of carbon concentration for 50 N load after  $10^7$  cycles at  $20^\circ\text{C}$

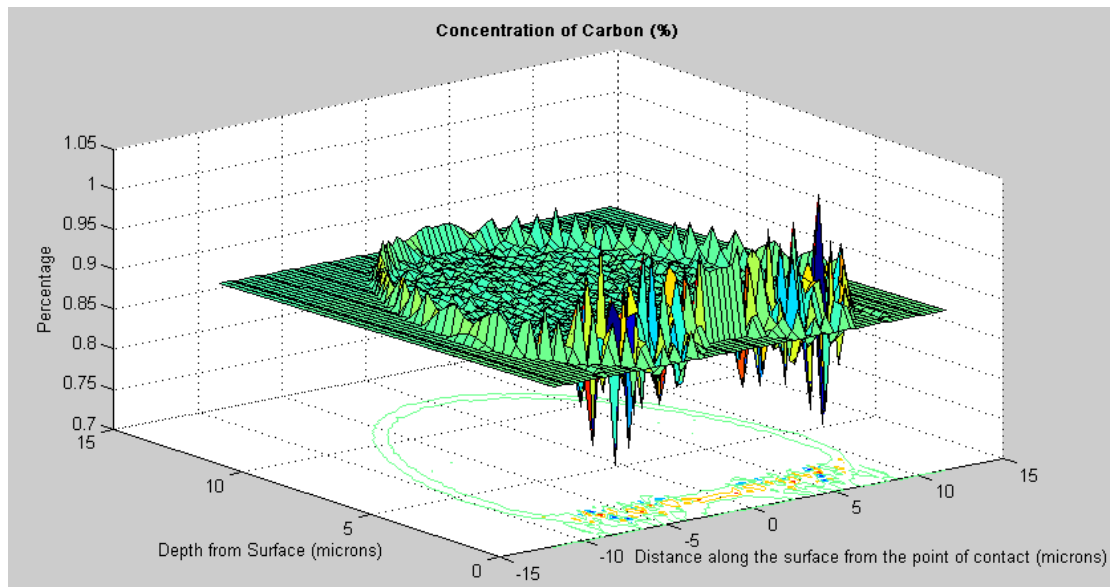


Fig. 4.25 3D plot of carbon concentration for 50 N load after  $10^7$  cycles, at  $40^\circ\text{C}$



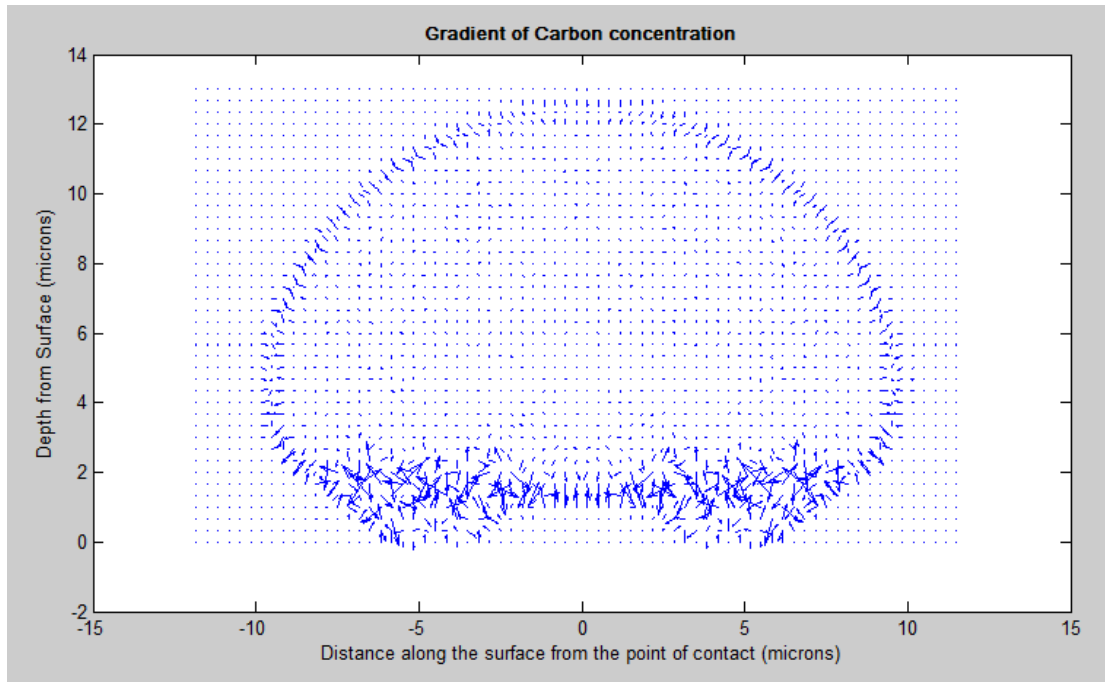


Fig. 4.26 Gradient plot of carbon concentration for 50 N load after  $10^7$  cycles at  $40^\circ\text{C}$

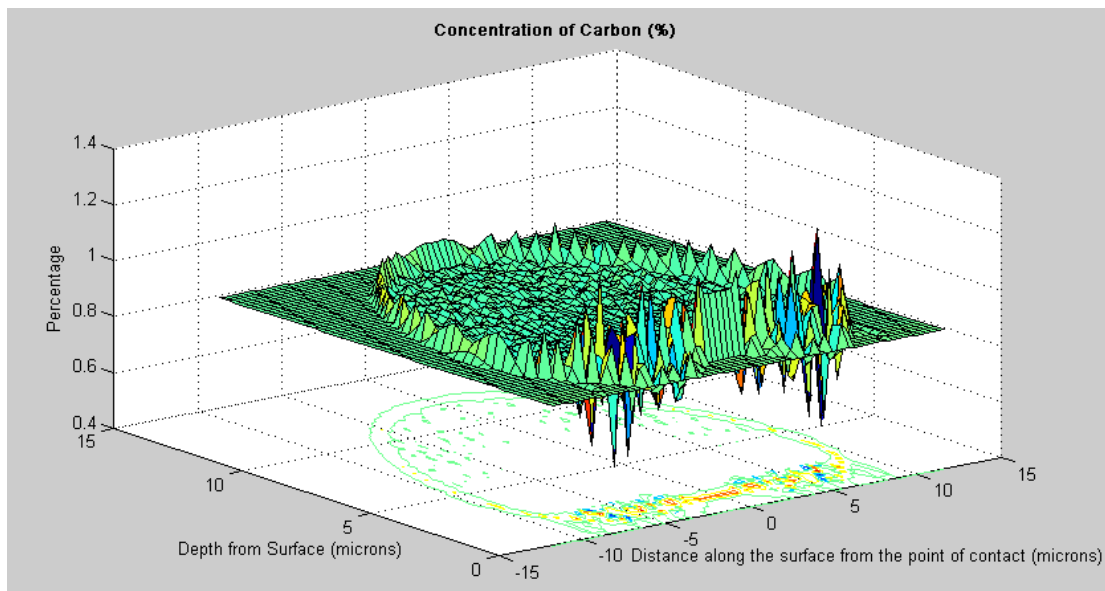


Fig. 4.27 3D plot of carbon concentration for 50 N load after  $10^7$  cycles, at  $50^\circ\text{C}$

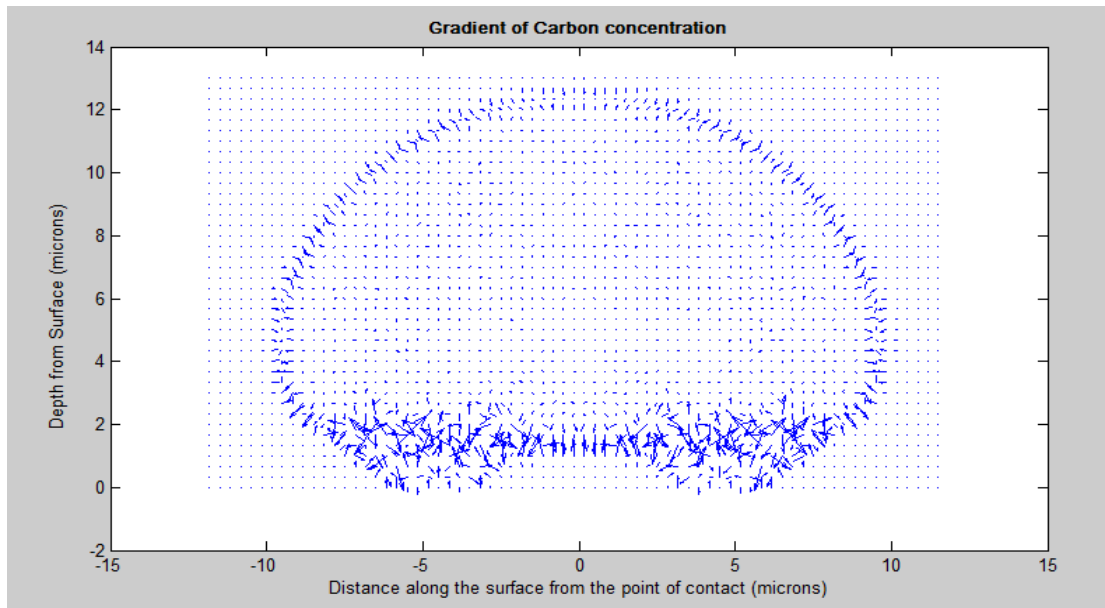


Fig. 4.28 Gradient plot of carbon concentration for 50 N load after  $10^7$  cycles at  $50^\circ\text{C}$

The maximum and minimum nodal carbon concentrations are 0.9167% and 0.8824% for Fig. 4.23 and Fig. 4.24 respectively resulting in a range of 0.0343 percentage points and a standard deviation of 0.0035 at  $20^\circ\text{C}$ . The corresponding maximum and minimum nodal carbon concentrations at  $40^\circ\text{C}$  are 1.0467% and 0.7647 % respectively resulting in a range of 0.2820 percentage points and a standard deviation of 0.0167 and the corresponding maximum and minimum nodal carbon concentrations at  $50^\circ\text{C}$  are 1.2685% and 0.5739% respectively resulting in a range of 0.6946 percentage points and a standard deviation of 0.0420. The minimum and maximum nodal concentrations under the same load and cycles at different temperatures are plotted in Fig. 4.29 and the variation of the range (difference between maximum and minimum values of carbon concentration) with temperature is shown in Fig. 4.30. The average concentration of carbon is 0.895% and is unaffected by the variation in temperature. The change in standard deviation of the carbon concentration with temperature is shown in Fig. 4.31.

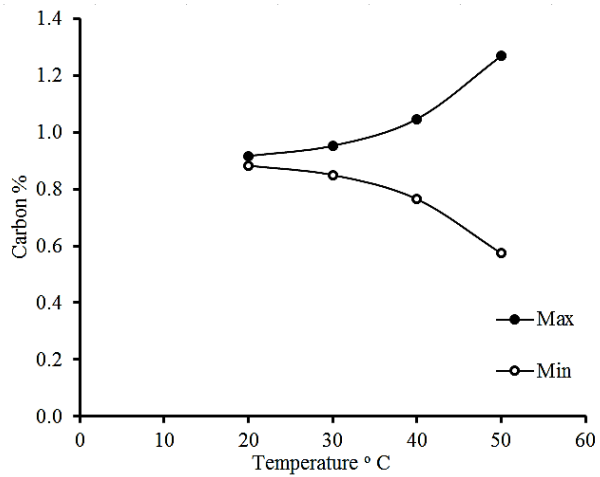


Fig. 4.29 Maximum and minimum carbon concentrations after stress assisted diffusion due to cyclic contact stress at different temperatures.

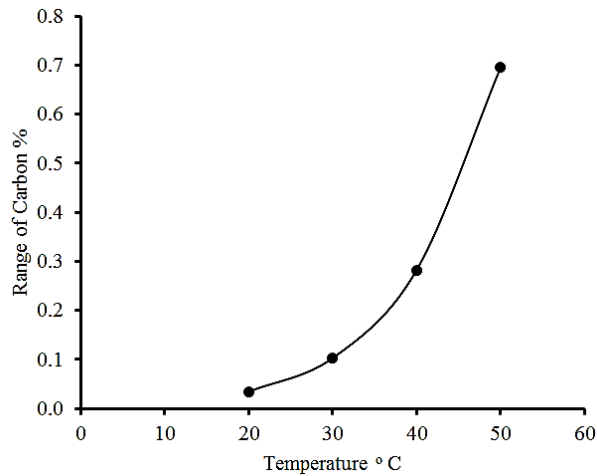


Fig. 4.30 Range of carbon concentration (difference between maximum and minimum values) after stress assisted diffusion at different temperatures.

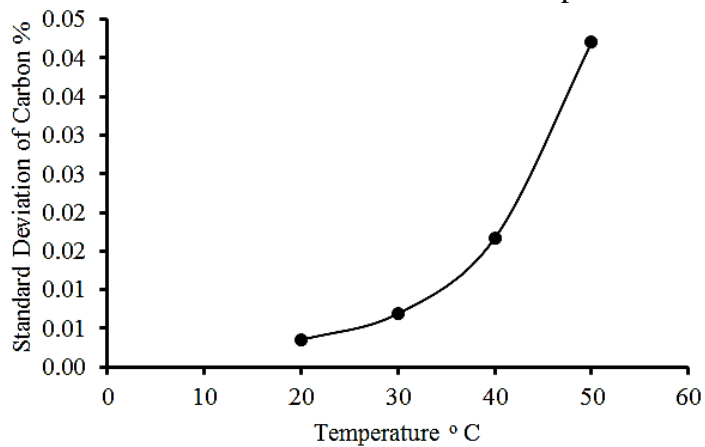


Fig. 4.31 Standard deviation of carbon concentration after stress assisted diffusion at different temperatures

#### 4.6 DISCUSSION ON THE RESULTS OF SIMULATION

The von Mises stress plot obtained in the pilot finite element analysis assuming pure elastic analysis to validate the methodology is shown in Fig. 4.10. The maximum von Mises stress obtained from the FE analysis is approximately 15% less than the results obtained as per the classical Hertzian theory of non-adhesive elastic contact. Considering the assumptions of Hertz theory this difference is reasonable and thus validates the FEA procedure.

The contour plots of equivalent stress and equivalent plastic strain for the elastic plastic analysis are shown in Fig. 4.11 and Fig. 4.12. The maximum equivalent stress has a lower value of 910.9 MPa in the elastic plastic analysis compared to the pure elastic analysis. This is expected since in the elastic plastic analysis, (as well as in the actual case) the yielding occurs at 869 MPa. Beyond the yield point, the characteristic curve is the hardening modulus, which is having a lower slope compared to the elastic modulus as can be seen from the line OABC in Fig. 4.7.

The dissipated plastic strain energy density in Fig. 4.13 is the source of potential gradient for stress assisted diffusion. The vector plot in Fig. 4.15 shows the gradient of dissipated plastic strain energy which is the potential gradient for stress assisted diffusion. The direction of arrows show the direction of gradient and the arrow size is proportional to the magnitude of the gradient. The potential gradient exists over a width of about 20 microns symmetrical to the point of contact and upto a depth of about 12 microns from the surface of contact for the given boundary conditions. The distribution is symmetrical to the Y axis. This is expected as the center of the point of contact is at the origin of the coordinate system and the Hertzian load is acting along the Y axis. The dissipated plastic strain energy reaches maximum value on a point at a

depth of approximately 5 microns from the surface, on the line perpendicular to the surface, passing through the point of contact (Fig. 4.13 and Fig. 4.14) and the potential gradient reach minimum values at same point (Fig. 4.15).

The 3D mesh and contour plots of carbon concentration is shown in Fig. 4.17. The peaks and valleys in carbon concentration within the diffusion affected region are indicated by the plot. This result in the clustering of carbon near the surface of the serrations, which is similar to the clustering of carbon and the corresponding martensite decay, resulting in dark and white bands reported for the bearing raceway (Mitamura *et al.*, 2007; Warhadpande *et al.*, 2014)

The 3D mesh and contour plots of the Laplacian of dissipated plastic strain energy shown in Fig. 4.16 has striking similarity to the 3D mesh and contour plots of carbon distribution plots like Fig. 4.17 etc. highlighting its influence on stress assisted diffusion.

It is interesting to note from Fig. 4.13, Fig. 4.14 and Fig. 4.17 that the regions of highest dissipated plastic strain energy has the lowest carbon diffusion. Fig. 4.13 and Fig.4.14 shows that the value of potential gradient is zero at the point of contact and it is skewed towards the surface of contact. The skewed shape implies more slope on one side and hence more diffusion of carbon on the skewed side as in Fig. 4.17 to Fig. 4.28.

It is attempted to quantify the redistribution of carbon in using following parameters,

1. Spread of redistribution - Defined by the area of the rectangle circumscribing the diffusion affected region in the XY plane.
2. Intensity of redistribution - The Range and Standard deviation of the carbon concentration in the diffusion affected region.

These measures are used to compare the amount of carbon redistribution due to stress assisted diffusion under different conditions.

Since stress assisted diffusion is caused by the potential gradient of plastic strain energy, the dimensions of diffusion affected region need not change when the gripper is operated for more number of cycles. Also it is logical to expect increased diffusion when the gripper is operated for more cycles as it is subjected to more stress cycles during the process. Fig. 4.17 and Fig. 4.18 correspond to  $10^7$  cycles and Fig. 4.19 and Fig. 4.20 corresponds  $10^8$  cycles respectively. As expected, the dimensions of the region of diffusion is unaffected by the number of cycles and are same as for all the four figures. The diffusion affected region is about 20 microns wide and 13 microns deep resulting in a spread of 260 square microns, for both cases. But the range of carbon concentration increased from 0.1029 to 0.9049 and the standard deviation of carbon concentration at the diffusion affected region increased from 0.0069 to 0.0594 as the number of cycles increased from  $10^7$  to  $10^8$ . In short, the intensity of redistribution increases and spread remains unchanged by the increase in number of cycles.

Fig. 4.19 and Fig. 4.20 correspond to load of 50 N, and Fig. 4.21 and Fig. 4.22 correspond to 40N. All other conditions are the same. Since the load acting is of lower value the plastic energy will be dissipated over a smaller area and hence the diffusion affected region will also be smaller. Since the values of the dissipated plastic strain energies are lower for lower load, the amount of diffusion also should be lower. The circumscribing rectangle of the diffusion affected region for 50N load as in Fig. 4.19 and Fig. 4.20, is about 20 microns wide and 13 microns deep resulting in a spread of 260 square microns whereas that for the lower load of 40N in Fig. 4.21 and Fig. 4.22

is about 17 microns wide and 11 microns deep resulting in a spread of 187 square microns. The range and standard deviation of carbon concentration corresponding to 40N are also lower than that corresponding to 50N load. Thus the change of the load results in corresponding change in both spread and intensity of diffusion as expected.

Fig. 4.23 and Fig. 4.24 shows the results corresponding to a temperature of 20° C, Fig. 4.17 and Fig. 4.18 correspond to 30° C, Fig. 4.25 and Fig. 4.26 correspond to 40° C and Fig. 4.27 and Fig. 4.28 correspond to 50° C. All other conditions like load, and number of cycles are same for all these cases. Since the range of temperature is only from 20° C to 50° C the effect of temperature on the mechanical properties like yield strength and elastic modulus is negligible (Chen *et al.*, 2006). Also as per Eurocode 3 (2005) the variation of  $S_y$  and  $E$  with temperature can be neglected upto 100°C (Kodur *et al.*, 2010). Since  $E$  and  $S_y$  are assumed to be same, the distribution of dissipated plastic strain energy density will be as in Fig. 4.13 in all these cases. The circumscribing rectangle of the diffusion affected region for different temperatures as can be seen from Fig. 4.18, Fig. 4.24, Fig. 4.26 and Fig. 4.28 are all same at about 20 microns wide and 13 microns deep resulting in a spread of 260 square microns as expected. However, the coefficient of diffusion,  $D$  increases with temperature as per equation (4.4) and hence the intensity of diffusion increases due to increase in temperature. This can be observed from Fig. 4.23, Fig. 4.17, Fig. 4.25 and Fig. 4.27. The change in intensity of diffusion with temperature is quantified and plotted in Fig. 4.29, Fig. 4.30 and Fig. 4.31. Thus the change of the temperature results in corresponding change in the intensity of diffusion as expected.

## 4.7 CONCLUSIONS

Modeling of stress assisted diffusion of carbon due to contact stress in steel grippers is conducted for the first time. The dissipated plastic strain energy which acts as the potential gradient for stress assisted diffusion is coupled with the concentration gradient for modeling the same. It is found that the elastic gradient created due to the high contact stress and its Laplacian has profound effect on the diffusion of carbon atoms compared to the concentration gradient. This in turn results in redistribution and clustering of carbon atoms near the surface of the serrations which can promote wear due to martensitic decay. The clustering of carbon near the surface of serration is verified by the FESEM with EDS micrograph of the sectional plane along the axis of serration.

Parameters for quantifying the redistribution of carbon in steel viz., spread and intensity are introduced. It is found that increasing the number of cycles results in increased intensity of redistribution without affecting the spread and increasing load will increase both spread and intensity of redistribution. Increased temperature will not have a significant effect on spread but will result in increased intensity.

In the next chapter, the feasibility of replacing serrated steel grippers with impactive grippers with an inexpensive and easily replaceable lining material like silica reinforced nitrile butadiene rubber (NBR), for applications like SFOPM are explored.



## CHAPTER 5

### FEASIBILITY OF SILICA LOADED NBR AS LINING MATERIAL FOR IMPACTIVE GRIPPER

#### 5.1 INTRODUCTION

Grippers in general can be ingressive or impactive (Monkman *et al.*, 2007). Ingressive grippers grasp the object by physically penetrating the surface of the object while impactive grippers grasp the object without physically penetrating the surface of the object. Ingressive gripping is not preferred in some applications as it can damage the grasped object. Ingressive grippers usually offer better grasp, but impactive grippers minimize the possibility of damage to the grasped object as there is no physical penetration. Thus impactive grippers that do not permeate into surface of grasped object have an advantage over ingressive grippers in some applications (Monkman *et al.*, 2007).

As an application, let us again consider the cylinder grippers of a sheet fed offset printing machine. Ingressive grippers, made of metallic jaws with serrations are commonly used in SFOPM. A firm grip is required to retain the positional accuracy of paper during the process and a gentle grip is preferred to avoid any marks or damage to the paper. The possibility of replacing ingressive grippers of metallic jaws with serrations, which permeate into the paper surface, with soft impactive grippers having high friction is explored in this chapter. Materials like NBR, with high coefficient of friction is a promising choice for making linings for such impacting gripping surfaces. Also NBR lining is more economical than metallic serrated tips and will not cause any marks even on very thin papers. Another advantage is that NBR can be made as thin gauge sheets and easily bonded to metallic surfaces.

### 5.1.1 Objectives and background

The feasibility study was conducted to assess the suitability of NBR as a lining material for impactive grippers. This study is important since certain materials like papers and polymers require highly precise and sensitive impactive gripping. In certain applications it may be possible to replace ingressive grippers with impactive grippers made of soft materials with high coefficient of friction.

The static coefficient of friction of NBR loaded with silica, when paired with different types of papers commonly used for offset printing, like Art paper, Maplitho, Executive bond, Color wove, Crème wove, Cover paper, Ledger and Grey board are explored in this chapter. The variation in mechanical properties of NBR, like hardness, tear strength, tensile strength, elongation at break, oil resistance etc. with the addition of silica fillers and the changes in these properties due to ageing are also investigated. These studies were conducted on NBR loaded with 45 phr to 65 phr of silica and the period taken for study of ageing is 18 months. SEM studies were also conducted to examine the surface of samples.

A higher coefficient of friction of gripper surface will result in a better grip on the paper. Hence the static coefficient of friction with paper is one of the desirable properties of the gripping surface / lining material for paper grippers. Since the application calls for contact with paper, carbon black was not considered as a filler material to prevent the possibility of any black stains on the paper handled (Wang *et al.*, 2006). High static friction and good mechanical properties are desirable in the context of lining for impactive grippers.

Fillers are added to NBR to improve its mechanical properties. The influence of filler content on the mechanical properties of reinforced elastomers has been extensively

reported in the literature (Fultz *et al.*, 1998; Schwaiger and Blume, 2000; Bachmann *et al.*, 1959; Wolff., 1996; Donnet, 1998; Treloar, 2005; Mostafa *et al.*, 2009). The hardness of NBR increases with addition of silica. Since a higher hardness is preferred for such applications, the study was focused in the region of 45 to 65 phr. The change of mechanical properties of NBR loaded with silica, due to ageing is seldom reported. The durability of the material is an important criterion in the selection of materials and hence it needs to be understood. Hence the effect of natural ageing on mechanical properties of NBR was explored.

Many studies have been conducted on friction of NBR and other elastomers (Donnet, 1998; Felhos *et al.*, 2008; Karger-Kocsis *et al.*, 2008; Sirinthorn Thongsang, *et al.*, 2012; Huang X *et al.*, 2007; Xu D. *et al.*, 2009; Palfi L. *et al.*, 2009). Investigations by Felhös *et al.* (2008) and Karger-Kocsis *et al.* (2008) on the dry sliding friction between steel and rubber showed that the coefficient of friction (COF) of EPDM rubbers gets reduced with increasing carbon black content in rubber. Studies by Thongsang *et al.*, (2012) have shown that the co-efficient of friction of NR when paired with stainless steel increases with the addition of silica, but the study was limited to NR with silica content upto 40 phr (parts per hundred rubber). Many studies are also available on paper to paper friction and on paper to steel friction (Back, 1991; Garoff *et al.*, 2004). However no literature on the friction of NBR to paper is available and needs to be determined. Since friction plays a crucial role in applications as discussed above, the coefficients of static friction of the samples when paired with different types of paper were determined.

## 5.2 EXPERIMENTAL

### 5.2.1 Materials

NBR having acrylonitrile content-33%, Mooney viscosity [ML (1 + 4) at 100 °C] of 40.9 was used for the study. Compounding ingredients, i.e., zinc oxide, stearic acid, dioctyl phthalate (DOP), silica, and sulfur, were of commercial grade. The mating materials used for evaluation of static frictional co-efficient were various types of offset printing papers viz. art paper, maplitho, executive bond, color wove, crème wove, cover paper, ledger and grey board.

### 5.2.2 Preparation of Samples

In this study, different quantities of silica powder fillers were added to NBR rubber in five samples from 45 to 65 phr. The NBR was compounded in a laboratory on a 15.25mm × 30.5 mm (6" × 12") two roll mixing mill according to formulations given in Table 5.1. The optimum cure times of the compounds were determined on RPA 2000. NBR compounds were molded in an electrically heated hydraulic press at a temperature of 150°C up to their optimum cure times at a pressure of 200 kg/cm<sup>2</sup>.

Table 5.1 Formulation of mixes (in phr)

Mix	A	B	C	D	E
NBR(medium Nitrile)	100	100	100	100	100
Sulfur	1.5	1.5	1.5	1.5	1.5
ZnO	4.0	4.0	4.0	4.0	4.0
Stearic acid	2.0	2.0	2.0	2.0	2.0
Precipitated Silica	45	50	55	60	65
DOP	5	5	5	5	5
CBS	1.0	1.0	1.0	1.0	1.0
TMTD	0.2	0.2	0.2	0.2	0.2

### 5.2.3 Tests

Static coefficients of friction for the five samples on the various types of papers mentioned above were determined as per ASTM D 1894- 01 using friction/slip apparatus. The rubbing face of the moving sled of the friction/slip apparatus was covered with one type of paper, say art paper, using cellophane tape. One sample of the NBR sheet, say sample A (with 45phr silica), was held stationary and the corresponding static coefficient of friction was determined. The first sliding was done in one direction and the subsequent three sliding in the opposite direction. The first value was ignored and the average of the last three readings was taken for each combination. The experiment was repeated with sheets of the remaining four samples of NBR and the same sled (covered with art paper).The whole experiment was again repeated with the moving sled covered with each type of paper, viz. maplitho, executive bond, color wove, crème wove, cover paper, ledger and grey board. The values of static frictional coefficients of each combination were noted. All the experiments were conducted at a relative humidity of 78%. The coefficients of friction for the different samples with various types of paper are thus determined.

SEM studies were also done on the surfaces of relevant samples. SEM model JSM-6390LA (JEOL Ltd., Tokyo, Japan) was used for the purpose.

For finding the tensile strengths, dumbbell-shaped tensile test pieces were punched out of the compression-molded sheets along the mill-grain direction. The tensile properties were determined on a Zwick Universal Testing Machine as per ASTM D412 - 06a (2013). Abrasion resistance was tested using a DIN abrader according to DIN 53516. The Shore hardness of the samples was measured and expressed in Shore A units. Tear strength of the samples was determined as per ASTM D624 - 00(2012). Swelling index of the samples was found, using methods outlined in ASTM D471 - 12a.

Another set of samples with the same levels of silica were tested after a period of 18 months to determine the change in mechanical properties due to ageing.

### 5.3 RESULTS AND DISCUSSION

The coefficient of friction of uncoated paper may decrease with repeated slides over the same track in the same direction and may increase when sliding direction is reversed (Niklas Garoff *et al.*, 2004). Also the coefficient of friction of paper depends on relative humidity (Back, E. L., 1991; Inoue M. *et al.*, 1990; Christer Fellers *et al.*, 1998). Hence the values of the coefficients of friction are approximate and adequate factor of safety shall be used. However, since the testing was done at identical conditions of relative humidity and sliding directions as indicated before, the results can be used for a comparative study of friction between different combinations of NBR samples and papers.

The static coefficient of friction of the five samples of NBR with silica content of 45 phr to 65 phr with the various types of papers are given in Table 5.2.

Table 5.2 Co-efficient of static friction of NBR loaded with different amounts of silica, when paired with different types of paper.

Phr of Silica in sample→	45	50	55	60	65
Type of Paper↓					
Art paper	0.693	0.772	0.894	0.890	0.772
Maplitho	0.575	0.599	0.693	0.549	0.556
Executive Bond	0.490	0.500	0.486	0.486	0.458
Color wove	0.496	0.496	0.536	0.496	0.516
Crème wove	0.488	0.472	0.500	0.472	0.475
Cover paper	0.641	0.644	0.772	0.653	0.599
Ledger	0.555	0.556	0.556	0.496	0.516
Grey board	0.577	0.577	0.644	0.577	0.516

The change in friction with the amount of added silica was found to depend on the type of paper it was paired with. The results showed a maximum coefficient of friction of 0.894 for art paper and NBR with 55 phr silica. The minimum COF of 0.458 was obtained when executive bond paper was paired with NBR of 65 phr silica.

Let us consider the case of grippers on sheet fed offset printing press. Tensile forces upto 70 N act on the paper during the printing process (Kipphan *et al.*, 2001). Usually such presses will have around 10 to 15 grippers per cylinder (Fig. 3.5). The tensile force on the paper will be shared by the grippers. Assuming only 10 grippers, the maximum tensile force per gripper is  $70/10 = 7$  N. Considering the minimum COF of 0.458 and a factor of safety of 2, the gripping force required is only  $7 \times 2/0.458 = 30.6$  N. This value is obtained by assuming that only one of the two jaws, (Fig. 3.5) is provided with NBR lining and without considering the friction of the other jaw. If the other jaw is also lined, the force required can be halved to 15.3 N. The value of 30.6 N itself is found to be well within the limits of values provided by press manufactures for setting the gripper pressure and will not overload the system. Hence NBR has sufficient static friction to be used as lining material for impactive grippers in sheet fed offset press.

Lining may be provided on the gripping surface of either on one jaw or both the jaws, depending on the specific application. Lining can be implemented by bonding a small strip of silica loaded NBR to the surface of the jaw using a suitable rubber metal adhesive. In case of wear, it can be easily, quickly and economically replaced. It also has the advantage of lower noise.

Table 5.2 shows that the coefficient of friction generally increases with addition of silica reinforcement upto 55 phr and above that it started to decline. In order to

investigate this phenomenon, the samples with 55 phr silica and 65 phr silica were examined using Scanning Electron Microscope. SEM micrographs in Fig. 5.1 show the comparison of the surfaces of samples with 55 phr and 65 phr of silica respectively.

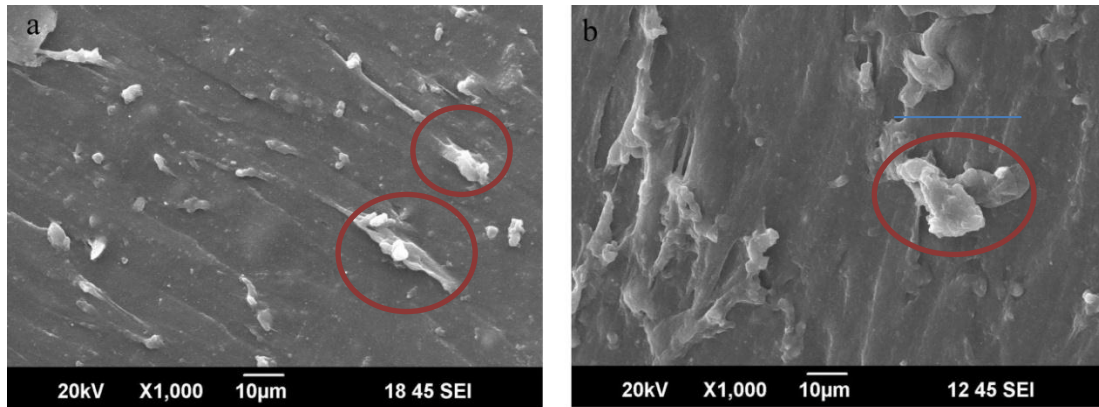


Fig 5.1 SEM micrographs of (a) NBR with 55 phr silica. (b) NBR with 65 phr silica. (Agglomeration shown in red circles)

It is observed that the large scale agglomeration of silica begins at around 55 phr and progresses as the silica content is increased beyond this point and becomes significant at around 65 phr.

Hardness is the resistance offered by the rubber surface against penetration by an indenter, and relates to the surface deformation of the rubber surface. The results are shown in Fig. 5.2.

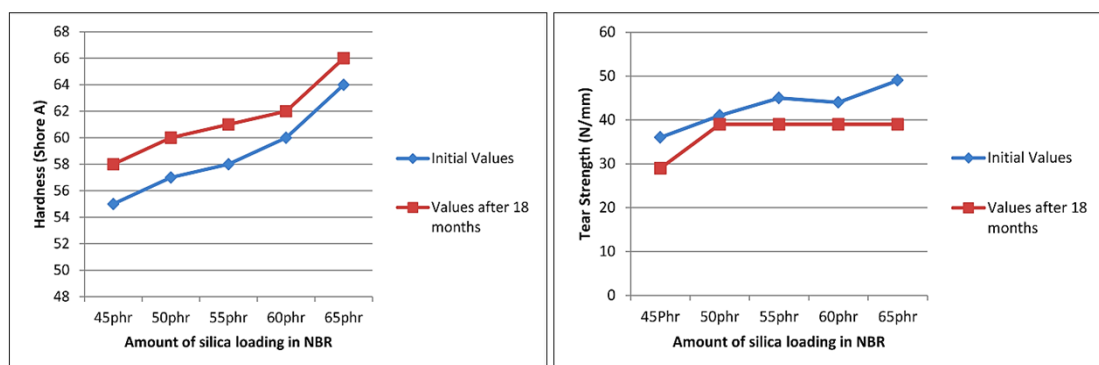


Fig. 5.2 Variations of Hardness of NBR with silica loading and natural ageing and Tear strength of NBR with silica loading and natural ageing



Comparing these five silica filler combinations, the sample with the lowest silica content of 45 phr demonstrated the lowest hardness of 54.8 Shore A and the sample with the highest silica content of 65phr in this study, demonstrated the best Shore hardness of 64.2 Shore A.

Unlike static coefficient of friction, Shore hardness increased almost linearly with addition of silica and kept on increasing beyond 55 phr. The variation of Shore hardness with addition of silica and the variation of the same after a period of 18 months are shown in Fig. 5.2. As expected, due to the marginal increase in cross-link density, the hardness also increased marginally.

The tear strength also showed a similar trend. The change in variation of tear strength of NBR with addition of silica and the variation of the same due to ageing over an 18 month period are both shown in Fig. 5.2. NBR with 65 phr and 45phr showed the highest and the lowest tear strengths of 49.35 N/m and 35.73 N/mm respectively. The tear strength showed a small deterioration on ageing.

Oxidation reduces the strength of rubber due to molecular weight degradation. However, additional crosslink formation imparted by the residual curing agents can result in increased hardness and strength (Blow and Hepburn, 1982). Thus due to environmental ageing, the crosslinking increases but rubber degrades, though marginally by oxidation. This explains increase in hardness and reduction in tear strength upon ageing.

The lining on the jaw of a paper gripper is not expected to be in contact with oil. However since paper gripper being a part of the machine, there is a chance of lubricating oil or oil based inks accidentally coming into contact with the gripper jaw. The swelling index when kept in oil showed a marginal decreasing trend with the

addition of silica reinforcement as shown in Fig. 5.3. The study showed that the resistance to oil increased with addition of silica. This is expected since an increase in the amount of filler material decreases the rubber content and hence the swelling index also decreases.

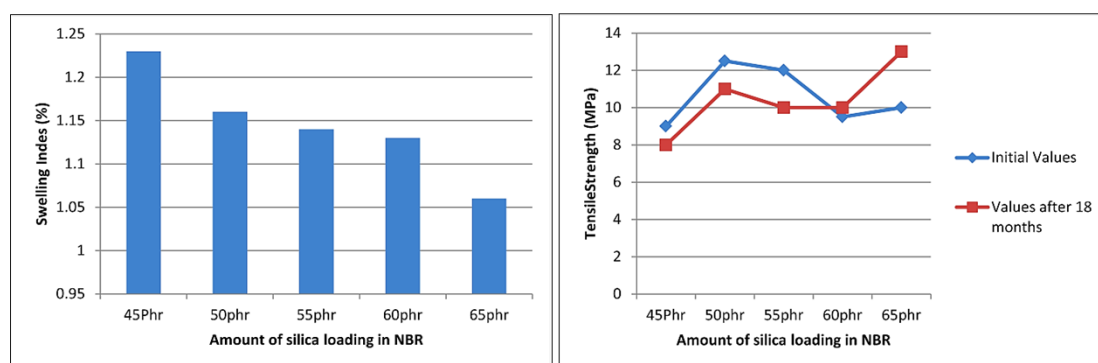


Fig. 5.3 Variations of Swelling Index of NBR in oil with silica loading and Tensile strength of NBR with silica loading and natural ageing

The tensile strength increased upto 50phr silica content and started to decline beyond this filler content (Fig. 5.3). The tensile strength showed marginal decrease due to ageing for NBR with silica upto 55 phr, but as the silica content reached 60 phr, the trend gets reversed and the tensile strength increased with ageing.

Generally tensile strength increases with filler content or crosslink density. However at higher filler content there is a possibility of formation of agglomerates. These agglomerates can act as points of weakness for initiating failures and reduce tensile strength. Also natural ageing reduces the strength of polymer due to oxidation but increases the strength due to additional cross link formation. At still higher filler content, even with agglomeration, the amount of silica may be sufficient to be distributed throughout the matrix. Thus the tensile strength is a balance of all these factors.

The abrasion loss for the various samples of NBR is shown in Fig 5.4. The lowest and highest abrasion resistance was observed at silica contents of 55 phr and 65 phr respectively. The abrasion loss increases as agglomeration sets in at around 55 phr. This is likely due to the removal of agglomerated portions as single entities. At 65 phr silica content, even with agglomeration, the amount of silica is sufficient for distribution throughout the matrix and provided sufficient strength to reduce loss due to abrasion.

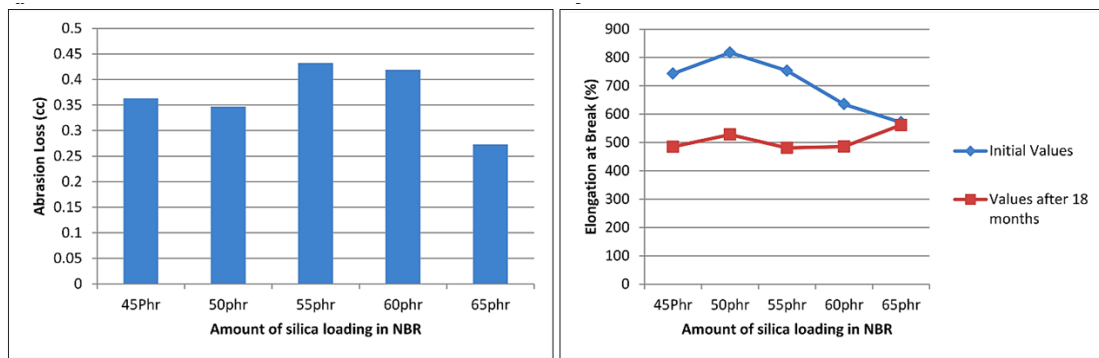


Fig. 5.4 Variations of Abrasion loss of NBR with silica loading and Elongation at break of NBR with silica loading and natural ageing.

Fig 5.4 also shows the variation of elongation at break with maximum and minimum values at silica contents of 50 phr and 60 phr respectively. The deterioration of elongation at break due to ageing decreased as silica content was increased and there was only marginal change due to ageing at 65 phr. As the rubber content becomes less, the change due to ageing also decreases.

Agglomeration gives points of weakness from where cracks can be initiated resulting in early failure and thus reduces the elongation at break. Increase in cross link density can also result in reduction of elongation at break. Ageing results in reduction of molecular weight and reduces elongation at break. Also additional crosslinking due to

residual curing agents during the ageing process can result in increased cross link density and hence lower elongation at break.

The coefficient of friction with paper is one of the most important properties to be considered in the selection of lining material for paper grippers. Higher values of mechanical properties like abrasion resistance, tensile strength, tear strength, hardness, elongation at break and lower value of swelling index in oil increases the durability of the lining material.

#### **5.4 CONCLUSIONS**

In this study, the variation of mechanical and frictional properties of NBR with addition of silica fillers was explored and the feasibility of employing it as a lining material for impactive printing grippers is established. The mechanical properties and coefficient of friction of NBR with paper can be altered by adding silica as filler material. The static frictional coefficient of NBR with most of the papers peaked at a silica content of about 55 phr. Mechanical properties like hardness, tear strength and resistance to oil increased with the amount of silica content. Agglomeration at higher filler content can results in reduction of tensile strength. The change in mechanical properties due to ageing was marginal.

## CHAPTER 6

### SUMMARY AND CONCLUSIONS

Gripper is a general name for any prehension device. In spite of its many applications in industry, from robots to printing to work-holding devices, the gripper design is almost always neglected and is not given the attention it deserves. The motivation of the study is the rapid wear and the requirement of frequent replacements of grippers in SFOPM and the dearth of literature on the subject.

In many designs, the surface of at least one of the jaws of the gripper is serrated. The serrations are provided to ensure sufficient grip while holding the part. The serrations usually result in point contact and are hence subjected to very high stress. Serrations on a printing gripper, significant for ensuring the register accuracy in sheet fed offset printing machines, also have to sustain severe contact stresses. Poorly designed serrations can have an adverse effect on its life and performance. However, literature on the design of serrations on grippers is scarce. In this study, using analytical solutions, we have developed an optimization framework that can help to quickly arrive at design solutions to maximize the durability and performance of a serrated printing gripper.

A cut section of the serrated portion of a gripper is subjected to the same cyclic stress as in the SFOPM, using a newly designed experimental setup and the carbon distribution is examined using FESEM with EDS. Clustering of carbon atoms near the surface of serrations is observed. The stress assisted diffusion of carbon atoms due to high stress cyclic loading of serrations on a case hardened steel gripper, leading to the redistribution of carbon near the surface of the serrations is modeled. An elastic

plastic finite element model coupled with modified Fick's law of diffusion is employed for the purpose. Commercial FEA software is used to model the contact of a serration and estimate the equivalent stress and equivalent plastic strain at the nodes of the FE model and these are used to calculate the dissipated plastic strain energy at the nodes of the FE model. Kinematic hardening rule is used to estimate the dissipated plastic strain energy due to the contact stress and these results are transferred to the nodes of a very fine square grid. Potential gradient due to dissipated plastic strain energy coupled with concentration gradient is employed to simulate the stress assisted diffusion of carbon near the surface of a serration on the gripper jaw. 3D and gradient plots of carbon concentration at the contact surface, after specified cycles, at different loads and at different temperatures are plotted. The contour plots of equivalent stress and equivalent plastic strain for the elastic plastic analysis are also made. Measures for quantifying the redistribution of carbon are introduced and the effect of the number of cycles, temperature and loading conditions on the redistribution of carbon in steel serrations are examined.

The feasibility of silica loaded NBR as a lining material for gripper jaw surfaces are studied and established. The effect of silica loading on the static frictional coefficient of nitrile rubber when paired with different types of papers is investigated. The influence of silica loading on the mechanical properties of nitrile rubber and its changes due to natural ageing are also examined. The change in the mechanical properties due to natural ageing varies, though marginally.

### **Directions of future work**

The simulation of carbon diffusion is conducted assuming that no carbon molecules flow from and into the gripper jaw. But this assumption may not be true in all cases.

For example, when uncoated carbon rich paper is gripped, there is a possibility of diffusion of carbon molecules between gripper surface and the paper. Further simulation and investigation can be conducted for the same.

Research can be done on the suitability of high strength / ultra high strength /duplex /super-duplex steels with or without wear resistant coatings like DLC / TiN/TiC for gripper.

Research can be done on the suitability of highly frictional surface for gripper by embedding high density of silicon carbide particles within a hard electroless nickel matrix.

## APPENDIX

### GENERAL THEORIES AND SOME RECENT DEVELOPMENTS IN DIFFUSION

Scientist	Development	Year	Remarks
Thomas Graham	<p>Conducted and published experiments in gases. Graham's law claims that the volumes of gas exchange are inversely proportional to the square root of their masses. He noticed that diffusion in liquids is by three orders of magnitude smaller than in gases and that the diffusion rate slowed down with increasing time.</p> <p>Also studied the diffusion of salt in water and the uptake of hydrogen by palladium and other metals</p>	<p>1829</p> <p>1833</p> <p>1868</p> <p>1869</p>	<p>First known quantitative study of diffusion in gases.</p> <p>Graham's work on diffusion in gases could be understood by the kinetic theory of gases developed afterwards.</p>
Adolf E. Fick	<p>Developed a mathematical framework to describe the phenomena of diffusion using results of Graham's experiments and perceiving the analogy of diffusion between Fourier's law of thermal conduction and diffusion. Used phenomenological approach and continuum description for the phenomenon of diffusion.</p> <p>Introduced the concept of the diffusion coefficient and measured it for salt in water</p>	1855	<p>A major milestone in the field of diffusion.</p> <p>The equations governing diffusion processes are Fick's laws.</p>



Jozef Stephan, <i>et al.</i>	Gave solutions of Fick's second law either as a trigonometric series or as the complementary error function.  Calculated numerical tables of concentration-depth profiles with $h/2\sqrt{Dt}$ as a parameter, where t is the time and h is the thickness of successive layers used for chemical analysis.	1879	Stefan's tables were used later by Roberts-Austen to evaluate his data
Albert Colson	Carbon diffusion in iron was measured.	1881	Colson also prepared platinum silicides by solid interdiffusion
Svante August Arrhenius	Proposed the Arrhenius equation to model the temperature dependence of diffusion coefficients.	1889	The Arrhenius equation is a general formula for the temperature dependence of reaction rates.
W.C. Roberts Austen	Performed experiments on the diffusion of precious metals (Au, Pt, Rh) in liquid lead, of Au and Ag in liquid tin, and Au in liquid bismuth.	1896	The first systematic study on solid state diffusion (diffusion of gold in solid lead) that was reported.  'Austenite' is named after him.
Dushman and Langmuir	Diffusion in solids also obey Arrhenius law	1922	Unconventional applications of the Arrhenius law include the chirping of tree crickets, creeping of ants, and the flashing of fireflies

Robert Brown	Discovered Brownian motion	1828	Brownian motion may be defined as the erratic random movement of microscopic particles in a fluid, as a result of continuous bombardment from molecules of the surrounding medium
Albert Einstein	There are two parts to Einstein's theory: the first part consists in the formulation of a diffusion equation for Brownian particles, in which the diffusion coefficient is related to the mean squared displacement of a Brownian particle (Einstein-Smoluchowski relation), while the second part consists in relating the diffusion coefficient to measurable physical quantities.	1905 1906	Explained the physics of Fick's phenomenological diffusion theory in terms of Brownian motion or random walks.
Marian Smoluchowski	Theory of Brownian motion based on a kinetic approach of collisions between particles.	1906	The Smoluchowski factor, related to inter-particle interactions, is named after him
Jean Baptiste Perrin	Experimentally proved Einstein-Smoluchowski theory	1908 1909	By verifying the Einstein's explanation of Brownian motion, he confirmed the atomic nature of matter.

Jakov Ilich Frenkel	Suggested transitions of atoms to interstitial positions resulting in lattice vacancies due to thermal agitation causes interstitial diffusion in crystalline solids.	1926	This is later known as Frenkel disorder or Frenkel defect.
Wagner and Schottky	Introduced point defects and generalized the concept of disorder.	1930	Atomic defects are a prerequisite for diffusion in crystals
Ernest Kirkendall, <i>et al.</i>	Kirkendall's experiment demonstrated the inequality of copper and zinc diffusion during interdiffusion between brass and copper. The Kirkendall effect is the motion of the boundary layer between two metals in contact that occurs as a consequence of the difference in diffusion rates of the metal atoms	1939 1942 1947	Kirkendall's discovery is taken as evidence for a vacancy mechanism of diffusion in metals and alloys.
Lawrence Stamper Darken	Darken's equations to be used in solid solution when two interdiffusing components do not have the same coefficient of diffusion.	1948	Darkens equations are the phenomenological description of Kirkendall effect
John Bardeen	Pointed out the role of correlation in defect-mediated diffusion in solids and recognized that the original Darken equations are approximations. Correlation factor depends on both the diffusion mechanism and on the lattice geometry and it play an important role for solid-state diffusion process, when point defects act as diffusion vehicles	1949	In the vacancy mechanism, there exists correlation between the directions of consecutive jumps of atoms.

J. C. Fisher	Theoretical model of grain-boundary diffusion	1951	First theoretical model of grain-boundary diffusion
R. E. Hoffman & David Turnbull	Systematic quantitative studies of grain-boundary diffusion in solids	1951	The absolute grain boundary diffusion coefficients are found to be independent of the grain size of the specimens.
John Randolph Manning	The role of correlation was explored in detail and modified the Darkens Equation with a correction term for the vacancy wind effect.	1968	Darker-Manning relations
Akira Okubo	Oceanic diffusion diagrams. - Empirical relations between diffusion characteristics are investigated by the use of carefully examined data from instantaneous dye-release experiments in the upper mixed layer of the sea and 'diffusion diagrams' are prepared.	1971	These diagrams provide a practical means to predict the rate of horizontal spread of substance from an instantaneous source.
Brebec, G, <i>et al.</i>	The diffusion of Si in amorphous silica was measured and diffusion profiles were obtained. A diffusion equation for correlation was also proposed	1980	Secondary-ion-mass-spectroscopy (SIMS) technique is used.
P. L. Gal, <i>et al.</i>	Experimental studies on bulk diffusion of metal particles on ceramic substrates - studied the dynamics of small copper particles on the surface of	1990	These diffusion processes may be important in electronics applications, which

	amorphous alumina in various oxidizing and reducing atmospheres based on in-situ electron microscopy for the diffusion of metal particles through the bulk of a ceramic substrate.		involve similar combinations of materials
Roder Holger, <i>et al.</i>	Method for the simultaneous formation of many densely packed nanostructures of various morphologies using diffusion-controlled aggregation on surfaces, to grow linear, two-dimensional or tenuous fractal aggregates of nanometer dimensions obtained by exploiting the dependence of the mobility of adsorbed atoms on substrate crystal face and temperature,	1993	The formation of nanometer-scale surface structures is done by atomic manipulation with the help of scanning tunneling microscope.
Alexandros Pertsinidis and X. S. Ling	Study on the dynamics of mono- and di-vacancies in two-dimensional colloidal crystals. Provided evidence that the excitation of point defects into dislocation pairs enhances the diffusion of di-vacancies and also found that the hopping of the defects does not follow a pure random walk, but exhibits memory effects.	2001	The results may be relevant for explaining the dynamics of other two-dimensional systems.
Shin-ichi Nishimura, <i>et al.</i>	Experimental visualization of lithium diffusion in $\text{Li}_x\text{FePO}_4$ . By combining high-temperature	2008	Experimental evidence for a curved one-dimensional chain for

	powder neutron diffraction and the maximum entropy method, lithium distribution along the [010] direction was clearly visualized		lithium motion is provided
Yaohong Suo and Shengping Shen	Diffusion–reaction–mechanics model of the metallic oxidation is developed. The coupled model shows that the hydrostatic pressure depending on the diffusion and reaction is a harmonic function if the body force is ignored.	2015	The chemical reaction during metal oxidation at high temperature is considered.
Shang Shun-Li, <i>et al.</i>	A compilation of vacancy formation energies, vacancy migration energies, vacancy activation energies, vacancy concentrations and vacancy-mediated self-diffusion coefficients as a function of temperature for 82 pure elements is made in bcc, fcc, and hcp structures by means of a comprehensive first-principles study. The researchers claim that the study of pure elements provides not only diffusion-related properties and a new understanding of diffusivity, but also a benchmark of first-principles calculations and a foundational dataset for the Materials Genome Initiative.	2016	The Materials Genome Initiative is a multi-agency initiative designed to create a new era of policy, resources, and infrastructure that support U.S. institutions in the effort to discover, manufacture, and deploy advanced materials twice as fast, at a fraction of the cost

## REFERECES

- [1] **Abbas, I. A., Kumar, R., & Kaushal, S.** (2015) Interaction Due to Thermal Source in Micropolar Thermoelastic Diffusion Medium. *Journal of Computational and Theoretical Nanoscience*. **12(8)**. 1780-1786.
- [2] **AbuZaiter, A., Nafea, M. and Ali, M. S. M.** (2016). Development of a shape-memory-alloy micromanipulator based on integrated bimorph microactuators. *Mechatronics*. **38**. 16-28.
- [3] **Aifantis, E. C.** (1979) *Comments on the calculation of the formation volume of vacancies in solids*. Physical Review B. **19(12)**. 6622.
- [4] **Aifantis, E.C.** (1980) On the problem of diffusion in solids. *Acta Mech.* **37**. 265-296.
- [5] **Aifantis, E.C. and Gerberich, W.W.** (1977a) Gaseous diffusion in a stressed thermoelastic solid, Part I: The thermomechanical formulation. *Acta Mechanica*. **28**. 1-24.
- [6] **Aifantis, E.C. and Gerberich W.W.** (1977b) Gaseous diffusion in a stressed thermoelastic solid, Part II: Thermodynamic structure and transport theory. *Acta Mechanica*. **28**. 25-47.
- [7] **Amend, J. R., Brown, E., Rodenberg, N., Jaeger, H. M. and Lipson, H.** (2012) A positive pressure universal gripper based on the jamming of granular material. *IEEE Transactions on Robotics*. **28(2)**. 341-350.
- [8] **Ames, K., Gibala, D. and Hamed, G. R.** (1996) Styrene-butadiene rubber filled with fluorinated carbon black: Part II. Effect of curative level. *Rubber chemistry and technology*. **69(2)**. 273-276.
- [9] **Arakere, N. K.** (2016) Gigacycle rolling contact fatigue of bearing steels: A review. *International Journal of Fatigue*. **93**. 238-249.
- [10] **Arrhenius, S.** (1889) "Über die Reaktionsgeschwindigkeit bei der Inversion von Rohrzucker durch Säuren, Zeitschrift für" *Phys. Chemie* **4**. 226 - 248.
- [11] **Ayasse, J.B. and Chollet, H.U.G.U.E.S.** (2005) Determination of the wheel rail contact patch in semi-Hertzian conditions. *Vehicle System Dynamics*. **43(3)**. 161-172.
- [12] **Bachmann, J.H., Sellers, J.W., Wagner, M.P. and Wolf, R.F.** (1959) Fine particle reinforcing silicas and silicates in elastomers. *Rubber Chemistry and Technology*. **32(5)**. 1286-1391.
- [13] **Back, E. L.** (1991) Paper-to-paper and paper-to-metal friction. *International Paper Physics Conference Proceedings*, TAPPI PRESS, Atlanta. 49-65.
- [14] **Bardeen, J.** (1949) Diffusion in binary alloys. *Physical Review*. **76(9)**. 1403-1405.

- [15] **Bibel, G. D., Kumar, A., Reddy, S., and Handschuh, R.** (1995) Contact stress analysis of spiral bevel gears using finite element analysis. *Journal of Mechanical Design*. **117(2A)**. 235-240.
- [16] **Bicchi, A. and Vijay Kumar,** (2000) Robotic Grasping and Contact: A Review. *International Conference on Robotics and Automation ICRA*. **1**. 348-353.
- [17] **Blow, C.M. and Hepburn, C.** *Rubber Technology and Manufacture*. 2nd ed. Elsevier Science & Technology Books, 1982.
- [18] **Bogdanski, S., Olzak, M. and Stupnicki, J.** (1996) Numerical stress analysis of rail rolling contact fatigue cracks. *Wear*. **191(1)**. 14-24.
- [19] **Bomidi, J. A., Weinzapfel, N., Sadeghi, F., Liebel, A. and Weber, J.** (2013) An improved approach for 3D rolling contact fatigue simulations with microstructure topology. *Tribology Transactions*. **56(3)**. 385-399.
- [20] **Borgese, S.** (1970) A study of the growth mechanism of lenticular carbides in cyclically stressed 52100 steel. *Journal of Lubrication Technology*. **92(1)**. 54-58.
- [21] **Brebec, G., Seguin, R. and Sella, C.** (1980) Diffusion of silicon in amorphous silica. *Acta Metall.* **28(3)**. 327-33.
- [22] **Brinke, J. W.** Silica reinforced tyre rubbers: mechanistic aspects of the role of coupling agents. Twente University Press, 2002.
- [23] **Brown, E., Rodenberg, N., Amend, J., Mozeika, A., Steltz, E., Zakin, M. R. and Jaeger, H. M.** (2010) Universal robotic gripper based on the jamming of granular material. *Proceedings of the National Academy of Sciences*. **107(44)**. 18809-18814.
- [24] **Brown, R.** (1828) A brief account of microscopical observations made in the months of June, July and August 1827, on the particles contained in the pollen of plants; and on the general existence of active molecules in organic and inorganic bodies. *Philosophical Magazine Series 2*, **4(21)**. 161-173.
- [25] **Buchwald, J., and Heckel, R. W.** (1968) An analysis of microstructural changes in 52100 steel bearings during cyclic stressing (Microstructural changes in 52100 steel bearing inner rings during cyclic stressing, obtaining thickening rate data on white-etching regions and lenticular carbides). *ASM Transactions Quarterly*. **61**. 750-756.
- [26] **Causey, G. C., and Quinn, R. D.** (1998) Gripper design guidelines for modular manufacturing. *Proceedings of IEEE International Conference on Robotics and Automation* **2**. 1453-1458.
- [27] **Chen, J., Young, B., and Uy, B.** (2006) Behavior of high strength structural steel at elevated temperatures. *Journal of structural engineering*. **132(12)**. 1948-1954.



- [28] **Chen, Y. C., and Tsay, C. B.** (2002) Stress analysis of a helical gear set with localized bearing contact. *Finite Elements in Analysis and Design*. **38(8)**. 707-723.
- [29] **Cottrell, A. H.** (1948) Effect of solute atoms on the behavior of dislocations. *In Report of a Conference on Strength of Solids*. Physical Society, London, 30-38.
- [30] **Cottrell, A. H., and Bilby, B. A.** (1949) Dislocation theory of yielding and strain ageing of iron. *Proceedings of the Physical Society*. Section A. **62(1)**. 49.
- [31] **Cox, R. W.** (1991) Stress-assisted diffusion: a free boundary problem. *SIAM Journal on Applied Mathematics*. **51(6)**. 1522-1537.
- [32] **Darken, L. S.** (1948) Diffusion, mobility and their interrelation through free energy in binary metallic systems. *Trans. Aime*. **175(1)**. 184-201.
- [33] **Dejak, B., Mlotkowski, A., and Langot, C.** (2012) Three-dimensional finite element analysis of molars with thin-walled prosthetic crowns made of various materials. *Dental Materials*. **28(4)**. 433-441.
- [34] **Desimone, H., Bernasconi, A., and Beretta, S.** (2006) On the application of Dang Van criterion to rolling contact fatigue. *Wear*. **260(4)**. 567-572.
- [35] **Donnet, J. B.** (1998) Black and white fillers and tire compound. *Rubber chemistry and technology*. **71(3)**. 323-341.
- [36] **Donnet, J.B. and Emmanuel Custodero** (2011) *Reinforcement of Elastomers by Particulate Fillers*. pp. 367-400. *In J.E. Mark, B.Erman and F.R. Eirich* (eds.) *Science and Technology of Rubber, 3rd ed.* Elsevier Academic Press, 2011.
- [37] **Dubbeldam, D., Calero, S., Ellis, D. E., and Snurr, R. Q.** (2016) RASPA: molecular simulation software for adsorption and diffusion in flexible nanoporous materials. *Molecular Simulation*. **42(2)**. 81-101.
- [38] **Dushman, S., and Langmuir, I.** (1922) The diffusion coefficient in solids and its temperature coefficient. *Phys. Rev.* **20**. 113.
- [39] **Eeten, V. P.** (2006) Constant and variable amplitude cyclic plasticity in 316L stainless steel. *Journal of Testing and Evaluation*. **34(4)**. 1-14.
- [40] **Einstein, A.** (1905) Über die von der molekularkinetischen Theorie der Wärme geforderte Bewegung von in ruhenden Flüssigkeiten suspendierten Teilchen. *Annalen der physik*, **322(8)**. 549-560. (English translation, *Investigations on the Theory of Brownian Movement*. Dover. New York. 1956.)
- [41] **Einstein, A.** (1906) Zur theorie der brownschen bewegung. *Annalen der physik*. **324(2)**. 371-381.
- [42] **Ekberg, A., Åkesson, B., and Kabo, E.** (2014) Wheel/rail rolling contact fatigue – probe, predict, prevent. *Wear*. **314(1)**. 2-12.

- [43] **El-Mellouhi, F., Mousseau, N. and Lewis, L. J.** (2008) Kinetic activation-relaxation technique: An off-lattice self-learning kinetic Monte Carlo algorithm. *Physical Review B*. **78(15)**. 153202.
- [44] **El-Thalji, I., and Jantunen, E.** (2015) Dynamic modelling of wear evolution in rolling bearings. *Tribology International*. **84**. 90-99.
- [45] **Eschenbach, W. and Wagenbauer, K.** (1961) *Impression forces and pressure distribution in the cylinder contact areas of a sheet-fed offset printing press*. 1.109. In **Banks** (ed) *Advances in Printing Science and Technology*. WH.
- [46] **Felhös, D. and Karger-Kocsis, J.** (2008) Tribological testing of peroxide-cured EPDM rubbers with different carbon black contents under dry sliding conditions against steel. *Tribology International*. **41(5)**. 404-415.
- [47] **Fellers, C., Backstrom, M., Htun, M., and Lindholm, G.** (1998) Paper-to-paper friction-paper structure and moisture. *Nordic Pulp & Paper Research Journal*. **13(3)**. 225-232.
- [48] **Fick, A.** (1855) Über diffusion. *Poggendorff's Annalen der Physik*. **94**. 59-86.
- [49] **Fick, A.** (1995) On liquid diffusion. *Journal of membrane science*. **100(1)**. 33-38.
- [50] **Fisher, J. C.** (1951) Calculation of diffusion penetration curves for surface and grain boundary diffusion. *Journal of Applied Physics*. **22(1)**. 74-77.
- [51] **Flores, P. and Lankarani, H. M.** (2016) *Contact Force Models for Multibody Dynamics* (Vol. 226). Springer.
- [52] **Flynn, C. P.** *Point defects and diffusion*. Oxford, Clarendon Press, 1973.
- [53] **Frenkel, J.** (1926) Über die Wärmebewegung in festen und flüssigen Körpern. *Zeitschrift für Physik*. **35(8-9)**. 652-669.
- [54] **Fultz, W. C. and Evans, L. R.** (1998) Tire tread compounds with silica/CB blends. *Rubber world*. **218(1)**. 39-43.
- [55] **Gabelli, A., Morales-Espejel, G. E. and Ioannides, E.** (2008) Particle damage in Hertzian contacts and life ratings of rolling bearings. *Tribology Transactions*. **51(4)**. 428-445.
- [56] **Gal, P. L., Smith, B. C. and Owen, G.** (1990) Bulk diffusion of metal particles on ceramic substrates. *Nature* **348**. 430-432.
- [57] **Garoff, N., Fellers, C. and Nilvebrant, N. O.** (2004) Friction hysteresis of paper. *Wear*. **256(1)**. 190-196.
- [58] **George, B. and Prasad, N. S.** (2007) Finite element analysis of squirrel cage ball bearings for gas turbine engines. *Defence Science Journal*. **57(2)**. 165.
- [59] **Girifalco, L. A. and Welch, D. O.** (1967) *Point defects and diffusion in strained metals*. Gordon & Breach, New York.

- [60] **Goldsmith, W.** *Impact: The Theory and Physical Behavior of Colliding Solids*, Edward Arnold Ltd, London, 1960.
- [61] **Graham, T.** (1829) A short Account of Experimental Researches on the Diffusion of Gases through each other, and their Separation by mechanical means. *Quarterly Journal of Science, Literature and Art.* **27**. 74-83.
- [62] **Graham, T.** (1833) On the law of the diffusion of gases. *The London, Edinburgh, and Dublin Philosophical Magazine and Journal of Science.* **2(9)**. 175-190
- [63] **Graham, T.** (1867) On the occlusion of hydrogen gas by metals. *Proceedings of the Royal Society of London.* **16**. 422-427.
- [64] **Graham, T.** (1868) On the relation of hydrogen to palladium. *Proceedings of the Royal Society of London.* **17**. 212-220.
- [65] **Gupta, M. B., Choubey, M. A. and Varde, M. G. V.** (2012) Contact stress analysis of spur gear. *International Journal of Engineering Research & Technology (IJERT).* **1(4)**.
- [66] **Halama, R., Šofer, M. and Fojtík, F.** (2012) Choice and Calibration of Cyclic Plasticity Model with Regard to Subsequent Fatigue Analysis. *Engineering Mechanics.* **19**. 87-97.
- [67] **Hassan, A. R.** (2009) Contact stress analysis of spur gear teeth pair. *World Academy of Science, Engineering and Technology.* **58(1)**. 597-602.
- [68] **Henak, C. R., Kapron, A. L., Anderson, A. E., Ellis, B. J., Maas, S. A., and Weiss, J. A.** (2014) Specimen-specific predictions of contact stress under physiological loading in the human hip: validation and sensitivity studies. *Biomechanics and modeling in mechanobiology.* **13(2)**. 387-400.
- [69] **Hertz, H.** (1882) Über die Berührung fester elastischer Körper und über die Harte. In Hertz, H., *Gesammelte Werke*, Band 1. Leipzig: Johann Ambrosius Barth (1895), 174–196. (English Translation: **Hertz, H.** (1896) *On the contact of rigid elastic solids and on hardness*. pp 163-183 In **Jones, Daniel Evan and Schott, George Adolphus** (eds) *Miscellaneous papers by Hertz, Heinrich*. Macmillan, London, 1896).
- [70] **Heuer, A. H. and Azar, M. Z.** (2015) A disconnection mechanism of enhanced grain boundary diffusion in Al<sub>2</sub>O<sub>3</sub>. *Scripta Materialia.* **102**. 15-18.
- [71] **Hill R.** *The mathematical theory of plasticity*, Oxford University Press, 1998.
- [72] **Hoffman, R. E. and Turnbull, D.** (1951) Lattice and Grain Boundary Self-Diffusion in Silver. *Journal of Applied Physics.* **22(5)**. 634-639.
- [73] **Huang, X., Tian, N., Wang, T., Wang, K. and Xue, Q.** (2007) Friction and wear properties of NBR/PVC composites. *Journal of applied polymer science.* **106(4)**. 2565-2570.

- [74] **Hwang, S. C., Lee, J. H., Lee, D. H., Han, S. H. and Lee, K. H.** (2013) Contact stress analysis for a pair of mating gears. *Mathematical and Computer Modelling*. **57(1)**. 40-49.
- [75] **Inoue, M., Gurnagul, N. and Aroca, P.** (1990) Static friction properties of linerboard. *Tappi journal*. **73(12)**. 81-85.
- [76] **Jackson, R. L. and Green, I.** (2005) A finite element study of elasto-plastic hemispherical contact against a rigid flat. *Journal of Tribology*. **127(2)**. 343-354.
- [77] **Jiang, Y. and Sehitoglu, H.** (1996) Rolling contact stress analysis with the application of a new plasticity model. *Wear*. **191(1)**. 35-44.
- [78] **Jiang, Y. and Sehitoglu, H.** (1999) A model for rolling contact failure. *Wear*. **224(1)**. 38-49.
- [79] **Jiang, Y. and Zhang, J.,**(2008) Benchmark experiments and characteristic cyclic plasticity deformation. *International Journal of Plasticity*. **24(9)**.1481-1515.
- [80] **Jiang, Y., Xu, B. and Sehitoglu, H.** (2002) Three-dimensional elastic-plastic stress analysis of rolling contact. *Journal of tribology*. **124(4)**. 699-708.
- [81] **Karger-Kocsis, J., Mousa, A., Major, Z. and Békési, N.** (2008) Dry friction and sliding wear of EPDM rubbers against steel as a function of carbon black content. *Wear*. **264(3)**. 359-367.
- [82] **Kipphan, H.** (Ed.) *Handbook of Print Media Technologies and Production Methods*. pp.109, 227,1066-1067. Springer, 2001.
- [83] **Kirkendall, E. O.** (1942) Diffusion of zinc in alpha brass. *Aime Trans*. **147**. 104-109.
- [84] **Kirkendall, E. O. and Smigelskas, A. D.** (1947) Zinc diffusion in alpha brass. *AIME TRANS*. **171**. 130-142.
- [85] **Kirkendall, T., Thomassen, L. and Upthegrove, C.** (1939) Rates of diffusion of copper and zinc in alpha brass. *AIME TRANS*. **133**. 186-203.
- [86] **Klepach, D. and Zohdi, T. I.** (2014) Strain assisted diffusion: Modeling and simulation of deformation-dependent diffusion in composite media. *Composites Part B: Engineering*. **56**. 413-423.
- [87] **Kodur, V., Dwaikat, M. and Fike, R.** (2010) High-temperature properties of steel for fire resistance modeling of structures. *Journal of Materials in Civil Engineering*. **22(5)**. 423-434.
- [88] **Leeuwen, V. H. P.** (1974) The kinetics of hydrogen embrittlement: a quantitative diffusion model. *Engineering Fracture Mechanics*. **6(1)**. 141-161.

- [89] **Li, J. C. M., Oriani, R. A. and Darken, L. S.** (1966) The thermodynamics of stressed solids. *Zeitschrift für Physikalische Chemie*. **49(3\_5)**. 271-290.
- [90] **Litvin, F. L., Lian, Q. and Kapelevich, A. L.** (2000) Asymmetric modified spur gear drives: reduction of noise, localization of contact, simulation of meshing and stress analysis. *Computer methods in applied mechanics and engineering*. **188(1)**. 363-390.
- [91] **Magel, E., Mutton, P., Ekberg, A. and Kapoor, A.** (2016) Rolling contact fatigue, wear and broken rail derailments. *Wear*. **366**. 249-257.
- [92] **Magne, P. and Belser, U. C.** (2002) Rationalization of shape and related stress distribution in posterior teeth: a finite element study using nonlinear contact analysis. *International Journal of Periodontics & Restorative Dentistry*. **22(5)**.
- [93] **Manning, J. R. & Bruner, L. J.** (1968) Diffusion kinetics for atoms in crystals. *American Journal of Physics*. **36(10)**. 922-923.
- [94] **Mitamura, N., Hidaka, H. and Takaki, S.** (2007) Microstructural development in bearing steel during rolling contact fatigue. In *Materials science forum* **539.543**. 4255-4260.
- [95] **Monkman, G. J., Hesse, S., Steinmann, R. and Schunk, H.** *Robot grippers*. John Wiley & Sons, 2007.
- [96] **Mostafa, A., Abouel-Kasem, A., Bayoumi, M. R. and El-Sebaie, M. G.** (2009) Effect of carbon black loading on the swelling and compression set behavior of SBR and NBR rubber compounds. *Materials & Design*. **30(5)**. 1561-1568.
- [97] **Newton I.**, *Philosophiae Naturalis Principia Mathematica* Reg. Soc. Preases, London, 1686.
- [98] **Nishimura, S. I., Kobayashi, G., Ohoyama, K., Kanno, R., Yashima, M. and Yamada, A.** (2008) Experimental visualization of lithium diffusion in  $\text{Li}_x\text{FePO}_4$ . *Nature materials*. **7(9)**. 707-711.
- [99] **Nunes, R. C. R., Fonseca, J. L. C. and Pereira, M. R.** (2000) Polymer–filler interactions and mechanical properties of a polyurethane elastomer. *Polymer testing*. **19(1)**. 93-103.
- [100] **Okel, T. A., Patkar, S. D. and Bice, J. A.** (1999) Advances in precipitated silicas for passenger and truck tyre treads. *Progress in rubber and plastics technology*. **15(1)**. 1-27.
- [101] **Okubo, A.** (1971) Oceanic diffusion diagrams. In *Deep sea research and oceanographic abstracts*. Elsevier. **18. 8**. pp. 789-802.
- [102] **Oriani, R.A.** (1969) Hydrogen in metals, *Fundamentals of stress corrosion cracking, Conference*, Ohio State University, NACE, 32-50.

- [103] **Pálfi, L., Goda, T. and Váradi, K.** (2009) Theoretical prediction of hysteretic rubber friction in ball on plate configuration by finite element method. *eXPRESS Polym. Lett.* **3(11)**. 713-723.
- [104] **Patil, S. S., Karuppanan, S. and Atanasovska, I.** (2015) Contact stress evaluation of involute gear pairs, including the effects of friction and helix angle. *Journal of Tribology.* **137(4)**. 044501.
- [105] **Patil, S. S., Karuppanan, S., Atanasovska, I. and Wahab, A. A.** (2014) Contact stress analysis of helical gear pairs, including frictional coefficients. *International Journal of Mechanical Sciences.* **85**. 205-211.
- [106] **Pau, M., Aymerich, F. and Ginesu, F.** (2002) Distribution of contact pressure in wheel–rail contact area. *Wear.* **253(1)**. 265-274.
- [107] **Paul, B.** (1975) A review of rail-wheel contact stress problems. *Railroad Track Mechanics and Technology.* 323-352.
- [108] **Pedrero, J. I., Pleguezuelos, M. and Muñoz, M.** (2011) Contact stress calculation of undercut spur and helical gear teeth. *Mechanism and Machine Theory.* **46(11)**. 1633-1646.
- [109] **Perrin, J.** (1908) La loi de Stokes et le mouvement brownien. *Comptes rendus.* **147**. 475-476.
- [110] **Perrin, J.** (1909) Mouvement brownien et réalité moléculaire. In *Annales de Chimie et de Physique.* **18**. 5-104.
- [111] **Pertsinidis, A. and Ling, X. S.** (2001) Diffusion of point defects in two-dimensional colloidal crystals. *Nature.* **413(6852)**. 147-150.
- [112] **Petković, D., Pavlović, N. D., Čojbašić, Ž. and Pavlović, N. T.** (2013) Adaptive neuro fuzzy estimation of underactuated robotic gripper contact forces. *Expert systems with Applications.* **40(1)**. 281-286.
- [113] **Piotrowski, J. and Kik, W.** (2008) A simplified model of wheel/rail contact mechanics for non-Hertzian problems and its application in rail vehicle dynamic simulations. *Vehicle System Dynamics.* **46(1-2)**. 27-48.
- [114] **Polonsky, I. A. and Keer, L. M.** (1995) On white etching band formation in rolling bearings. *Journal of the Mechanics and Physics of Solids.* **43(4)**. 637-669.
- [115] **Popescu, G., Morales-Espejel, G. E., Wemekamp, B. and Gabelli, A.** (2006) An engineering model for three-dimensional elastic-plastic rolling contact analyses. *Tribology transactions.* **49(3)**. 387-399.
- [116] **Raghavan, R., Wheeler, J. M., Esqué-de los Ojos, D., Thomas, K., Almandoz, E., Fuentes, G. G. and Michler, J.** (2015) Mechanical behavior of Cu/TiN multilayers at ambient and elevated temperatures: Stress-assisted diffusion of Cu. *Materials Science and Engineering: A.* **620**. 375-382.

- [117] **Ramesan, M. T.** (2005) The effects of filler content on cure and mechanical properties of dichlorocarbene modified styrene butadiene rubber/carbon black composites. *Journal of Polymer Research*. **11(4)**. 333-340.
- [118] **Roberts-Austen, W.C.** (1896) On the Diffusion of Metals. *Phil. Trans. Roy. Soc. London A*. **187**. 383-415.
- [119] **Robertson, I. M., Sofronis, P., Nagao, A., Martin, M. L., Wang, S., Gross, D. W. and Nygren, K. E.** (2015) Hydrogen embrittlement understood. *Metallurgical and Materials Transactions B*. **46(3)**. 1085-1103.
- [120] **Robeson, L. M., Liu, Q., Freeman, B. D. and Paul, D. R.** (2015) Comparison of transport properties of rubbery and glassy polymers and the relevance to the upper bound relationship. *Journal of Membrane Science*. **476**. 421-431.
- [121] **Roch, I., Bidaud, P., Collard, D. and Buchailot, L.** (2003). Fabrication and characterization of an SU-8 gripper actuated by a shape memory alloy thin film. *Journal of Micromechanics and Microengineering*. **13(2)**. 330.
- [122] **Roder, H., Hahn, E., Brune, H., Bucher, J. P. and Kern, K.** (1993) Building one-dimensional and 2-dimensional nanostructures by diffusion-controlled aggregation at surfaces. *Nature*. **366(LNS-ARTICLE-1993-004)**. 141-143.
- [123] **Rodgers, B. and Walter Waddell** *The Science of Rubber Compounding*. pp 401-454. In **J.E. Mark, B. Erman and F.R. Eirich** (eds.) *Science and Technology of Rubber, 3rd ed.* Elsevier Academic Press, 2011.
- [124] **Rodriguez, J. and Hamed, G. R.** (1993) Styrene-butadiene rubber filled with fluorinated carbon black. *Rubber chemistry and technology*. **66(2)**. 286-294.
- [125] **Routh, Edward John** *Dynamics of a system of rigid bodies*. New York, Dover, 1960.
- [126] **Schwaiger, B. and Blume, A.** (2000) FEATURES-Silica/silane--A winning reinforcement formula-The silica/silane system is finding favor in tire reinforcement due to its wet traction and rolling resistance performance. *Rubber World*. **222(1)**. 32-38.
- [127] **Seita, M., Hanson, J. P., Gradečak, S. and Demkowicz, M. J.** (2015) The dual role of coherent twin boundaries in hydrogen embrittlement. *Nature communications*, **6**.
- [128] **Seo, J. W., Yoo, O. S., In, Y., Kang, B. M., Sun, D. H. and Kim, Y. S.** (2016) Evaluation of contact pressure at articular surface of knee implant in neutral, varus and valgus alignment. *Bone Joint J*. **98(SUPP 10)**. 25-25.
- [129] **Shang, Shun-Li, Bi-Cheng Zhou, William Y. Wang, Austin J. Ross, Xuan L. Liu, Yong-Jie Hu, Hua-Zhi Fang, Yi Wang and Zi-Kui Liu** (2016) A comprehensive first-principles study of pure elements: Vacancy formation and migration energies and self-diffusion coefficients. *Acta Materialia*. **109**. 128-141.

- [130] **Sherief, H. H.** and **Hussein, E. M.** (2016) Two-dimensional problem for a half-space with axi-symmetric distribution in the theory of generalized thermoelastic diffusion. *Mechanics of Advanced Materials and Structures*. **23(2)**. 216-222.
- [131] **Shewmon, P.** *Diffusion in Solids*. 2nd ed. Wiley, 1991.
- [132] **Shigley, J. E.** *Mechanical engineering Design*. Mc. Graw Hill, Singapore, 1986.
- [133] **Shiller, Z.** and **Dubowsky, S.** (1989) Robot path planning with obstacles, actuator, gripper, and payload constraints. *The International Journal of Robotics Research*. **8(6)**. 3-18.
- [134] **Shuqin, W., Wang Yiming, Chai Chengwen** and **Bai Jianjun** (2009) Research on the Methods of the Measurement of Printing Pressure in Offset Press, *International Conference on Measuring Technology and Mechatronics Automation IEEE*. **1**. 342-344.
- [135] **Smoluchowski, V. M.** (1906) Zur kinetischen theorie der brownschen molekularbewegung und der suspensionen. *Annalen der physik*. **326(14)**. 756-780.
- [136] **Smoluchowski, V. M.** (1916) Drei vortrage uber diffusion. Brownsche bewegung und koagulation von kolloidteilchen. *Z. Phys.* **17**. 557-585.
- [137] **Song, Y., Shao, X., Guo, Z.** and **Zhang, J.** (2013) Role of material properties and mechanical constraint on stress-assisted diffusion in plate electrodes of lithium ion batteries. *Journal of Physics D: Applied Physics*. **46(10)**. 105307.
- [138] **Stefan, J.** (1879) Sitzungsberichte d. *Kaiserl. Akad. d. Wissenschaften II*. **79**. 161-214.
- [139] **Suo, Y.** and **Shen, S.** (2015) Coupling diffusion–reaction–mechanics model for oxidation. *Acta Mechanica*. **226(10)**. 3375-3386.
- [140] **Swahn, H. P. C. O., Becker, P. C.** and **Vingsbo, O.** (1976) Martensite decay during rolling contact fatigue in ball bearings. *Metallurgical Transactions A*. **7(8)**. 1099-1110.
- [141] **Tang, X., Chen, R., Yin, W., Wang, J., Tang, X., Lee, D.** and **Yan, A.** (2015) Mechanism of texture enhancement in nanocomposite magnets during process of die upsetting coupled with Nd–Cu grain boundary diffusion. *Journal of Alloys and Compounds*. **623**. 386-392.
- [142] **Thongsang, S., Vorakhan, W., Wimolmala, E.** and **Sombatsompop, N.** (2012) Dynamic mechanical analysis and tribological properties of NR vulcanizates with fly ash/precipitated silica hybrid filler. *Tribology International*. **53**. 134-141.
- [143] **Timoshenko, S. P.** and **J N Goodier** *Theory of Elasticity*. Mc Graw Hill, Singapore, 1970.



- [144] **Tjaden, B., Lane, J., Withers, P. J., Bradley, R. S., Brett, D. J. and Shearing, P. R.** (2016) The application of 3D imaging techniques, simulation and diffusion experiments to explore transport properties in porous oxygen transport membrane support materials. *Solid State Ionics*. **288**. 315-321.
- [145] **Treloar, L.R.G.** *The Physics of Rubber Elasticity*. 3rd ed. Clarendon Press, Oxford, 2005.
- [146] **Tremblay, M. R. and Cutkosky, M. R.** (1993) Estimating friction using incipient slip sensing during a manipulation task. *Proceedings of IEEE International Conference on Robotics and Automation*. May, 429-434.
- [147] **Tsay, C. B.** (1988) Helical gears with involute shaped teeth: geometry, computer simulation, tooth contact analysis, and stress analysis. *Journal of mechanisms, transmissions, and automation in design*. **110(4)**. 482-491.
- [148] **Vadivu, K. S., Sankaranarayanan, N. and Mahalakshmi, N. V.** (2006) Design and development of a pressure sensing device in offset printing machine. *Journal of the Institution of Engineers(India), Part MC, Mechanical Engineering Division*. **87(2)**. 12-14.
- [149] **Varotsos, P. and Aifantis, E. C.** (1980) *Comments on the diffusion of a gas in a linear elastic solid*. *Acta Mechanica* **36(1)**. 129-133.
- [150] **Vijayarangan, S. and Ganesan, N.** (1994) Static contact stress analysis of a spur gear tooth using the finite element method, including frictional effects. *Computers & structures*. **51(6)**. 765-770.
- [151] **Wagner, C. and Schottky, W.** (1930) Theory of arranged mixed phases. *Z. Physik. Chem.* **11**. 163-210.
- [152] **Wang, L., Lin, Y. and Zhang, A.** (2006) Dispersion of carbon black in high-abrasion furnace black filled nonsulfur modified powdered polychloroprene rubber. *Journal of applied polymer science*. **101(1)**. 192-196.
- [153] **Wang, M., Wang, L., Li, P. and Fu, Y.** (2016) A novel modelling and simulation method of hip joint surface contact stress. *Bioengineered*. 1-8.
- [154] **Warhadpande, A., Sadeghi, F. and Evans, R. D.** (2014) Microstructural Alterations in Bearing Steels under Rolling Contact Fatigue: Part 2—Diffusion-Based Modeling Approach. *Tribology Transactions*. **57(1)**. 66-76.
- [155] **Weinzapfel, N. and Sadeghi, F.** (2013) Numerical modeling of sub-surface initiated spalling in rolling contacts. *Tribology International*. **59**. 210-221.
- [156] **Wilson, R. K. and Aifantis, E. C.** (1982) On the theory of stress-assisted diffusion, I. *Acta Mechanica*. **45(3-4)**. 273-296.
- [157] **Wilson, R. K., and Aifantis, E. C.** (1979) *A coupled diffusion-deformation theory*. *Developments in Mechanics*. **10**. 255-260.

- [158] **Wolff, S.** (1996) Chemical aspects of rubber reinforcement by fillers. *Rubber Chemistry and Technology*. **69(3)**. 325-346.
- [159] **Xu, D., Karger-Kocsis, J. and Schlarb, A. K.** (2009) Friction and wear of HNBR with different fillers under dry rolling and sliding conditions. *Express Polymer Letters*. **3(2)**. 126-136.
- [160] **Yan, W. and Fischer, F. D.** (2000) Applicability of the Hertz contact theory to rail-wheel contact problems. *Archive of applied mechanics*. **70(4)**. 255-268.
- [161] **Zhang, T., Cheung, L. and Goldberg, K.** (2001) Shape tolerance for robot gripper jaws. Proceedings of *2001 IEEE/RSJ International Conference on Intelligent Robots and Systems*. **3**. 1782-1787.
- [162] **Zhao, X. and Li, Z.** (2011) The solution of frictional wheel–rail rolling contact with a 3D transient finite element model: Validation and error analysis. *Wear*. **271(1)**. 444-452.
- [163] **Zhao, X., Zhao, X., Liu, C., Wen, Z. and Jin, X.** (2016) A Study on Dynamic Stress Intensity Factors of Rail Cracks at High speeds by a 3D Explicit Finite Element Model of Rolling Contact. *Wear*.
- [164] **Zwirlein, O. and Schlicht, H.** (1982) Rolling contact fatigue mechanisms—accelerated testing versus field performance. *Rolling contact fatigue testing of bearing steels*. ASTM International.

**LIST OF PAPERS**  
**SUBMITTED ON THE BASIS OF THIS THESIS**

**I REFEREED JOURNALS**

1. **O. Thomas and V.N.N. Namboothiri** (2014) A framework for optimised design of serrations on a printing gripper. *Procedia Materials Science*, **5**, 1509-1518. *Elsevier Publication*, doi: 10.1016/j.mspro.2014.07.338; ISSN: 2211-8128.
2. **O. Thomas, V.N.N. Namboothiri and Rani Joseph** (2016) Feasibility of silica loaded NBR as lining material for impactive gripper, *Procedia Technology*, **25**, 900-907. *Elsevier Publication*, doi: 10.1016/j.protcy.2016.08.175; ISSN: 2212-0173.
3. **Oommen Thomas and Narayanan V. N. Namboothiri** (2017) Diffusion of carbon in steel grippers due to cyclic contact stress, *Journal of Failure Analysis and Prevention*, **17(2)**, 275-290. *Springer US (ASM International) Publication*, doi: 10.1007/s11668-017-0244-0; ISSN: 1547-7029.

**II PRESENTATIONS IN CONFERENCES.**

1. **O. Thomas and V.N.N. Namboothiri** (2016) On stress assisted Diffusion. *International Conference On Recent Trends In Engineering & Technology*, Kochi, October 2016.

## **CURRICULAM VITAE**

**1. NAME** : Oommen Thomas

**2. DATE OF BIRTH** : 01 March 1961

**3. EDUCATIONAL QUALIFICATIONS**

**1983 Bachelor of Engineering BSc (Engg)**

Institution : College of Engineering, Trivandrum

Specialization : Mechanical Engineering

Marks : 74.5%

**1992 Master of Technology (M.Tech)**

Institution : Indian Institute of Technology, Madras

Specialization : Mechanical Engineering

CGPA : 8.83/10

**2003 Master of Business Administration (MBA)**

Institution : Indira Gandhi National Open University

**Doctor of Philosophy (Ph.D)**

Institution : Cochin University of Science and Technology

Registration Date : 29-12-2006

**INDUSTRIAL EXPERIENCE**

**Institution** : **HMT Machine Tools Limited, Kochi, India.**

2006 till date : Dy. General Manager - Design and development

2000 –2006 : Dy. Chief Engineer - Design and development

1992 - 2000 : Senior Engineer - Manufacturing

1986 - 1992 : Dy. Engineer / Engineer- Engineering

1984 - 1986 : Engineer Trainee